IOWA STATE UNIVERSITY
Digital Repository

Retrospective Theses and Dissertations

Iowa State University Capstones, Theses and Dissertations

2006

Comparison of alternative laboratory dowel bar testing procedures

John Francis Harrington
Iowa State University

Follow this and additional works at: https://lib.dr.iastate.edu/rtd

 Part of the Civil Engineering Commons

Recommended Citation
Harrington, John Francis, "Comparison of alternative laboratory dowel bar testing procedures " (2006). *Retrospective Theses and Dissertations*. 854.
https://lib.dr.iastate.edu/rtd/854

This Thesis is brought to you for free and open access by the Iowa State University Capstones, Theses and Dissertations at Iowa State University Digital Repository. It has been accepted for inclusion in Retrospective Theses and Dissertations by an authorized administrator of Iowa State University Digital Repository. For more information, please contact digirep@iastate.edu.

www.manaraa.com

Comparison of alternative laboratory dowel bar testing procedures

by

John Francis Harrington

A thesis submitted to the graduate faculty

in partial fulfillment of the requirements for the degree of

MASTER OF SCIENCE

Major: Civil Engineering (Structural Engineering)

Program of Study Committee:
Max Porter, Major Professor
Fouad Fanous
Lester Schmerr

Iowa State University

Ames, Iowa

2006

UMI Number: 1439886

UMI Microform 1439886
Copyright 2007 by ProQuest Information and Learning Company.
All rights reserved. This microform edition is protected against unauthorized copying under Title 17, United States Code.

ProQuest Information and Learning Company
300 North Zeeb Road
P.O. Box 1346
Ann Arbor, MI 48106-1346

TABLE OF CONTENTS

LIST OF FIGURES iv

LIST OF TABLES vii

ABSTRACT viii

1. INTRODUCTION 1
   - 1.1 Background 1
   - 1.2 Research approach 5
   - 1.3 Research objectives 6
   - 1.4 Scope 6

2. LITERATURE REVIEW 7
   - 2.1. Modulus of Dowel Support 7
   - 2.2. Relative deflection between slabs 10

3. TESTING PROGRAM 14
   - 3.1 Test descriptions 14
   - 3.2 Construction 22

4. ANALYSIS AND RESULTS 25
   - 4.1. Modified AASHTO test 25
   - 4.2. Cantilever test 30

5. CONCLUSIONS 32
   - 5.1 Modified AASHTO T253 32
   - 5.2 Cantilever test 32
   - 5.3 Conclusion summary 33

6. FUTURE NEEDS AND RECOMMENDATIONS 34
   - 6.1 Modified AASHTO T253 34
   - 6.2 Cantilever test 37

REFERENCES 39

ACKNOWLEDGEMENTS 42

APPENDIX A. MODIFIED AASHTO LOAD VS. DEFLECTION PLOTS. 43

APPENDIX B. CANTILEVER TEST LOAD VS. DEFLECTION PLOTS.....70

APPENDIX C. MODULUS OF DOWEL SUPPORT PLOTS. 81

APPENDIX D. SUGGESTED REVISION OF AASHTO T273 DOWEL TEST. 86

LIST OF FIGURES

Figure 1.1. Iosipescu elemental dowel shear test....2
Figure 1.2. AASHTO T253-76 procedure [2]. 4
Figure 2.1. Deflected beam on an elastic foundation 8
Figure 2.2. Point load and moment acting on semi-finite beam 9
Figure 2.3. Relative deflection of slab sections [4] 11
Figure 3.1. Modified AASHTO T253 test diagram [2] 14
Figure 3.2. Load test frame....15
Figure 3.3. Locations of DCDTs on specimen 17
Figure 3.4. Cantilever test specimen....18
Figure 3.5. Cantilever dowel bar test....18
Figure 3.6. String line around dowel bar. 19
Figure 3.7. Instrumentation of cantilever specimen 21
Figure 3.8. Cantilever test loading brackets 21
Figure 3.9. Modified AASHTO specimen forms....23
Figure 3.10. Cantilever dowel forms. 24
Figure 6.1. Proposed revised modified AASHTO specimen....34
Figure 6.2. Proposed cantilever dowel specimen 37
Figure A.1. Round stainless steel #1, 0.5-in. gap load vs. deflection....45
Figure A.2. Round stainless steel #2, 0.5-in. gap load vs. deflection....45
Figure A.3. Round stainless steel #3, 0.5-in. gap load vs. deflection....46
Figure A.4. Round stainless steel #1, 0.125-in. gap load vs. deflection....46
Figure A.5. Round stainless steel #2, 0.125-in. gap load vs. deflection....47
Figure A.6. Round stainless steel #1, no gap load vs. deflection 47
Figure A.7. Round stainless steel #2, no gap load vs. deflection 48
Figure A.8. Round stainless steel #3, no gap load vs. deflection 48
Figure A.9. Round epoxy-coated steel #1, 0.5-in. gap load vs. deflection....49
Figure A.10. Round epoxy-coated steel #2, 0.5-in. gap load vs. deflection....49
Figure A.11. Round epoxy-coated steel #3, 0.5-in. gap load vs. deflection....50
Figure A.12. Round epoxy-coated steel #1, 0.125-in. gap load vs. deflection....50
Figure A.13. Round epoxy-coated steel #2, 0.125-in. gap load vs. deflection....51
Figure A.14. Round epoxy-coated steel #3, 0.125-in. gap load vs. deflection....51
Figure A.15. Round epoxy-coated steel #1, no gap load vs. deflection 52
Figure A.16. Round epoxy-coated steel #2, no gap load vs. deflection 52
Figure A.17. Round epoxy-coated steel #3, no gap load vs. deflection 53
Figure A.18. Round GFRP #1, 0.5-in. gap load vs. deflection....53
Figure A.19. Round GFRP #2, 0.5-in. gap load vs. deflection....54
Figure A.20. Round GFRP #3, 0.5-in. gap load vs. deflection....54
Figure A.21. Round GFRP #1, 0.125-in. gap load vs. deflection....55
Figure A.22. Round GFRP #2, 0.125-in. gap load vs. deflection....55
Figure A.23. Round GFRP #3, 0.125-in. gap load vs. deflection....56
Figure A.24. Round GFRP #1, no gap load vs. deflection 56
Figure A.25. Round GFRP #2, no gap load vs. deflection 57
Figure A.26. Round GFRP #3, no gap load vs. deflection 57

Figure A.27. Elliptical GFRP #1, 0.5-in. gap load vs. deflection 58
Figure A.28. Elliptical GFRP #2, 0.5-in. gap load vs. deflection 58
Figure A.29. Elliptical GFRP #3, 0.5-in. gap load vs. deflection 59
Figure A.30. Elliptical GFRP #1, 0.125-in. gap load vs. deflection 59
Figure A.31. Elliptical GFRP #2, 0.125-in. gap load vs. deflection 60
Figure A.32. Elliptical GFRP #3, 0.125-in. gap load vs. deflection 60
Figure A.33. Elliptical GFRP #1, no gap load vs. deflection 61
Figure A.34. Elliptical GFRP #2, no gap load vs. deflection 61
Figure A.35. Large elliptical steel #1, 0.5-in. gap load vs. deflection 62
Figure A.36. Large elliptical steel #2, 0.5-in. gap load vs. deflection 62
Figure A.37. Large elliptical steel #3, 0.5-in. gap load vs. deflection 63
Figure A.38. Large elliptical steel #1, 0.125-in. gap load vs. deflection 63
Figure A.39. Large elliptical steel #3, 0.125-in. gap load vs. deflection 64
Figure A.40. Large elliptical steel #1, no gap load vs. deflection 64
Figure A.41. Large elliptical steel #3, no gap load vs. deflection 65
Figure A.42. Small elliptical steel #1, 0.5-in. gap load vs. deflection 65
Figure A.43. Small elliptical steel #2, 0.5-in. gap load vs. deflection 66
Figure A.44. Small elliptical steel #3, 0.5-in. gap load vs. deflection 66
Figure A.45. Small elliptical steel #1, 0.125-in. gap load vs. deflection 67
Figure A.46. Small elliptical steel #2, 0.125-in. gap load vs. deflection 67
Figure A.47. Small elliptical steel #3, 0.125-in. gap load vs. deflection 68
Figure A.48. Small elliptical steel #1, no gap load vs. deflection 68
Figure A.49. Small elliptical steel #2, no gap load vs. deflection 69
Figure B.1. Round stainless steel #1 cantilever load vs. deflection 72
Figure B.2. Round stainless steel #2 cantilever load vs. deflection 72
Figure B.3. Round stainless steel #3 cantilever load vs. deflection 73
Figure B.4. Round epoxy-coated steel #1 cantilever load vs. deflection 73
Figure B.5. Round epoxy-coated steel #2 cantilever load vs. deflection 74
Figure B.6. Round epoxy-coated steel #3 cantilever load vs. deflection 74
Figure B.7. Round GFRP #1 cantilever load vs. deflection 75
Figure B.8. Round GFRP #2 cantilever load vs. deflection 75
Figure B.9. Round GFRP #3 cantilever load vs. deflection 76
Figure B.10. Elliptical GFRP #1 cantilever load vs. deflection 76
Figure B.11. Elliptical GFRP #2 cantilever load vs. deflection 77
Figure B.12. Elliptical GFRP #3 cantilever load vs. deflection 77
Figure B.13. Large elliptical steel #1 cantilever load vs. deflection 78
Figure B.14. Large elliptical steel #2 cantilever load vs. deflection 78
Figure B.15. Large elliptical steel #3 cantilever load vs. deflection 79
Figure B.16. Small elliptical steel #1 cantilever load vs. deflection 79
Figure B.17. Small elliptical steel #2 cantilever load vs. deflection 80
Figure B.18. Small elliptical steel #3 cantilever load vs. deflection 80
Figure C.1. Round stainless steel k_0 comparison 83
Figure C.2. Round epoxy-coated steel k_0 comparison 83
Figure C.3. Elliptical GFRP k_0 comparison 84
Figure C.4. Round GFRP k_0 comparison 84
Figure C.5. Large elliptical steel k_0 comparison 85

Figure C.6. Small elliptical steel k_0 comparison 85
Figure D-1. Modified dowel test procedure 90

LIST OF TABLES

Table 1.1. Dowel bar properties....6
Table 4.1. Load vs. deflection behavior of 0.125-in. gap AASHTO specimens. 26
Table 4.2. Load vs. deflection behavior of 0.5-in. gap AASHTO specimens 26
Table 4.3. Load vs. deflection behavior of no-gap AASHTO specimens 27
Table 4.4. Modified AASHTO k_0 values....29
Table 4.5. Load vs. deflection behavior of cantilever dowel specimens....30
Table 4.6. Cantilever k_0 values 31

ABSTRACT

The objective of this study was to evaluate the performance of a modified version of the AASHTO T253 dowel bar test procedure. The modified AASHTO test was developed based upon comparisons to previous ISU projects and was compared to an alternate cantilevered dowel bar test. The dowel bar tests were conducted for the purpose of finding a preferred method of obtaining the Modulus of Dowel Support, k_0. The series of tests included 54 modified AASHTO specimens and 18 cantilever specimens. Six different dowel bar types were included in the laboratory tests. The bar shapes were both round and elliptical. The dowel bars were made of epoxy-coated steel, stainless steel, and glass fiber-reinforced polymer (GFRP).

The study was conducted in the Iowa State University Structural Engineering Laboratories. The data gathered from the laboratory tests was analyzed using modified theories developed by Timoshenko and Friberg.

The results in this study determined that the modified AASHTO test was superior to the experimental cantilever test in both accuracy and precision for the determination of k_0. Recommendations are given for an improved AASHTO T253 procedure. Recommendations for further research regarding the determination of k_0 are noted at the end of this study.

1. INTRODUCTION

1.1 Background

Load transfer across transverse joints has always been a factor in the useful life of concrete pavements. For many years, round steel dowels have been the conventional shear transfer implement in concrete slab sections. Although an effective transfer method, many concerns have been associated with the round steel dowels such as higher bearing stresses and deformation of surrounding concrete. The most detrimental contribution of the steel dowel to a pavement joint is corrosion. When steel corrodes, it increases in volume and loses density. When the steel expands, unwanted stresses are applied to its surrounding concrete. The corroded steel also allows for small void spaces to surround the dowel. These small void spaces are capable of holding water and other detrimental salt solutions, which contribute even further to the detriment of the joint. The exposure of salt solutions to the dowel steel leads to corrosion due to chloride ion exchanges between the steel and solution [1]. The expanded, corroded steel will also prevent the proper lateral movement between the two slab sections in order to accommodate concrete expansion and contraction due to temperature changes. The prevention of free lateral movement between slab sections during thermal expansion and contraction contributes to cracks in the pavement around the sawed joints.

Repeated loading also contributes to damaged joints. When a dowel is repeatedly loaded over a long period of time, the surrounding concrete found at the top and bottom edge of the dowel bar is finely pulverized. The small-scale pulverization of the concrete surrounding the dowel distorts the shape of the dowel hole within the slab. The distortion of the shape of the surrounding concrete is called oblonging. This dowel hole oblonging

creates multiple problems in the joint. The void spaces allow greater and more dynamic deflections of the dowel within the concrete. Increased dowel movement for a given load means that load which was once transferred to the adjacent slab by the dowel bar is now transferred into the subgrade. When the shear load is not transferred efficiently from slab to slab by a dowel bar, the subgrade experiences increased loading and erosion due to the movement of the concrete. Over time, the damaged subgrade is eroded due to increased water infiltration and concrete movement. The lack of subgrade support below the joint causes the pavement to crack and sink at the joint locations. The increased void spaces between the dowel bars and concrete also allow greater infiltration of water and chemicals containing chloride ions to contribute further to steel corrosion.

Over the past decade, extensive research has been performed at Iowa State University (ISU) on new dowel shapes and materials to mitigate the joint-damaging effects of oblonging and corrosion. The past ISU studies included analyses of k_0 by implementing the Iosipescu elemental shear test (See Figure 1.1) and the standard AASHTO T253 procedure [2, 3, 4].

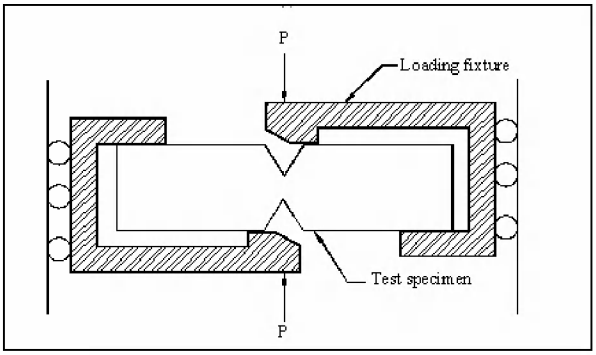

Figure 1.1. Iosipescu elemental dowel shear test

Other laboratory dowel studies involved full-scale slab tests and gap width analyses. In addition to laboratory simulations, studies were performed on existing Iowa roadways to evaluate the field capabilities of alternate dowel bar shapes and materials [5, 6].

This particular study was conducted for two reasons. The first goal of this study was to evaluate the performance of six different dowel bar types subjected to two different test methods. The second goal of the dowel study was to evaluate the current dowel shear testing procedures and recommend improvements. This document focuses primarily on the second goal.

The Iosipescu procedure was not implemented in this study because of the difficulties involved in fabricating a testing frame and performing the procedure. Although the Iosipescu test yielded preferable results due to the fact that the geometry of the test produced an inflection point of zero moment at the mid point of the joint, there were difficulties involved in the execution of the procedure. One significant obstacle involved in the Iosipescu test was maintaining adequate lubrication in the glides located in the test frame in order to create the roller end conditions shown above in Figure 1.1. There was no way of determining the amount of force that was dissipated due to frictional effects when the Iosipescu test was implemented.

Because of the difficulties associated with the Iosipescu procedure, the primary dowel test method applied in this study was an ISU-modified version of the AASHTO T253 dowel shear test. The standard AASHTO dowel shear procedure is shown below in Figure 1.2.

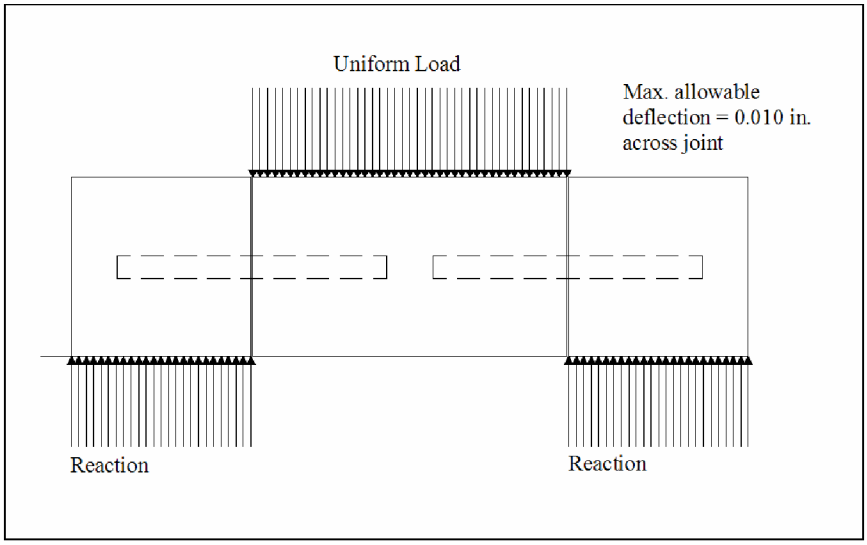

Figure 1.2. AASHTO T253-76 procedure [2].

The next test method was an experimental cantilever dowel bar specimen. The cantilever dowel bar specimen was designed to be a simpler, more economical, and more accurate test alternative to the AASHTO method. The modified AASHTO and cantilever test specimens and procedures will be shown and discussed in greater detail in Chapter 3 of this study. The AASHTO test was implemented at ISU in past studies to calculate k_0 by determining relative deflection between concrete block sections [4]. The constant, k_0, quantifies the amount of bearing stress applied to concrete and is directly related to the deflection of the bar and is defined as the amount of bearing stress produced by a unit bar deflection. Determination of k_0 is useful to designers in selecting an optimal bar shape or material in order to extend the useful design life of a pavement.

The AASHTO test blocks presented many difficulties and ambiguities with regard to executing the test procedure and measuring relevant deflections and loads. The

AASHTO procedure allowed for measurement of concrete blocks, but not actual dowel movement within the joint.

Because of the limitations present with respect to instrumentation, all crucial deflections with respect to solving for k_0 were calculated and not directly measured. The AASHTO test also required the use of heavy lifting equipment in order to move the test specimens. A cantilever dowel test is one possible alternative to reduce the shortcomings and equipment requirements of the AASHTO test. The test allowed direct measurements that were not allowed by the AASHTO procedure.

Another benefit of the smaller cantilever specimens was that their significantly reduced weight allowed them to be moved and placed by hand. In this study, a revised k_0 was calculated using data collected from both test methods and a determination was made for or against a cantilever test being used as an acceptable alternative to the AASHTO procedure in the verification of a k_0 value.

1.2 Research approach

A literature review covered the past dowel research conducted at ISU. The theory examining the structural behavior of a beam on an elastic foundation was also reviewed. Concrete dowel shear specimens containing dowel bars were constructed and tested in the laboratory using both the AASHTO and cantilever methods. The applicable theory of the behavior of a beam on an elastic foundation was implemented to determine k_0 for each specimen.

1.3 Research objectives

The objective of this investigation was to further improve the current AASHTO T253 dowel shear procedure and explore the use of an alternative test.

1.4 Scope

A total of 72 dowel bar tests were performed in this study. Fifty-four dowel tests were performed using a modified version of the AASHTO T253 test. An additional 18 tests were executed using a new experimental cantilever dowel test. Each dowel bar shape is listed below in Table 1.1. The table also includes physical properties of the dowel bars. The bars are listed in descending order with respect to flexural rigidity, *EI*.

Table 1.1. Dowel bar properties

Bar Type	AASHTO Quantity	Cantilever Quantity	Dimensions* in.	E lb/in.^{2}	I in.^{4}	EI lb*in.^{2}
Stainless Steel	9	3	1.5	2.80E+07	0.2485	6.96E+05
Epoxy-Coated Steel	9	3	1.5	2.90E+07	0.2485	7.21E+06
Small Elliptical Steel	9	3	1.66 x 1.333	2.90E+07	0.2552	7.40E+06
Round GFRP	9	3	1.875	6.51E+06	0.6067	3.95E+06
Large Elliptical Steel	9	3	2 x 1.375	2.90E+07	0.1176	3.41E+06
Elliptical GFRP	9	3	2.25 x 1.27	8.66E+06	0.2157	1.87E+06

*A single dimension denotes a round bar diameter. Elliptical dimensions are listed as horizontal x vertical.

The quantity of AASHTO test specimens was three times the amount of cantilever specimens because three different gap widths were used with the AASHTO test. Three individual specimens were tested for each gap width. The gap widths evaluated in the AASHTO test were 0.5, 0.125, and 0 in.

2. LITERATURE REVIEW

The theory in the following chapter was obtained through a literature review of information pertinent to the study of the behavior of dowel bars in pavements. The literature review was conducted through sources obtained in the Parks Library located at ISU and in the Structural Engineering Library of Town Engineering Building. Other sources in this study were publications from the Transportation Research Board (TRB), the Iowa Department of Transportation (IDOT), and the American Association of State Highway and Transportation officials (AASHTO).

2.1. Modulus of Dowel Support

The *Modulus of Dowel Support,* k_0, was calculated using Timoshenko's model of a beam resting uniformly on an elastic foundation [7]. Timoshenko's model stated that as a beam is deflected into an elastic foundation, the continuous reaction at each section of the beam is directly proportional to the deflection at each particular section. The reaction per unit length of the beam is given using the expression Ky. The variable K represents the *Modulus of Foundation* and y represents the downward deflection of the beam within the foundation. The modulus of foundation is defined by Timoshenko as "the reaction per unit length, provided the deflection is equal to unity" [7]. The variable K is related to the deflected shape of an unloaded beam, as shown below in Equation 2.1.

$$EI\frac{d^4y}{dx^4} = -Ky \tag{2.1}$$

The deflected shape of the unloaded beam supported on both surfaces is shown below in Figure 2.1.

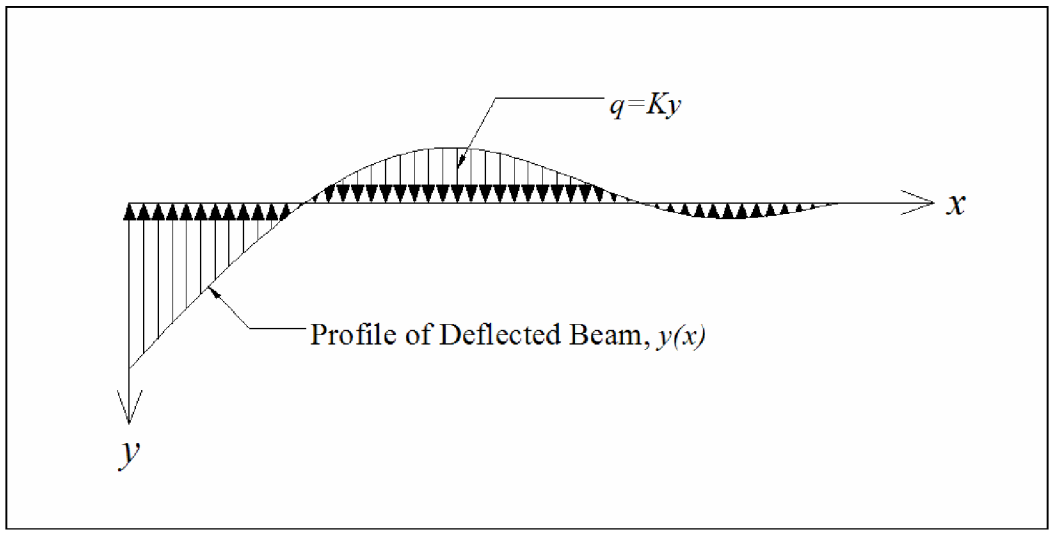

Figure 2.1. Deflected beam on an elastic foundation

The general solution of the above differential equation is denoted below in Equation 2.2.

$$y = e^{\beta x}(A\cos\beta x + B\sin\beta x) + e^{-\beta x}(C\cos\beta x + D\sin\beta x) \tag{2.2}$$

The variable β represents the relative stiffness (in.$^{-1}$) of the beam on foundation. The definition of β is shown below in Equation 2.3.

$$\beta = \sqrt[4]{\frac{K}{4EI}} \tag{2.3}$$

After applying the appropriate boundary conditions to Equation 2.2, Timoshenko's equation of the deflected shape of a beam on an elastic foundation became:

$$y = \frac{e^{-\beta x}}{2\beta^3 EI}[P\cos\beta x - \beta M_0(\cos\beta x - \sin\beta x)] \tag{2.4}$$

A semi-finite beam resting on an elastic foundation with a point load, P, and a moment, M_0 at the origin is shown below in Figure 2.2.

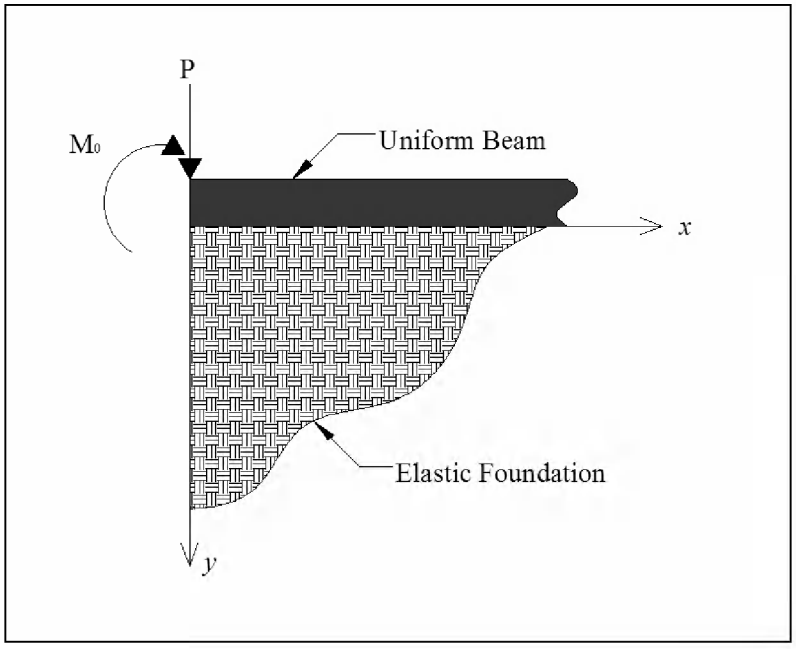

Figure 2.2. Point load and moment acting on semi-finite beam

Equation 2.4 was applied by Friberg to simulate a dowel bar of semi-finite length embedded in concrete [8]. In order to evaluate the behavior of the dowel bar at the joint face, the initial condition $x=0$ was applied, making Equation 2.4 become Equation 2.5.

$$y_0 = \frac{1}{2\beta^3 EI}(P - \beta M_0) \tag{2.5}$$

Where,

- $M_0 = \frac{Pz}{2}$ for the modified AASHTO specimens under the assumption that the inflection point occurs at the middle of the joint
- $M_0 = Pz$ for the cantilever specimens, with z representing the distance of load placement from the face of the concrete.

The variable β was modified to account for the bar width, b because k_0 is used to quantify stress produced by a unit deflection, rather than a reaction by a unit deflection.

- $\beta = \sqrt[4]{\frac{k_0 b}{4EI}}$

Where,

- k_0 = Modulus of Dowel Support (pci)

2.1.1. Dowel bar embedment length

Although the semi-finite beam assumed by Friberg is not the same as a dowel bar of relatively short length, Albertson determined that the semi-finite assumption is applicable to a dowel of finite length, provided that $\beta L > 2$ [9]. Work by Porter and Barnes also supports the assertion that $\beta L > 2$ is adequate to apply the semi-finite beam assumption by Friberg [10].

2.2. Relative deflection between slabs

The modified AASHTO test was used to determine the downward deflection of the dowel within the face of each joint, y_0. The modified AASHTO test specimen allowed measurements of slab sections and not of actual dowel bars. Because y_0 was not measured directly, a series of calculations was performed to determine the actual bar deflection. A diagram showing the deflected shape of two slab sections connected by a dowel bar is shown below in Figure 2.3.

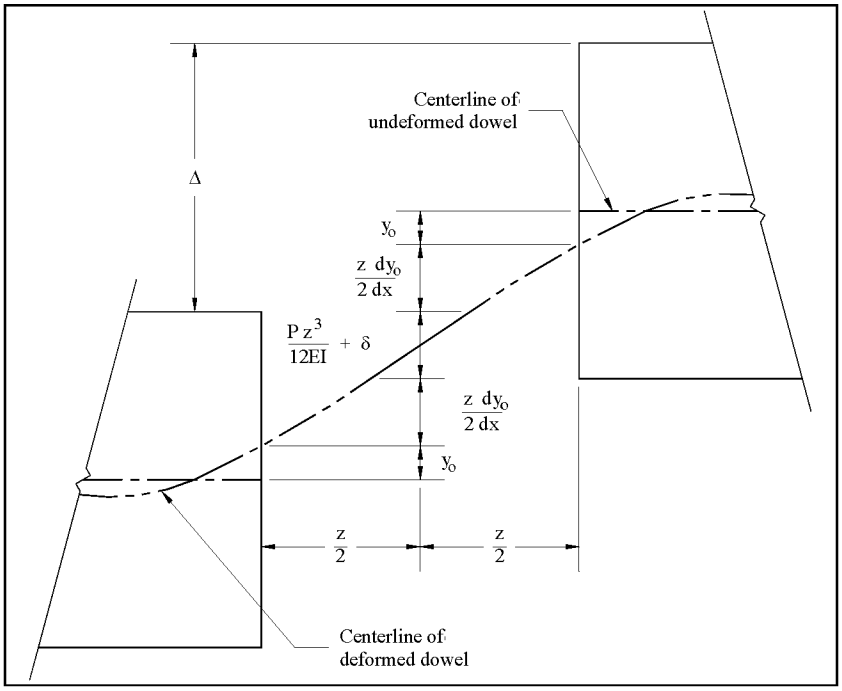

Figure 2.3. Relative deflection of slab sections [4]

The deflection between the two slab surfaces was calculated using Equation 2.6.

$$\Delta = 2y_0 + \frac{zdy_0}{dx} + \frac{Pz^3}{12EI} + \delta \tag{2.6}$$

Where,

- Δ = measured deflection between slab surfaces, in. (AASHTO)
- y_0 = deflection of dowel bar within concrete at joint face, in.
- z = gap width, in.
- $\frac{dy_0}{dx}$ = slope of dowel bar within joint
- $\frac{Pz^3}{12EI}$ = dowel deflection due to flexural effects, in.
- δ = shear deflection, in. [11]

The shear deflection of the dowel bar was calculated using the following

equation:

$$\delta = \frac{\lambda P z}{AG}, \text{ in.}$$

Where,

- λ = shear shape factor=10/9 for round and elliptical bars
- P = shear force transferred by dowel, lbs
- A = cross-sectional area of dowel bar, in.^2
- G = dowel bar shear modulus, psi

The gap widths of the modified AASHTO specimens were not large enough to warrant inclusion of deflection due to bar slope or flexural effects. The 0.5-in. gap AASHTO specimens experienced downward deflection due to flexural effects on the order of hundred-thousandths of an inch. After removing the deflection term due to flexure, Equation 2.6 became:

$$\Delta = 2y_0 + \delta \tag{2.7}$$

By solving for y_0, Equation 2.7 becomes:

$$y_0 = \frac{\Delta - \delta}{2} \tag{2.8}$$

Equation 2.8 was used to calculate y_0 from the data obtained in the modified AASHTO tests. Equation 2.8 was modified for use with cantilever test data and is shown below as Equation 2.9.

$$y_0 = \Delta \tag{2.9}$$

Equation 2.8 became Equation 2.9 because the objective of the cantilever test was to directly measure the value of y_0 at the face of the concrete joint. In the case of the cantilever test, Δ is equal to the measured dowel bar deflection at the concrete face.

3. TESTING PROGRAM

3.1 Test descriptions

3.1.1 AASHTO T-253

Tests were performed at ISU in the Structural Engineering Laboratories located in Town Engineering Building with the assistance of laboratory supervisor Douglas Wood. The tests were part of ongoing research to investigate the current AASHTO T253 testing method for dowel bars. The test specimens were constructed using concrete and various dowel shapes. Epoxy-coated steel, stainless steel and glass fiber-reinforced polymer (GFRP) dowels were tested. Each specimen consisted of three concrete blocks connected with two dowel bars (See Figure 3.1).

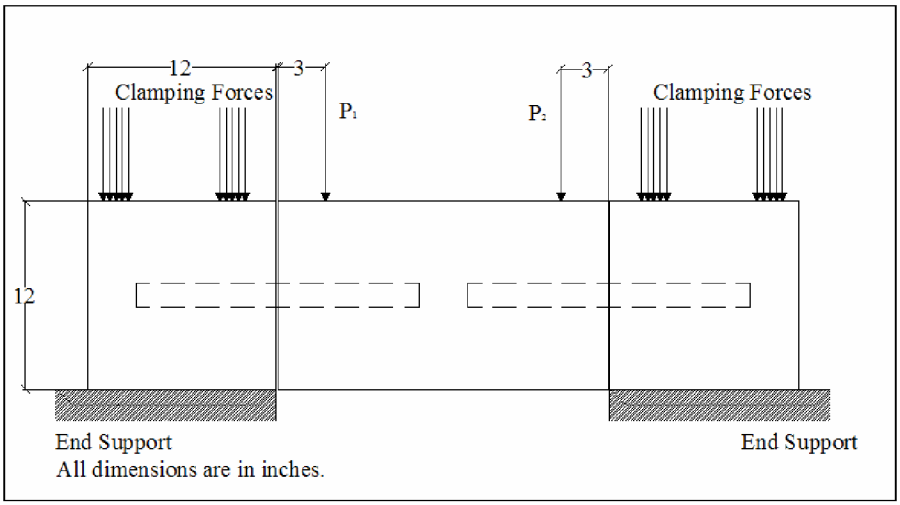

Figure 3.1. Modified AASHTO T253 test diagram [2]

The specimens were placed into a load frame shown below in Figure 3.2.

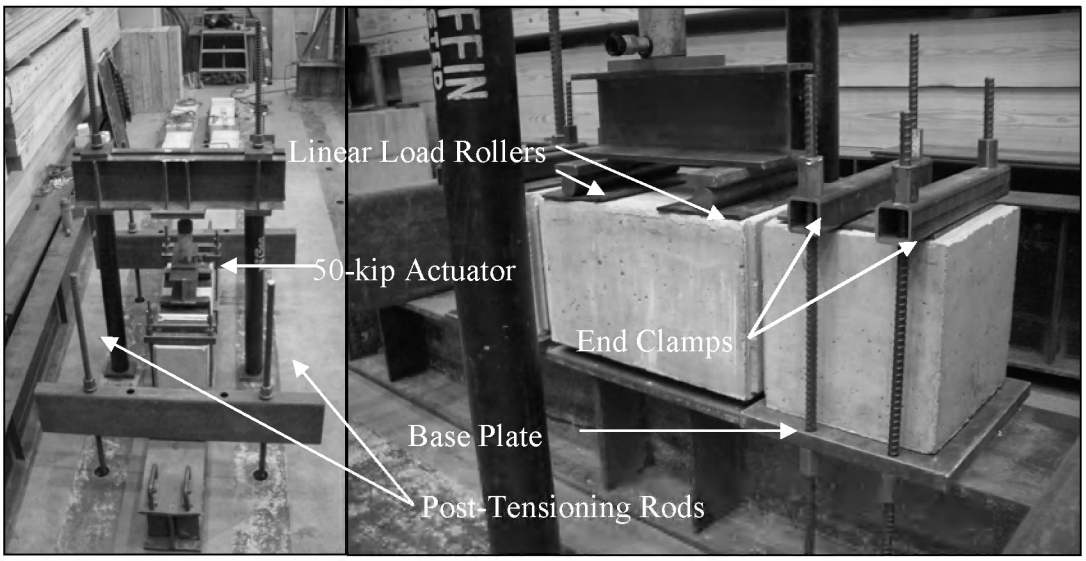

Figure 3.2. Load test frame

The vertical structural iron tubes supporting the top cross beam were secured to the reaction floor by post-tensioning high-strength Dywidag® rods to a stress of 3,000 psi per bar. The post-tensioning was done to ensure smooth load transfer from the hydraulic actuator to the concrete test specimen. Downward load was transferred from the hydraulic jack to the concrete by using a stiffened steel beam section. The load transfer beam was simply supported using two 1.25-in. diameter solid steel bars placed 3 in. inside and parallel to each specimen joint in order to transfer the downward load from the beam to the concrete. Thin sheets of neoprene were placed beneath the loaded rollers to allow for an even, transverse load application along the middle concrete block. Steel plates were not placed beneath the rollers shown in Figure 3.2 because trial tests determined that the neoprene provided adequate protection from localized concrete bearing failure. The absence of steel plates below the rollers allowed for more consistent load placement along the joints.

The end blocks of the specimen were clamped down to the lower steel support plates using high strength Dywidag® steel rods. The goal of applying each end support was to create a fixed-end condition on each side of the specimen. The clamping mechanisms were tightened by hand with wrenches. A hydraulic jack was not used to tension the clamping rods because outside stresses acting on the dowels would have affected the deflection behavior of the bar under a load. The fixed-end conditions were applied to prevent rotation in the end blocks. By preventing the end block rotation, the dowels were subjected to minimal bending effects. The reduction in bending of the dowel was necessary to promote load transfer primarily through dowel shear. Two clamps per end block were used because the preliminary tests involving one clamp per end yielded significantly higher end block rotations. The addition of the second clamp per side produced greater resistance to the moments produced at the end blocks due to dowel shear loading.

The specimens were instrumented with direct current deflection transducers (DCDTs). There were a total of eight DCDTs used. Four were used to measure relative deflections on the right and left ends of the specimen. Two were placed at the far ends of the end blocks to monitor the movement in the restrained ends. Two more were placed on the base plates that support the specimen in order to monitor movement of the entire testing surface. The DCDTs placed on the reaction beam did not monitor significant deflections and were not included in the calculation of y_0 from the laboratory data. The placement of DCDTs on the modified AASHTO specimen is illustrated below in Figure 3.3.

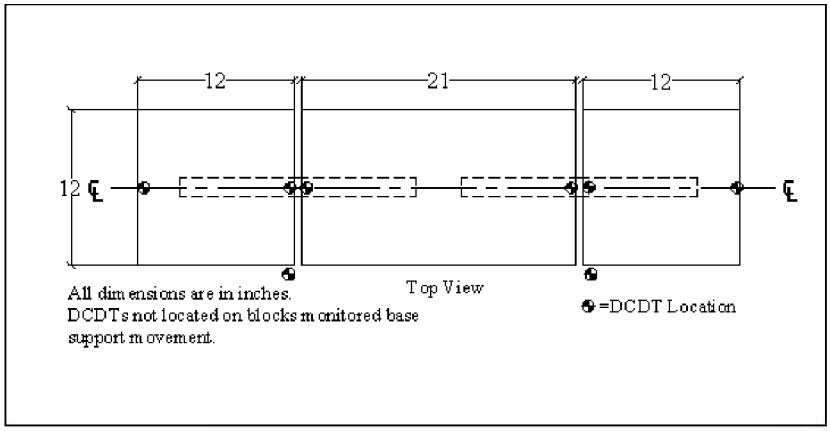

Figure 3.3. Locations of DCDTs on specimen

The AASHTO test specimens were constructed so that the relative deflection, Δ, was measured between the end and middle block sections at the joint locations. This deflection, along with a theoretical shear deflection, δ, was used to calculate the dowel deflection within the concrete, y_0.

The specimens also weighed over 600 pounds per specimen, making them somewhat heavy and awkward to move and place by hand within a test apparatus. The large AASHTO specimens required the use of a crane for placement within the test apparatus.

3.1.2 Cantilever test

The cantilever test was a new experimental test method. The aim of the new test was to eliminate some of the unknown parameters involved with the AASHTO test. The physical properties of the test were also a more accurate simulation of the semi-finite beam undergoing a concentrated load and moment at the origin. The cantilever test

consisted of a 12-in. concrete cube and a single 18-in. dowel. The dowel bar was placed with 9 in. embedded in the concrete. The cantilever specimen is shown below in Figure 3.4.

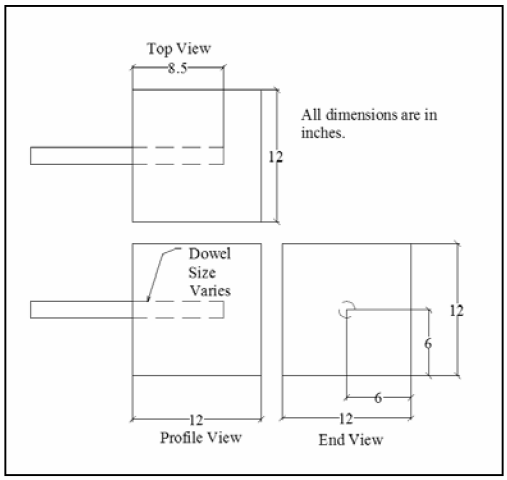

Figure 3.4. Cantilever test specimen

The new test allowed for direct measurement of the dowel deflection at the face of the concrete block. A diagram of the cantilever test is shown below in Figure 3.5.

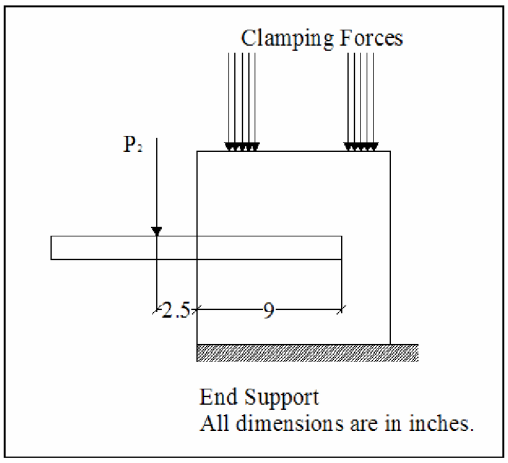

Figure 3.5. Cantilever dowel bar test

The specimens were also cast with the bar oriented vertically, allowing uniform concrete consolidation around the dowel. The test specimen was also significantly lighter than the AASHTO specimen, weighing only 150 pounds. The investigators were able to move and place the blocks by hand.

The test apparatus was the same one used during the AASHTO test with minor modifications. The base beam was moved in order to apply the load closer to the face of the test block. Like the AASHTO test, there was no hydraulic prestressing of the test specimens to the base plate. The test specimens were clamped down with the Dywidag® rods and square steel tubing and tightened by hand with wrenches. Although the cantilever test required greater moment resistance due to the increased distance of the load from the block, the high prestress forces would have had an unknown influence on the behavior of the dowel bar.

Dowel deflection was measured using a string line transducer. The string line was wrapped around the base of the dowel in order to measure bar deflection at the active face of the dowel. The string-dowel configuration is shown below in Figure 3.6.

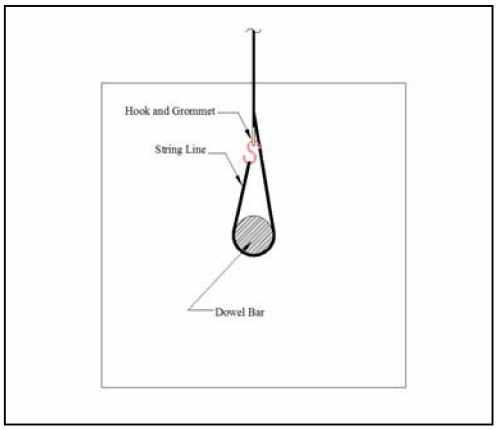

Figure 3.6. String line around dowel bar.

The geometry and dimensions of the specimen made the use of a DCDT very difficult. The direct measurement of y_0 had to be made from the bottom surface of the dowel bar, requiring an upside-down DCDT.

The other issue presented with the use of DCDTs was the inability to place the pin directly at the face of the joint. The clamps used to support the DCDTs were also contributing factors to the difficulty of pin placement at the joint face. Although the string transducer did not have as high precision as the DCDTs, the string apparatus allowed for more direct measurement at the face of the dowel. The use of a DCDT to measure dowel bar deflection anywhere but at the face would have nullified the goals of implementing the cantilever test. The string transducer was precise to the nearest thousandth of an inch. The researchers assumed that the difference in precision between the string transducers and the DCDTs would not have a significant effect on the results of the test. The direct measurement was assumed to allow for more consistent results and that one-thousandth of an inch was sufficient measurement precision. The investigators also assumed that even with the instrument's reduced precision, the DCDT would still be precise enough to calculate a reasonable value of k_0, since the values of k_0 were calculated to a precision of 10^4 pci.

The concrete block deflection was measured with a single 0.1-in. stroke DCDT. The block deflection was measured at the face of the block. This quantity was to be subtracted from the dowel deflection in order to account for the predicted concrete block movement. Two DCDTs were placed at the back top corners for two tests to quantify block rotation. The locations of the DCDTs are shown below in Figure 3.7.

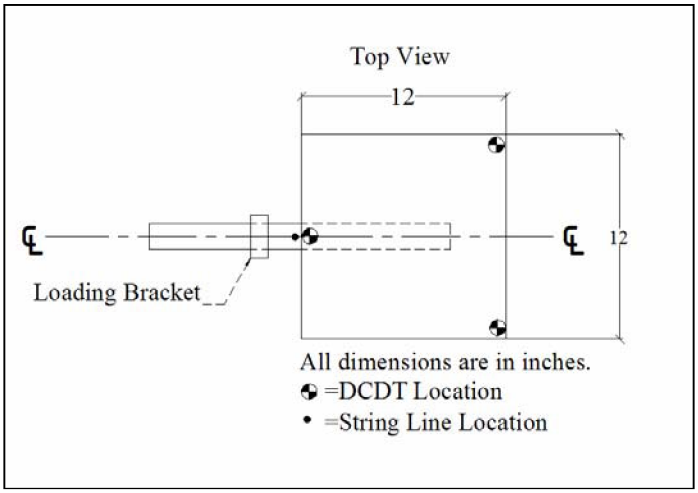

Figure 3.7. Instrumentation of cantilever specimen

Loads were applied using the same 50-kip capacity actuator used in the static modified AASHTO test. In order to apply a stable load directly to the center of each bar, a series of steel brackets were milled to fit the shape of each dowel bar. The series of steel brackets is shown below in Figure 3.8.

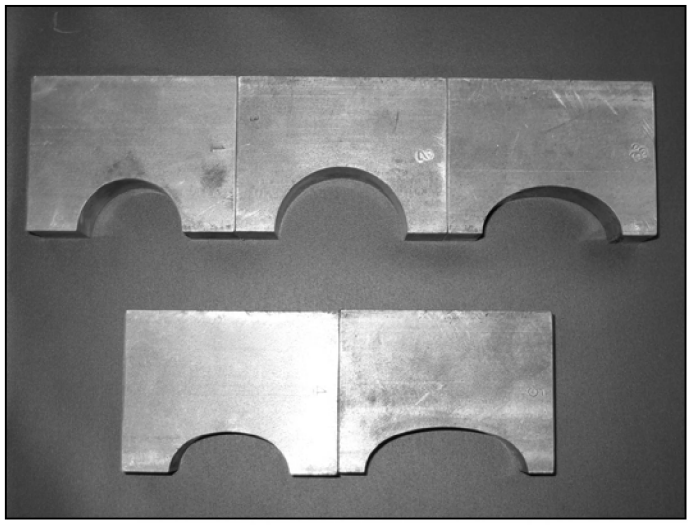

Figure 3.8. Cantilever test loading brackets

The brackets shown above in Figure 3.8 were placed on the top surface of the dowel bar. The brackets were centered at 2.5 in. from the face of the test block. The hydraulic actuator was positioned above the brackets and applied downward force to the top, flat surface.

3.2 Construction

3.2.1 AASHTO T-253

The three-block AASHTO specimen was constructed using prefabricated steel forms by EFCO Manufacturing. The steel forms were fabricated into 12-in. wide by 12-in. tall troughs. Each trough was 12-ft long and contained three specimens per trough. The specimens were formed using 1/8-in. polyvinyl chloride (PVC) sheets. The sheets were secured into place with ½-in. plywood strips and clear silicon adhesive. The dowels were placed across the PVC bulkheads and supported with steel chairs at each end. PVC bulkheads were also used to separate individual specimens. The steel trough forms are pictured below in Figure 3.9. The PVC bulkheads shown on the ends of the troughs were supported laterally with steel plates. The end bulkheads did not necessarily need to be flat. Lateral support was only required to keep the concrete from forcing the bulkhead out of the trough.

Figure 3.9. Modified AASHTO specimen forms

The concrete was a Class-C Portland Cement mix with a target compressive strength of 4000 psi. Concrete was delivered to the laboratory in mixer trucks from Ames Ready Mix and placed by hand using wheelbarrows, shovels, and hand scoops. Special care was taken to not disturb the alignment of the two dowels. A vibrator was used with care to properly consolidate the concrete.

3.2.2 Cantilever

The individual cantilevered dowels were built using the same steel troughs used in the construction of the AASHTO test specimens. Plywood bulkheads were used to separate the individual 12-in. blocks. The bulkheads were secured using clear silicon adhesive. The dowels were placed vertically with one end supported by a PVC chair at the center of the bottom surface. The dowels were secured with plywood strips cut to fit

the respective shape of each dowel bar. The plywood strips were secured to the formwork with wire ties after each bar was vertically plumbed by a hand level. The concrete was the same 4000 psi Class-C mix used in the AASHTO test specimens, and placed entirely by hand with scoops due to the small open spaces in the tops of the forms. An example of the formwork used to create the cantilever dowel specimens is shown below in Figure 3.10.

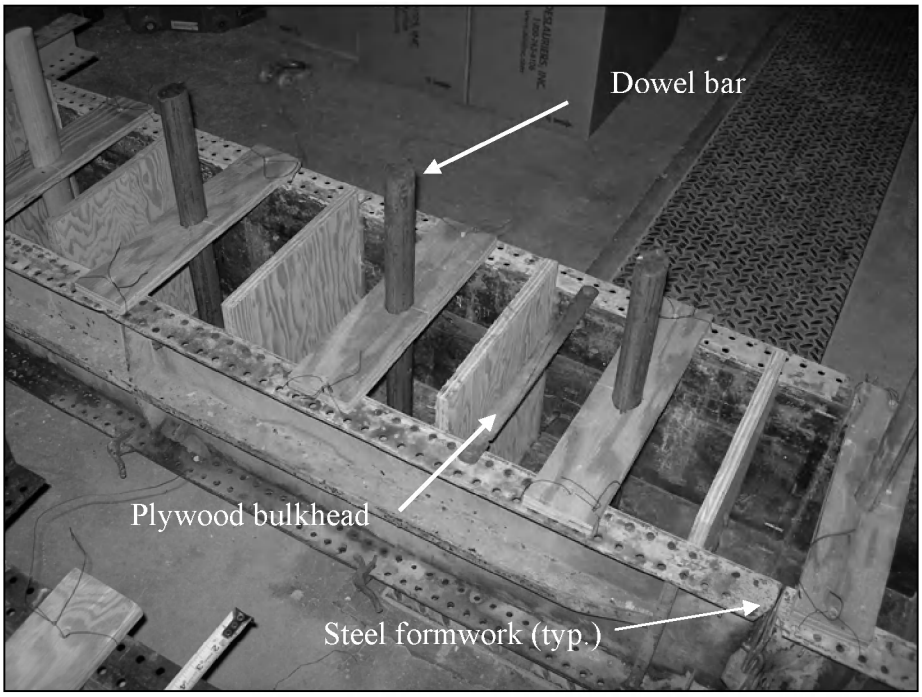

Figure 3.10. Cantilever dowel forms.

4. ANALYSIS AND RESULTS

4.1. Modified AASHTO test

4.1.1. Load vs. deflection

The data used in this experiment was collected from within the linear range of the load-deflection curve for each dowel bar. The load-deflection data was evaluated and the average load per in. of downward deflection was tabulated below in Table 4.1 through Table 4.3. Specimens with zero gap width were tabulated even though they contained misleading test results. The slope of the load-deflection curve of each specimen was tabulated along with the shear modulus, G and flexural rigidity, EI, of each specimen. The variable G is the ratio of shear stress to engineering shear strain in an isotropic material. The values of G were calculated by using the equation $G = \frac{E}{2(1+\upsilon)}$, where E is equal to the Modulus of Elasticity and υ is Poisson's Ratio [12].

The slopes are shown in descending order of shear modulus. The specimens with the same value of G were sorted in descending order of flexural rigidity, EI. The expected behavior of the bar with respect to the load per unit deflection slope is related to the shear modulus of dowel material, G. If values of G were very similar between two specimens, the bar with the larger value of EI was expected to undergo smaller deflections under the same loading. The "slope" term in the Tables 4.1-4.3 is a behavioral parameter indicating that a bar with a smaller "slope" demonstrated a higher defection than a bar of a higher "slope". The column entitled "Average Slope" is the calculated average of the three "slope" values per specimen.

Table 4.1. Load vs. deflection behavior of 0.125-in. gap AASHTO specimens.

Specimen	G lb/in.^{2} (10^6)	EI lb*in.^{2} (10^6)	Slope lb/in. (10^5)	Average Slope lb/in. (10^5)
Large Elliptical Steel 1	11.20	7.4	10.80	
Large Elliptical Steel 2	11.20	7.4	n/a	9.89
Large Elliptical Steel 3	11.20	7.4	8.98	
Epoxy Steel 1	11.20	7.21	9.30	
Epoxy Steel 2	11.20	7.21	1.82	6.10
Epoxy Steel 3	11.20	7.21	7.18	
Small Elliptical Steel 1	11.20	3.41	5.07	
Small Elliptical Steel 2	11.20	3.41	4.67	5.26
Small Elliptical Steel 3	11.20	3.41	6.05	
Stainless Steel 1	10.70	6.96	4.26	
Stainless Steel 2	10.70	6.96	9.19	6.72
Stainless Steel 3	10.70	6.96	n/a	
Elliptical GFRP 1	3.45	1.87	5.20	
Elliptical GFRP 2	3.45	1.87	6.21	5.36
Elliptical GFRP 3	3.45	1.87	4.68	
Round GFRP 1	2.60	3.95	4.25	
Round GFRP 2	2.60	3.95	4.37	3.51
Round GFRP 3	2.60	3.95	1.92	

Table 4.2. Load vs. deflection behavior of 0.5-in. gap AASHTO specimens

Specimen	G lb/in.^{2} (10^6)	EI lb*in.^{2} (10^6)	Slope lb/in. (10^5)	Average Slope lb/in. (10^5)
Large Elliptical Steel 1	11.20	7.4	8.14	
Large Elliptical Steel 2	11.20	7.4	8.55	8.34
Large Elliptical Steel 3	11.20	7.4	n/a	
Epoxy Steel 1	11.20	7.21	5.39	
Epoxy Steel 2	11.20	7.21	6.72	4.71
Epoxy Steel 3	11.20	7.21	2.03	
Small Elliptical Steel 1	11.20	3.41	4.78	
Small Elliptical Steel 2	11.20	3.41	3.93	3.56
Small Elliptical Steel 3	11.20	3.41	1.96	
Stainless Steel 1	10.70	6.96	6.65	
Stainless Steel 2	10.70	6.96	8.23	6.52
Stainless Steel 3	10.70	6.96	4.69	
Elliptical GFRP 1	3.45	1.87	3.67	
Elliptical GFRP 2	3.45	1.87	5.55	4.33
Elliptical GFRP 3	3.45	1.87	3.77	
Round GFRP 1	2.60	3.95	2.95	
Round GFRP 2	2.60	3.95	3.64	3.64
Round GFRP 3	2.60	3.95	4.31	

Table 4.3. Load vs. deflection behavior of no-gap AASHTO specimens

Specimen	G lb/in.^{2} (10^6)	EI lb*in.^{2} (10^6)	Slope lb/in. (10^5)	Average Slope lb/in. (10^5)
Large Elliptical Steel 1	11.20	7.4	276.60	
Large Elliptical Steel 2	11.20	7.4	n/a	146.20
Large Elliptical Steel 3	11.20	7.4	15.80	
Epoxy Steel 1	11.20	7.21	24.55	
Epoxy Steel 2	11.20	7.21	12.30	17.14
Epoxy Steel 3	11.20	7.21	14.58	
Small Elliptical Steel 1	11.20	3.41	16.54	
Small Elliptical Steel 2	11.20	3.41	17.78	17.16
Small Elliptical Steel 3	11.20	3.41	n/a	
Stainless Steel 1	10.70	6.96	21.02	
Stainless Steel 2	10.70	6.96	17.18	19.58
Stainless Steel 3	10.70	6.96	20.55	
Elliptical GFRP 1	3.45	1.87	8.45	
Elliptical GFRP 2	3.45	1.87	7.59	8.02
Elliptical GFRP 3	3.45	1.87	n/a	
Round GFRP 1	2.60	3.95	10.71	
Round GFRP 2	2.60	3.95	7.82	8.23
Round GFRP 3	2.60	3.95	6.17	

Overall, the bar shapes deflected in the fashion that was expected with respect to the shear modulus of each bar. The bars with the greater values of G underwent the least deformation with respect to shear load. The only exception to the load-deflection prediction with respect to G was the behavior of the stainless steel bar. The exception to the bar behavior with respect to G was as predicted: The difference between the deflection behavior of the round stainless steel bar and the small elliptical steel bar occurred because the cross section of the stainless steel bar was significantly larger with more than double the value of EI for the small elliptical steel bar. The difference in shear modulus values between the two materials was very small compared to the difference in rigidity properties. Although the epoxy-coated round steel bar had a higher flexural rigidity and shear modulus, the epoxy-coated bar tended to deflect more than the stainless steel bar. The confounding variable that could account for the difference in load-

deflection behavior is the thin layer of epoxy coating on the steel bar. Although the coating was very thin, the epoxy material could have had a slight effect on these results, given the fact that the deflections which were measured in this study were on the order of thousandths of an inch. Neglecting the epoxy coating on the epoxy-coated steel bar, both stainless and epoxy-coated bars had very similar physical characteristics.

The load-deflection slope for the no-gap specimens was significantly higher than those found in the 0.5 and 0.125-in. test specimens. Although the differential deflections on each end of the middle block were very small and did not have a significant effect on the calculation of k_0 when larger gaps were present, the absence of a joint width restricted free movement of the middle block. This restriction of rotation and translation produced high normal forces between the faces of the middle block and end blocks. These high normal forces created high frictional forces. The frictional forces between the joint faces dissipated force from the loading mechanism and did not allow full load transfer through the dowel bars. This "arching action" resulted in significantly smaller deflections at high loads. When downward deflection at a given load decreases, the value of k_0 increases. The significantly high values of k_0 shown in Table 4.4 are evidence of the arching action behavior.

4.1.2. Modulus of Dowel Support

The modified AASHTO test yielded the following average values of k_0 shown below in Table 4.4.

Table 4.4. Modified AASHTO k_0 values

Bar Type	*EI* lb*in^2(10^6)	0.5-in. Gap Average k_0 pci (10^5)	0.125-in. Gap Average k_0 pci (10^5)	No Gap Average k_0 pci (10^5)
Large Elliptical Steel	7.4	5.40	4.80	13.00
Epoxy Steel	7.21	6.10	9.40	28.00
Stainless Steel	6.96	7.90	7.00	36.00
Round GFRP	3.95	4.00	3.40	11.00
Small Elliptical Steel	3.41	5.80	5.20	38.00
Elliptical GFRP	1.87	4.90	5.90	12.00

Table 4.4 shows that the absence of gap widths in the test specimen joints yielded undesirable results in the determination of k_0. The poor results obtained from the specimens with no gap width stem from the fact that the middle block did not undergo a perfect downward translation.

The average values of k_0 calculated from the 0.5 and 0.125-in. gap specimens were very similar for each bar type. Both average k_0 values were within the standard deviations of each value. They did not appear to be different from one another. From this series of tests involving the modified AASHTO specimen with the exception of the 0.0-in. gap width, joint width did not appear to have a significant effect on the determination of k_0 in this study.

The distribution of k_0 results calculated from the modified AASHTO test was very scattered. Appendix C contains plots showing the wide spread of k_0 values obtained from the modified AASHTO procedure.

4.2. Cantilever test

4.2.1. Load vs. deflection

The load vs. deflection results of the cantilever test are shown below in Table 4.5. The bar types are sorted in descending order of flexural rigidity

Table 4.5. Load vs. deflection behavior of cantilever dowel specimens

Specimen	G lb/in.^{2}(10^6)	EI lb*in.^{2} (10^6)	Slope, lb/in. (10^5)	Average Slope, lb/in. (10^5)
Large Elliptical Steel 1	11.20	7.4	1.68	
Large Elliptical Steel 2	11.20	7.4	3.58	2.88
Large Elliptical Steel 3	11.20	7.4	3.38	
Epoxy Steel 1	11.20	7.21	n/a	
Epoxy Steel 2	11.20	7.21	n/a	3.28
Epoxy Steel 3	11.20	7.21	3.28	
Stainless Steel 1	11.20	3.41	2.31	
Stainless Steel 2	11.20	3.41	2.24	2.55
Stainless Steel 3	11.20	3.41	3.11	
Round GFRP 1	10.70	6.96	2.39	
Round GFRP 2	10.70	6.96	1.40	2.33
Round GFRP 3	10.70	6.96	3.21	
Small Elliptical Steel 1	3.45	1.87	26.60	
Small Elliptical Steel 2	3.45	1.87	4.15	11.37
Small Elliptical Steel 3	3.45	1.87	3.36	
Elliptical GFRP 1	2.60	3.95	3.11	
Elliptical GFRP 2	2.60	3.95	51.80	27.46
Elliptical GFRP 3	2.60	3.95		

The load vs. deflection behavior for the cantilever specimens was not as reliable as the results obtained through the modified AASHTO procedure. The blank entries seen in Table 4.5 correspond to load versus deflection plots that were not linear. All cantilever load vs. deflection plots are shown in Appendix B. By observation, these results were not considered due to their nonlinearity. The averages in Table 4.5 do not appear to follow the same load versus deflection behavior that was seen in the AASHTO

test results. A major cause of this discrepancy is the absence of load versus deflection slope values for the epoxy steel and elliptical GFRP specimens. The other main reason for the large difference in these averages from the modified AASHTO data is the abnormally large slopes seen in the small elliptical steel specimens.

4.2.2 Modulus of Dowel Support

The values of k_0 calculated from the cantilever test were significantly different from those obtained using the modified AASHTO test data. Half of the cantilever results were also much more scattered than those values found in from the modified AASHTO test. The calculated k_0 results are summarized below in Table 4.6.

Table 4.6. Cantilever k_0 values

Bar Type	*EI* lb*in.^{2}(10^6)	Average k_0 pci (10^5)
Large Elliptical Steel	7.4	1.59
Epoxy Steel	7.21	1.13
Stainless Steel	6.96	1.99
Round GFRP	3.95	0.89
Small Elliptical Steel	3.41	1.29
Elliptical GFRP	1.87	5.14

With the exception of outliers, the general trend of the k_0 calculations gathered from the cantilever test was much lower than the values calculated from the modified AASHTO test data. The plots in Appendix C show the trend in the lower k_0 values resulting from the cantilever test, as opposed to the modified AASHTO test.

5. CONCLUSIONS

5.1 Modified AASHTO T253

The modified AASHTO test specimens yielded scattered results but overall were more consistent than those numbers obtained during the cantilever test. The results calculated from the modified AASHTO test data were also more accurate with respect to previous studies at ISU. The modified version also yielded more consistent values of k_0 with less scatter than in previous studies. [3,4]

Gap width in the modified AASHTO series of tests for this particular study was shown to be insignificant in the specimens containing a gap width not equal to zero. Both the 0.5-and 0.125-in. gap widths yielded k_0 results that were not significantly different from one another. Although this study did not display differences in k_0 values between the two small gap widths, it is very likely that larger widths would yield significantly different values of k_0.

5.2 Cantilever test

The cantilever test was less reliable than the modified AASHTO test and less reliable than predicted. Although y_0 was measured directly, other factors, as will be described below, had an effect on the test results. The base support beam experienced small, erratic deflections. The end block rotation was another concern. For the cantilever test, the load was moved from a maximum of 0.5 in. to a distance of 2.5 in.

The increase in distance of the load placement created significantly larger moments in the dowel bar than seen in the modified AASHTO series of tests. The large moments produced by the greater loading distance increased the demand for a more sophisticated clamping mechanism to resist block rotation. The clamping method applied to this test allowed undesirable effects such as large normal forces on the dowel and small, unpredictable rotations.

5.3 Conclusion summary

Although the cantilever test is a more accurate simulation of theory derived by Timoshenko and Friberg, the modified AASHTO test yielded more desirable results. The results obtained in this study show that the modified AASHTO test is the recommended dowel shear procedure for future study. The procedure illustrated in Appendix D displays the recommended changes to the current AASHTO standard. Although the modified AASHTO procedure is an improvement over the standard procedure, future investigation recommendations are displayed in Chapter 6.

Although the cantilever test did not yield desirable k_0 values, the tight data spreads observed for the stainless steel, round GFRP, and small elliptical steel specimens indicate that future analysis of an improved cantilever test may increase its viability as an alternative method for the determination of k_0. A recommended change to the cantilever test procedure is outlined in Chapter 6 in addition to the future AASHTO procedure recommendations.

6. FUTURE NEEDS AND RECOMMENDATIONS

Whereas tests conducted during this experiment provided good information resulting from the modified AASHTO test, improvements are still desired in order to obtain more precise results for calculation of k_0. After performing the modified AASHTO and cantilever tests, certain observations were made in order to improve future dowel test procedures.

6.1 Modified AASHTO T253

A revised version of the modified AASHTO T253 procedure and specimen is recommended for future testing of dowel bar bearing stresses. The proposed modified specimen is shown below in Figure 6.1.

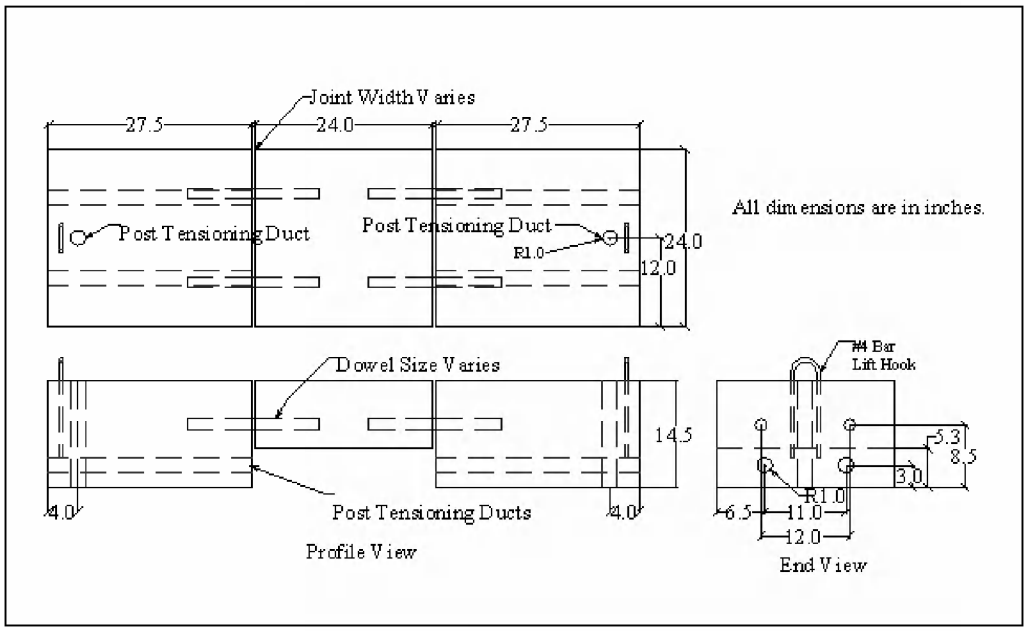

Figure 6.1. Proposed revised modified AASHTO specimen

The possibility of block rotation would be reduced with the addition of at least one more pair of dowels. For greater ease of load calculation per dowel, a four-bar specimen is recommended for future tests, but requires further experimental investigation. This configuration would be much more economical and simple than a full-scale slab test. Although the three-block model still poses the possibility of uneven deflections at each joint, the researchers found that simply dividing the load in half did not significantly affect k_0 results, provided that the possibility of uneven deflection was controlled.

The joint width should be kept at 1/8-in. for a modified test. The 1/2-in. joint yielded the most consistent results, but as Table 4.1 and Appendix A show, they were not significantly different than the 1/8-in. gap. The 1/8-in. gap specimen provides for a closer proximity to actual pavement joint widths. The zero-gap joint did not allow the dowels to carry the entire applied load in shear. As mentioned earlier, the zero-gap joints experienced significant "arching action" and carried high compressive stresses while the center block was loaded. The zero-gap joint specimen is not recommended for future study. In addition to the 1/8-in. gap, a wider gap of 1 in. or greater should be investigated to observe dowel behavior within a control or contraction joint. The conclusions found in this study for small gaps could have different results for large gaps, and therefore, large gaps require further research.

The load shall continue to be applied as two linear loads spanning perpendicular to the dowel bars at the joint locations. This application method produced limited rotation effects and allowed for adequate load distribution estimation.

A staggered block design (Figure 6.1) would eliminate the need for steel

baseplates to be used on the testing surface. The larger, staggered block configuration would allow direct placement and post-tensioning of the end blocks on the reaction floor or test frame. The new proposed block design will be larger than the current blocks used in this study. The bars will be placed 12 in. on center from each other. The bars will have an additional 6 in. of concrete on their outside edges in order to simulate an incremental piece of a full highway slab.

The new test will also need to include tension ties between the two end blocks. The tension ties will serve two purposes. The first use is to protect the specimen from damage while being moved with an overhead crane. The second purpose of the tension ties is to resist end block rotation during the load test. The block shown previously in Figure 6.1 is designed to be post-tensioned to a floor with 3-ft spaces between tie-down holes.

The horizontal tension tie must only be hand-tightened to a nominal force of roughly 200 pounds. The bars need only act as regular reinforcement and not as a prestressed tendon. Any reverse moment effect of the tension ties due to excessive tensioning will distort results. The end blocks shall be post-tensioned to the load floor or test frame with a force of 4000 pounds in each end block. A rough analysis was performed on the proposed block found that the force of 4000 pounds per side would be more than adequate to support the middle block loading.

6.2 Cantilever test

The cantilever test was much more vulnerable to block rotation due to the large couple produced when the dowel bar was loaded directly. Verification of this test is required before it can be accepted as an adequate tool to test for k_0.

A possible solution to this verification is to cast a longer cantilever specimen with a hole at the end of the block in order to allow the block to be post-tensioned down to the loading floor. Post tensioning would greatly reduce the chances of block rotation during the test. The location of the tie-down hole allows the post tensioning without adding excess compressive stresses on the embedded dowel. An example of this proposed test specimen is shown below in Figure 6.2.

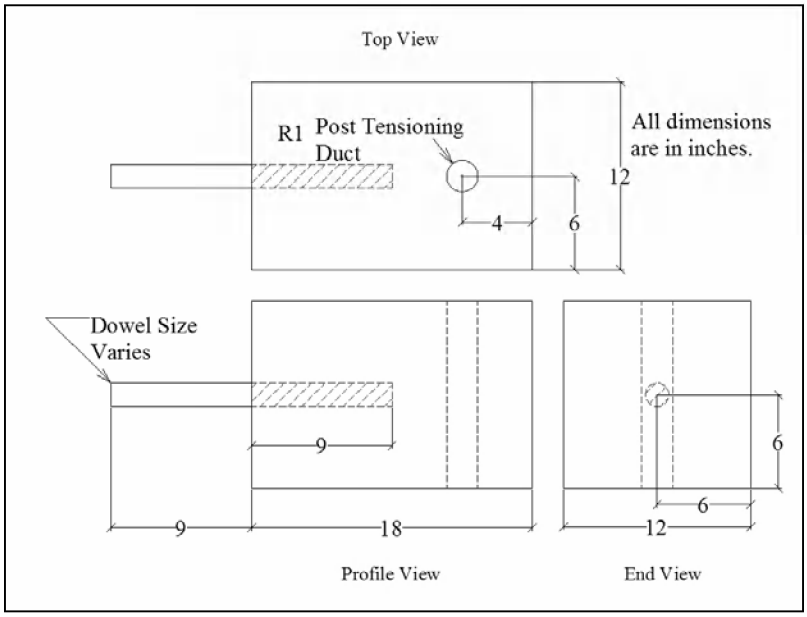

Figure 6.2. Proposed cantilever dowel specimen

The specimens would be better suited to be cast horizontally instead of vertically because of the addition of the tie-down hole. The vertical casting ensured more optimal concrete consolidation, but consolidation is not a concern with the round and elliptical dowel shapes used in the modified AASHTO specimens.

Although the cantilever results in this particular study were undesirable, future research is recommended to improve its viability as a cost-effective and precise dowel bar test procedure.

REFERENCES

1. Boris, T.A. *Performance of glass fiber reinforced polymer reinforcements in simulated concrete environments*. Masters Thesis. Iowa State University. Ames, Iowa. 1999.

2. American Association of State, Highway, and Transportation Officials (AASHTO). *AASHTO Guide for Design of Pavement Structures*. AASHTO. Washington D.C. 1993.

3. Lundy, A.L. *The effects of slope and flexural deflection on the concrete dowel-bar system*. Masters Thesis. Iowa State University. Ames, Iowa. 2003

4. Porter, M.L., R.J. Guinn, Jr., A.L. Lundy, D.D. Davis, and J.G. Rohner. *Investigation of Glass Fiber Composite Dowel Bars for Highway Pavement Slabs: Final Report*. Iowa Highway Research Board Project TR-408. Engineering Research Institute. Iowa State University. Ames, Iowa. 1993.

5. Cable, J.K., M.L. Porter, J. Hoffman, L.L. Rold, L.E. Edgar. *Demonstration and Field Evaluation of Alternative Portland Cement Concrete Pavement Reinforcement Material, HR-1069*. The Highway Division of the Iowa Department of Transportation, the Iowa Highway Research Board, and the Federal Highway Administration Demonstration Projects Program. Iowa State University. Ames, Iowa. 2003.

6. Porter, M.L., J.F. Harrington, N.J. Pierson, and A.W. Post. *Field Evaluation of Elliptical Fiber Reinforced Polymer Dowel Performance*. Center for Transportation Research and Education, Center for Portland Cement Concrete Pavement Technology, Federal Highway Administration, and Iowa Department of Transportation. Iowa State University. Ames, Iowa. 2005.

7. Timoshenko, S. and J.M. Lessels. *Applied Elasticity*. Westinghouse Technical Night School Press. Pennsylvania. 1925.

8. Friberg, B.F. Design of Dowels in Transverse Joints of Concrete Pavements. *Transactions, American Society of Civil Engineers*, Vol. 105, No. 2081. 1940.

9. Albertson, M.D. *Fibercomposite and steel pavement dowels*. Masters Thesis. Iowa State University. Ames, Iowa. 1992.

10. Porter, M.L., B.A. Barnes, B. Hughes, and K. Viswanath. *Non-Corrosive Tie Reinforcing and Dowel Bars for Highway Pavement Slabs, Final Report HR-343. Submitted to Highway Division of the Iowa Department of Transportation and Iowa Highway Research Board*. Iowa State University. Ames, Iowa. 1993.

11. Young, W.C. and R.G. Budynas. *Roark's Formulas for Stress and Strain, 7th Edition*. McGraw-Hill, Inc. New York, New York. 2002.

12. *Finding the Elastic Constants G and K*.

http://www.efunda.com/formulae/solid_mechanics/mat_mechanics/elastic_constants_G_K.cfm. Accessed June 17, 2006.

ACKNOWLEDGEMENTS

I would like to thank my family for all of their support during my entire educational career. I could not have done this without their help.

I would also like to acknowledge Iowa State University Structures Laboratory Manager Douglas Wood. His assistance and expertise during the construction and testing phases of this project were essential to the completion of this study.

I would like to express my gratitude to Dr. Fouad Fanous and Dr. Lester Schmerr for serving on my graduate committee.

Finally, I would like to thank my major professor, Dr. Max Porter for all of his assistance towards the completion of this study. His technical knowledge, patience, and persistence proved to be invaluable throughout this research process.

APPENDIX A. MODIFIED AASHTO LOAD VS. DEFLECTION PLOTS.

This section displays all deflections recorded by the center block DCDTs with respect to the adjusted load corresponding to each deflection. Each series of plots is plotted on the same *x*-and *y*-axis scales to display the differences in load vs. deflection slopes among each specimen type.

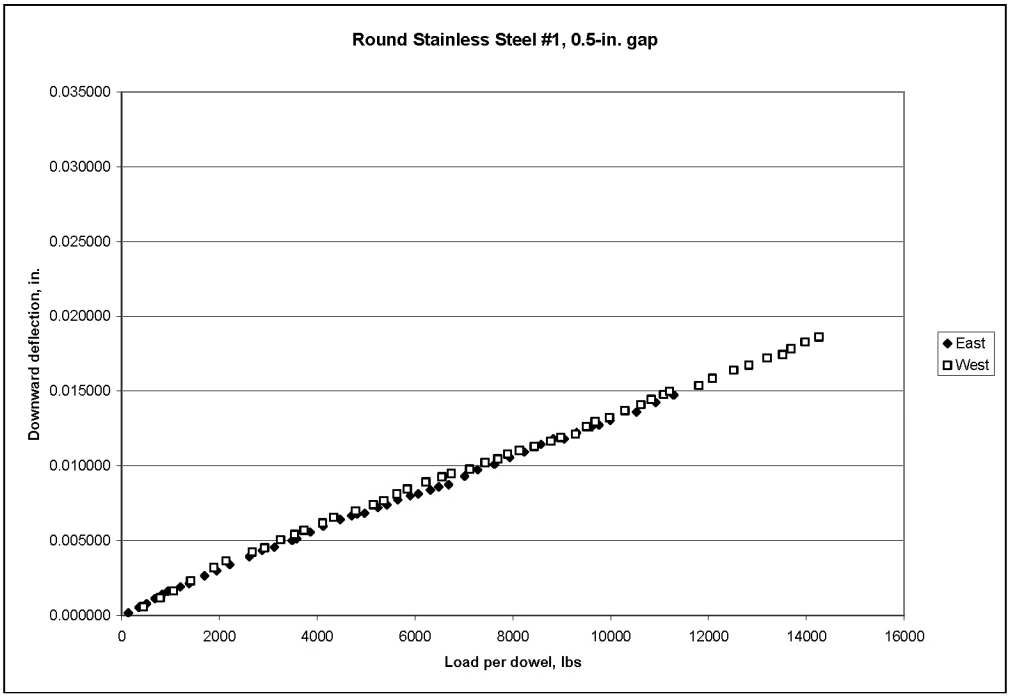

Figure A.1. Round stainless steel #1, 0.5-in. gap load vs. deflection

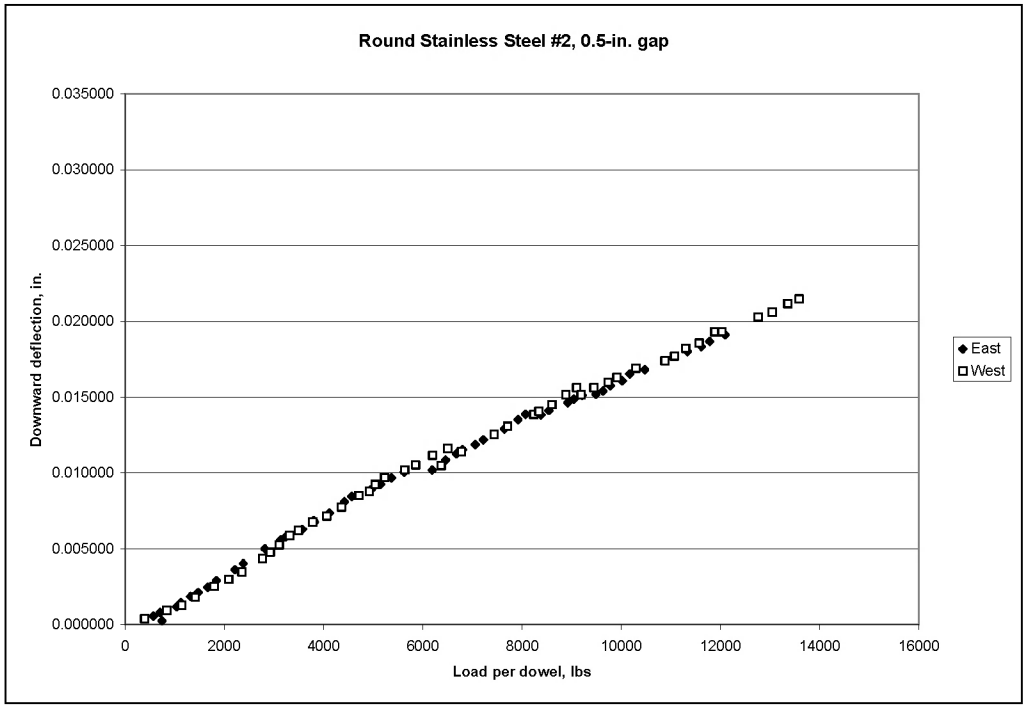

Figure A.2. Round stainless steel #2, 0.5-in. gap load vs. deflection

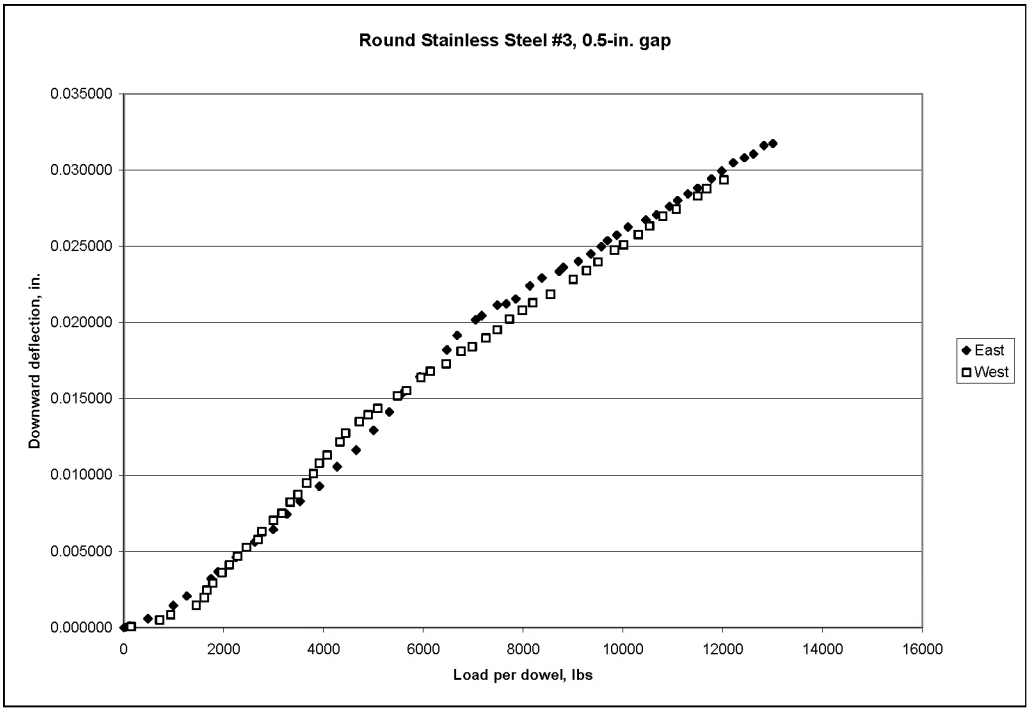

Figure A.3. Round stainless steel #3, 0.5-in. gap load vs. deflection

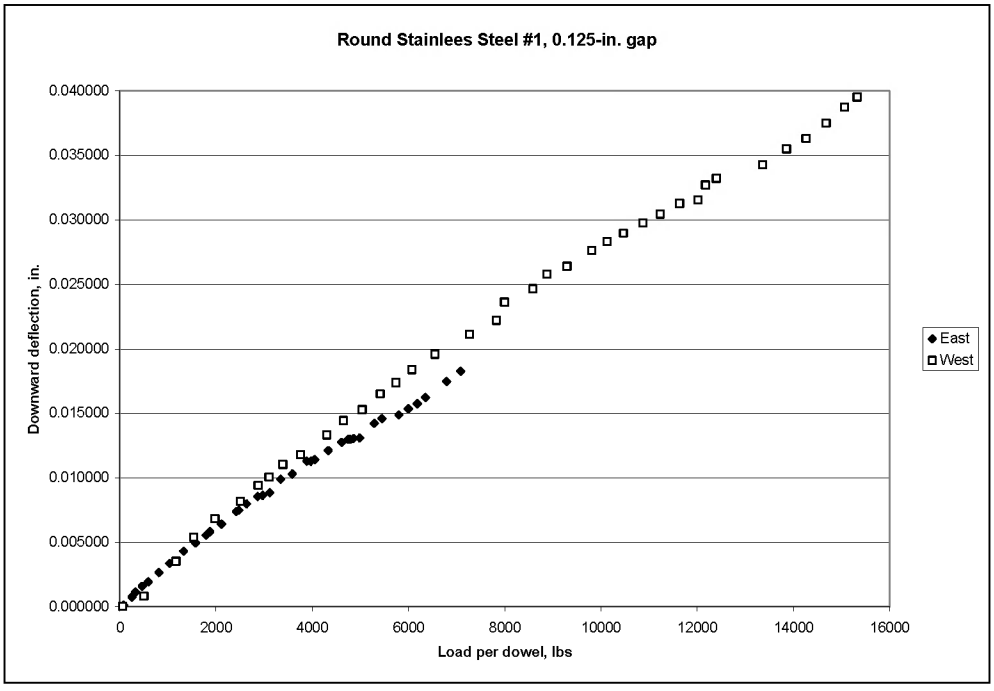

Figure A.4. Round stainless steel #1, 0.125-in. gap load vs. deflection

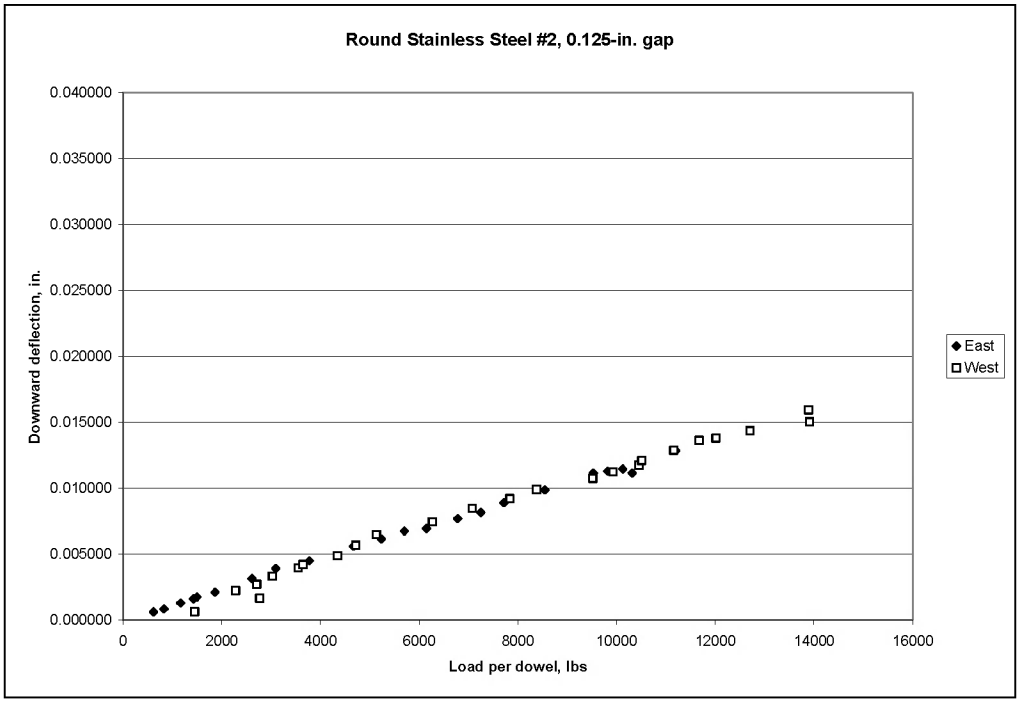

Figure A.5. Round stainless steel #2, 0.125-in. gap load vs. deflection

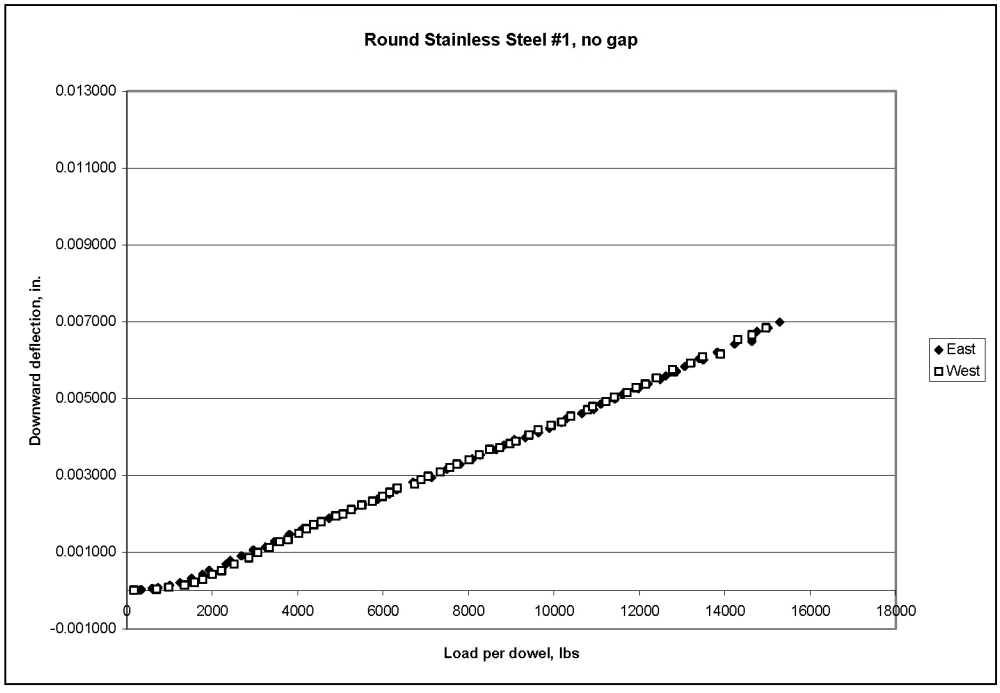

Figure A.6. Round stainless steel #1, no gap load vs. deflection

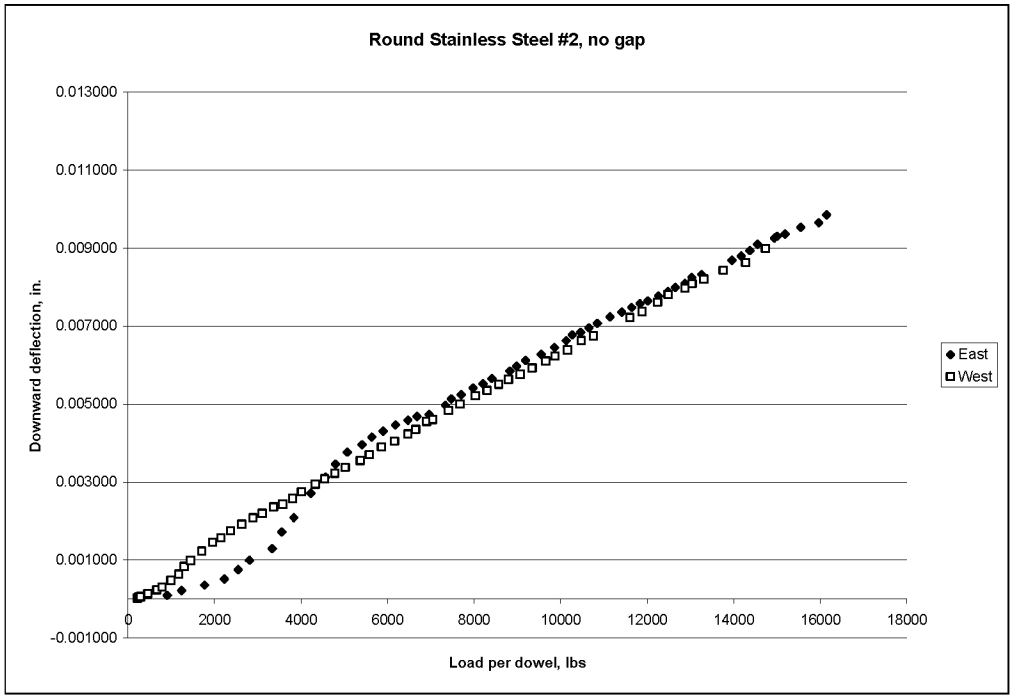

Figure A.7. Round stainless steel #2, no gap load vs. deflection

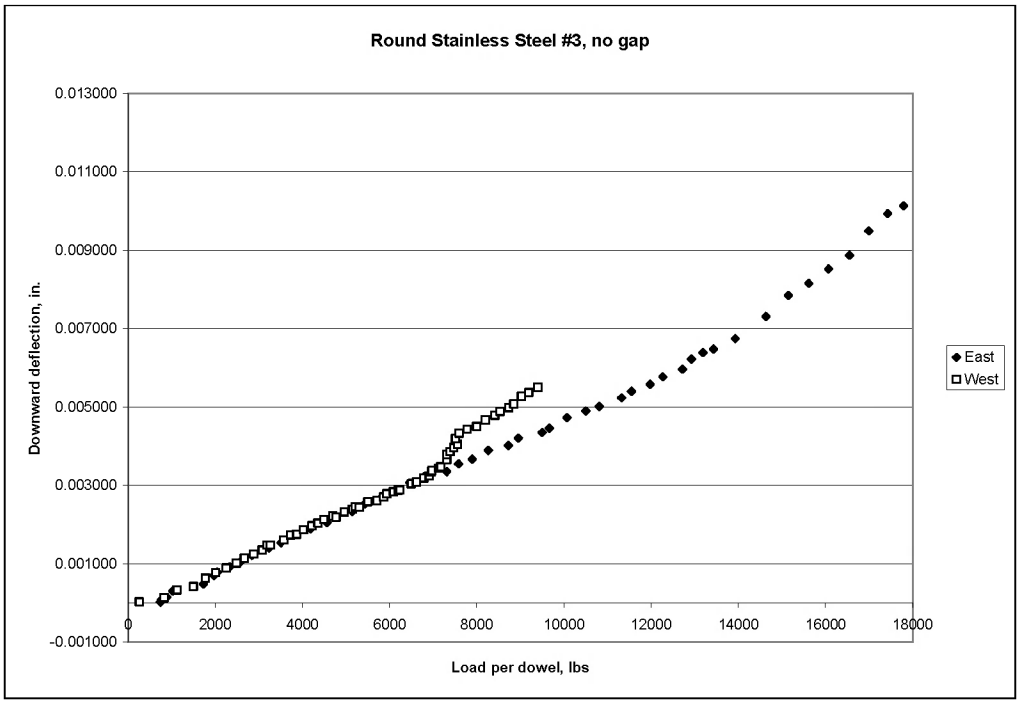

Figure A.8. Round stainless steel #3, no gap load vs. deflection

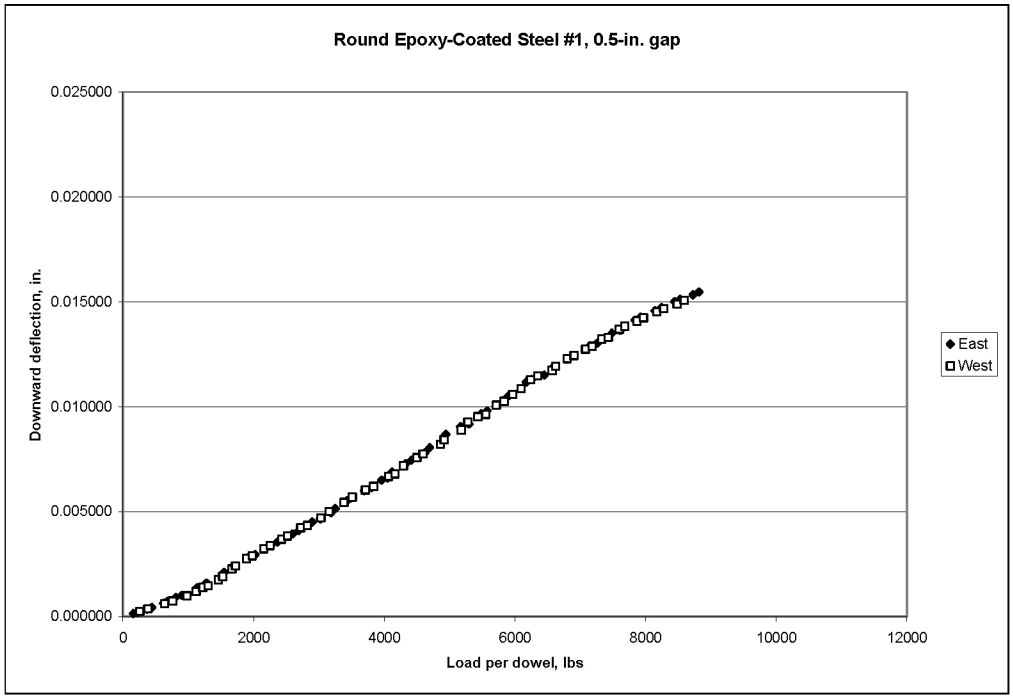

Figure A.9. Round epoxy-coated steel #1, 0.5-in. gap load vs. deflection

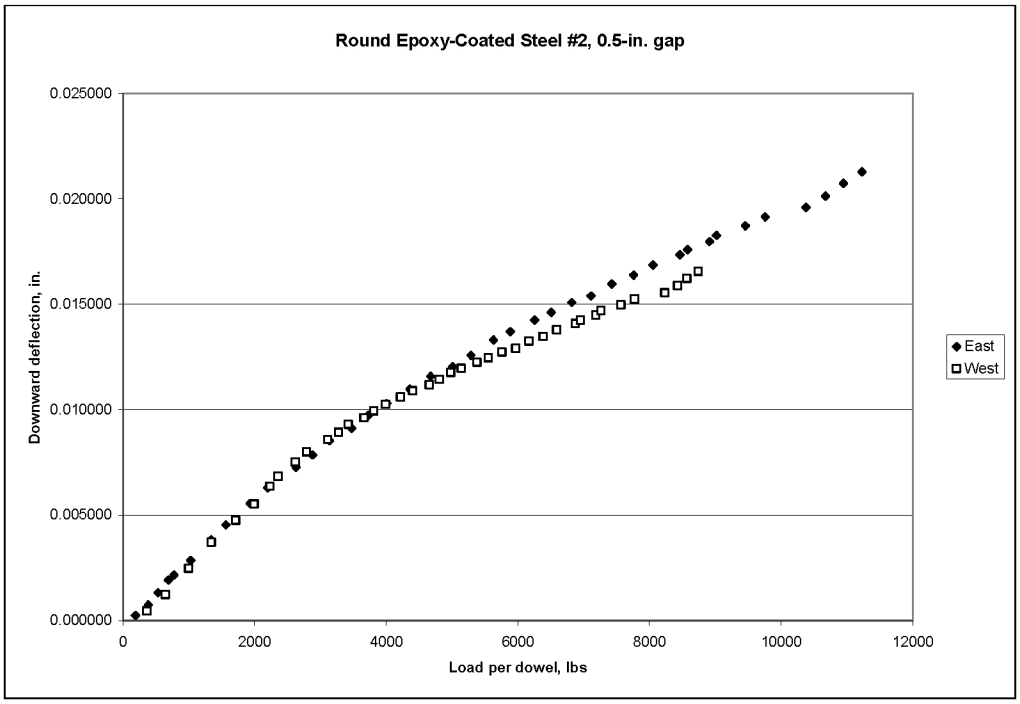

Figure A.10. Round epoxy-coated steel #2, 0.5-in. gap load vs. deflection

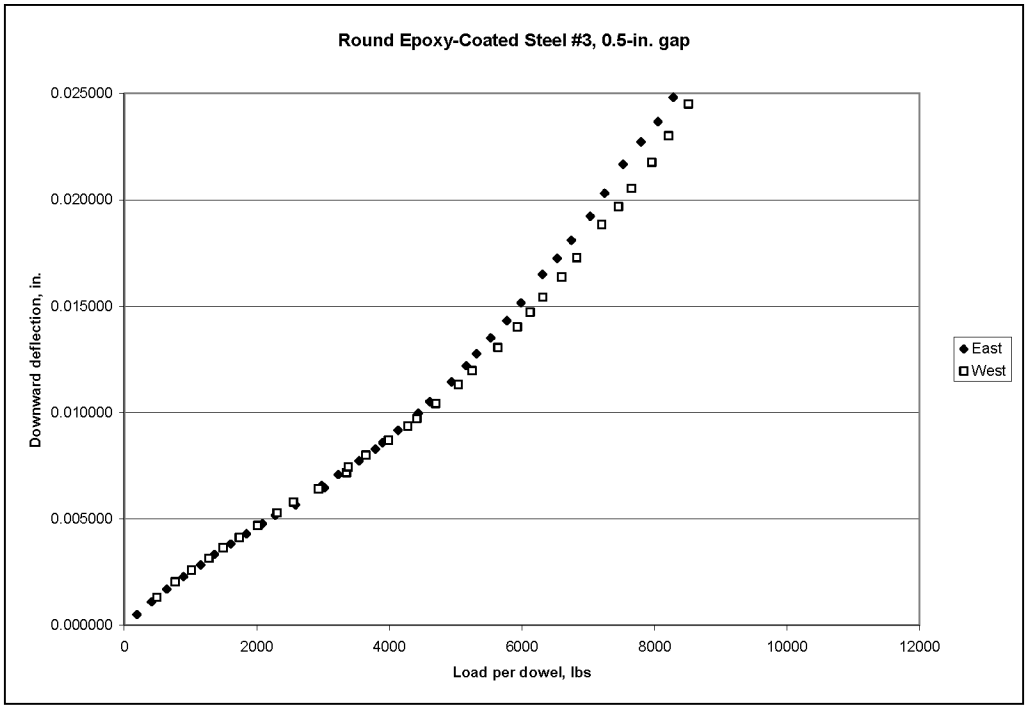

Figure A.11. Round epoxy-coated steel #3, 0.5-in. gap load vs. deflection

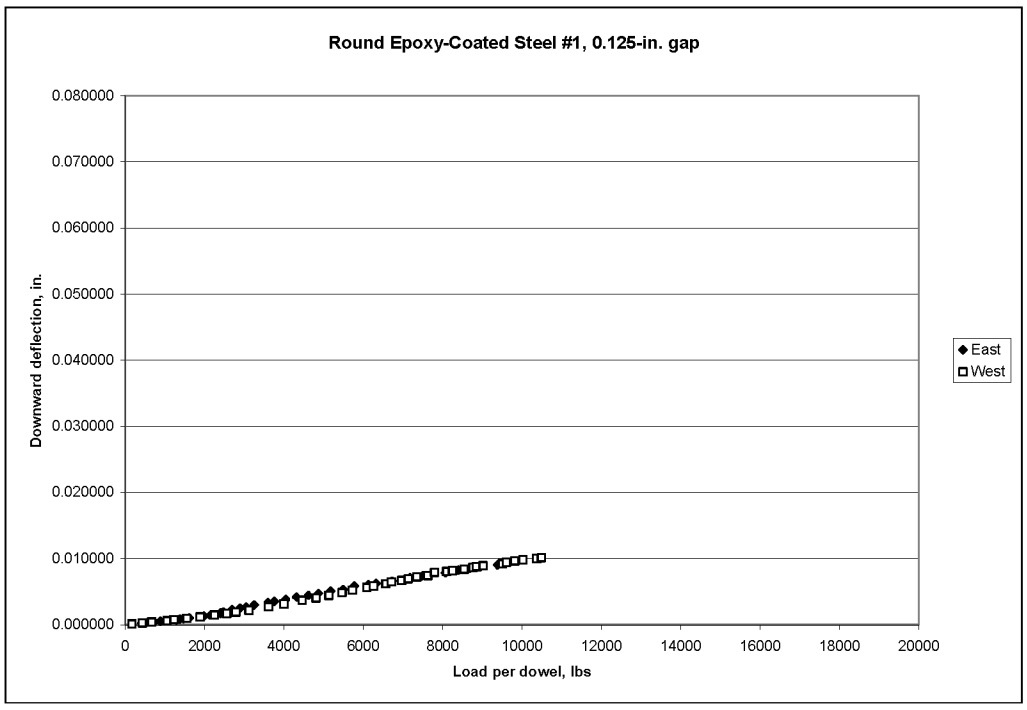

Figure A.12. Round epoxy-coated steel #1, 0.125-in. gap load vs. deflection

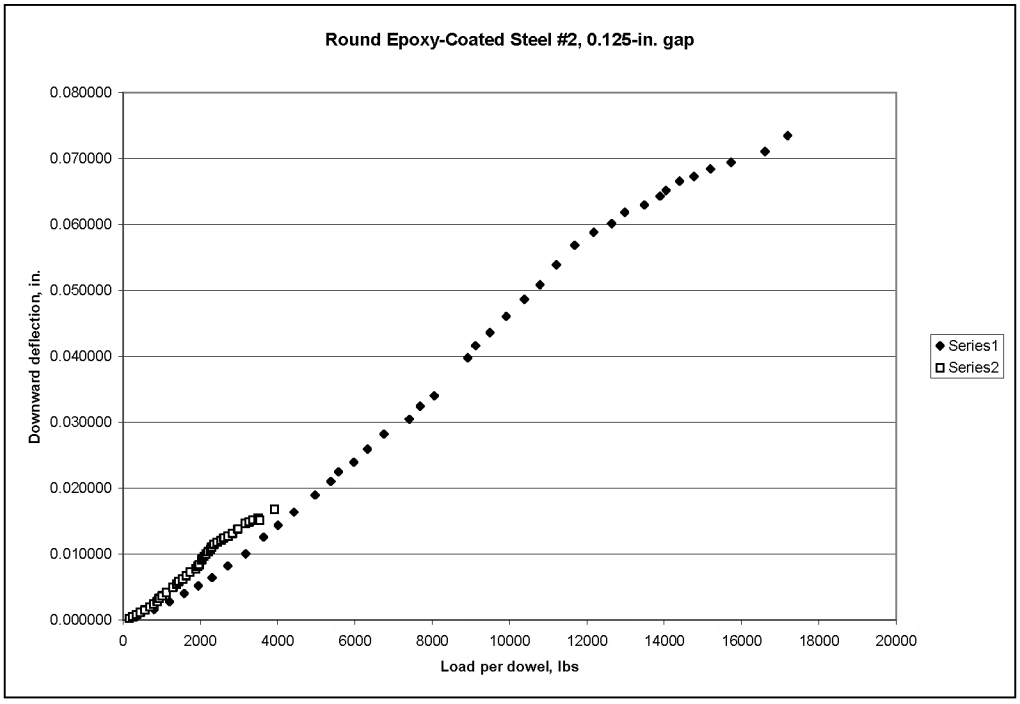

Figure A.13. Round epoxy-coated steel #2, 0.125-in. gap load vs. deflection

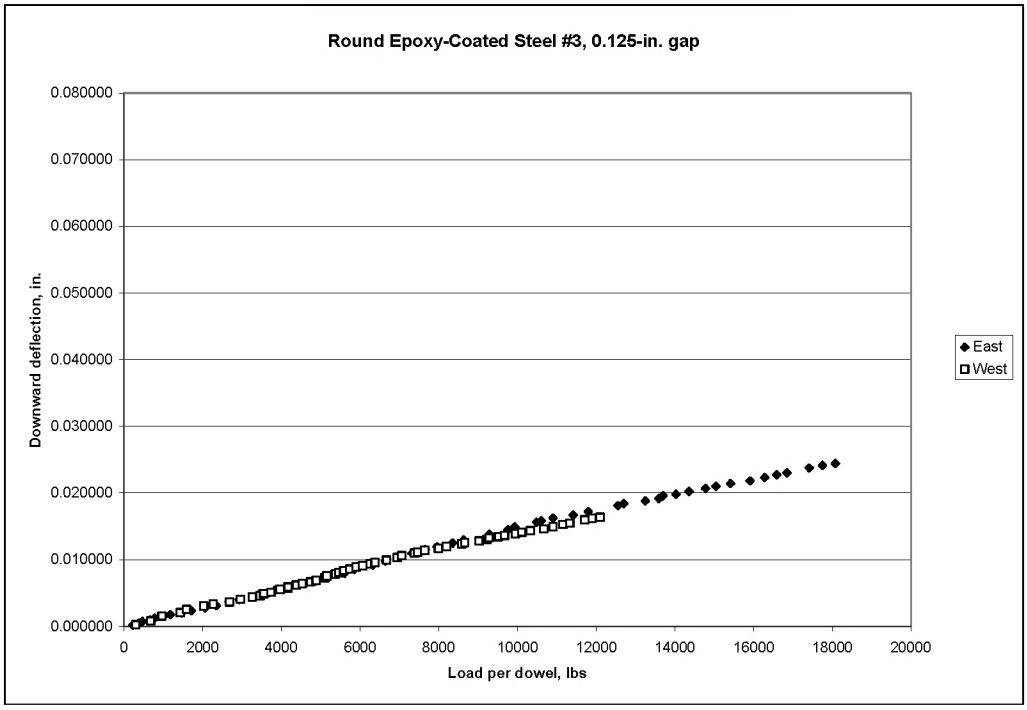

Figure A.14. Round epoxy-coated steel #3, 0.125-in. gap load vs. deflection

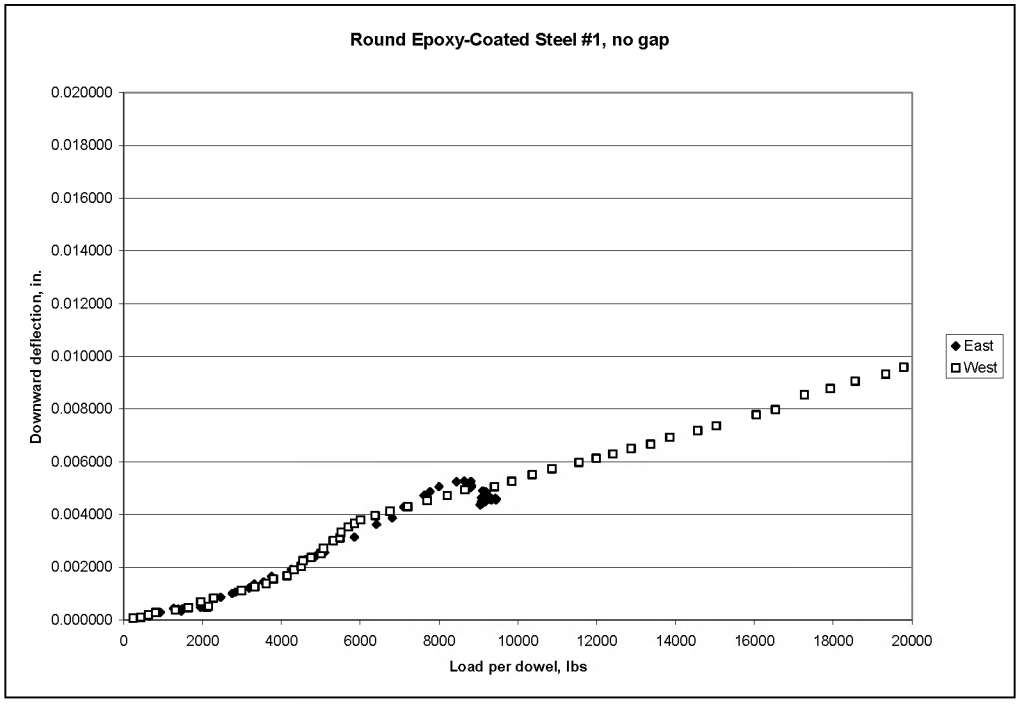

Figure A.15. Round epoxy-coated steel #1, no gap load vs. deflection

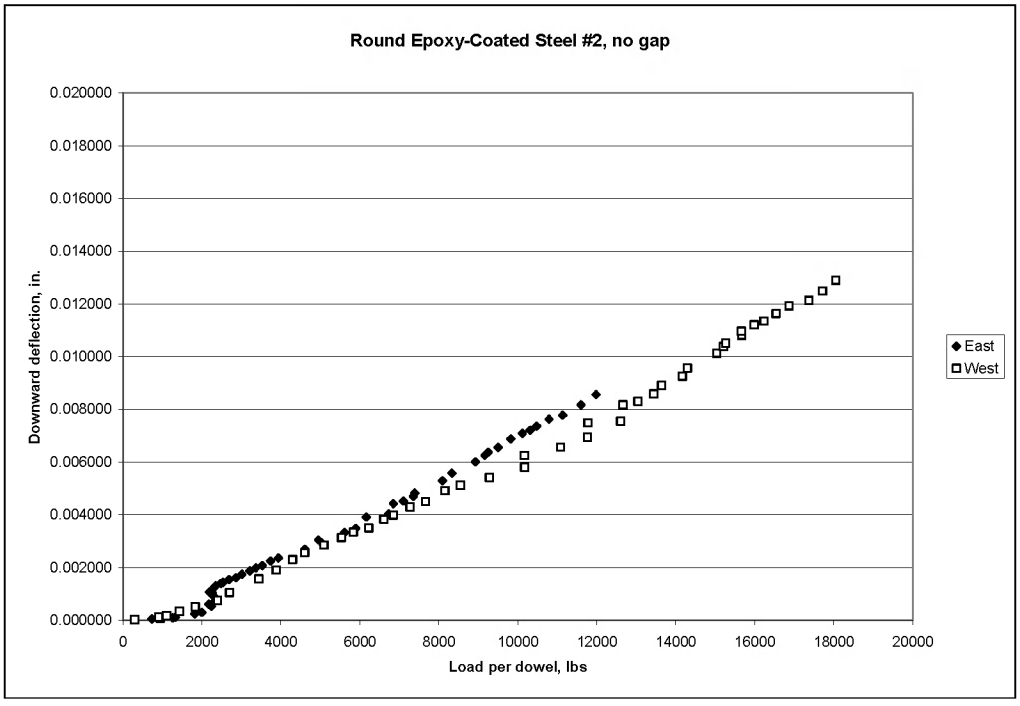

Figure A.16. Round epoxy-coated steel #2, no gap load vs. deflection

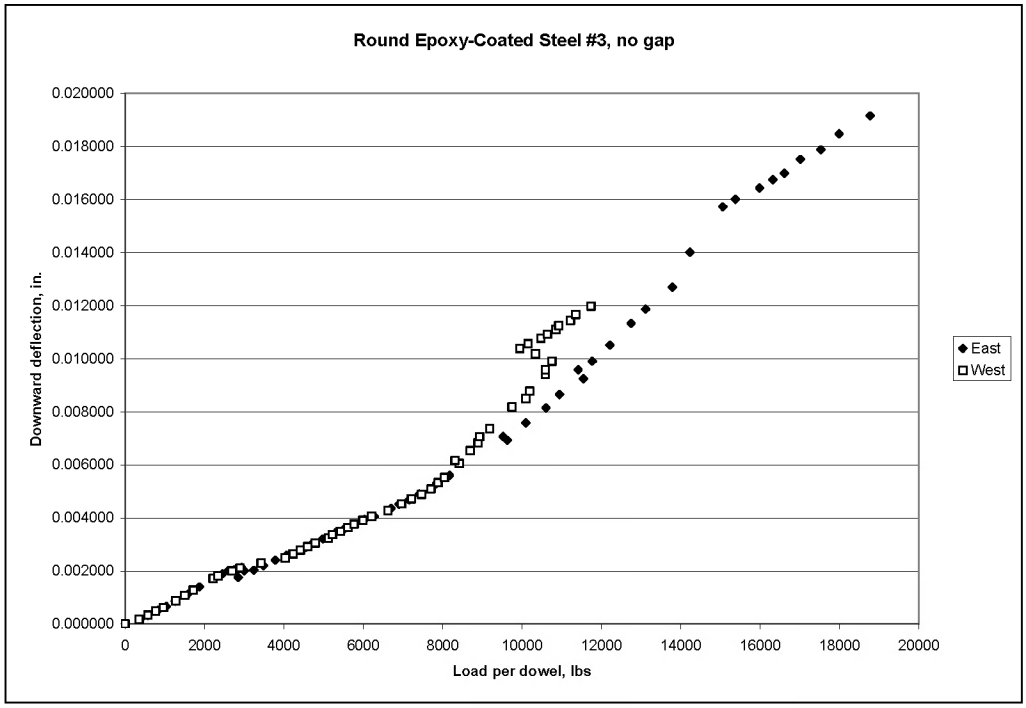

Figure A.17. Round epoxy-coated steel #3, no gap load vs. deflection

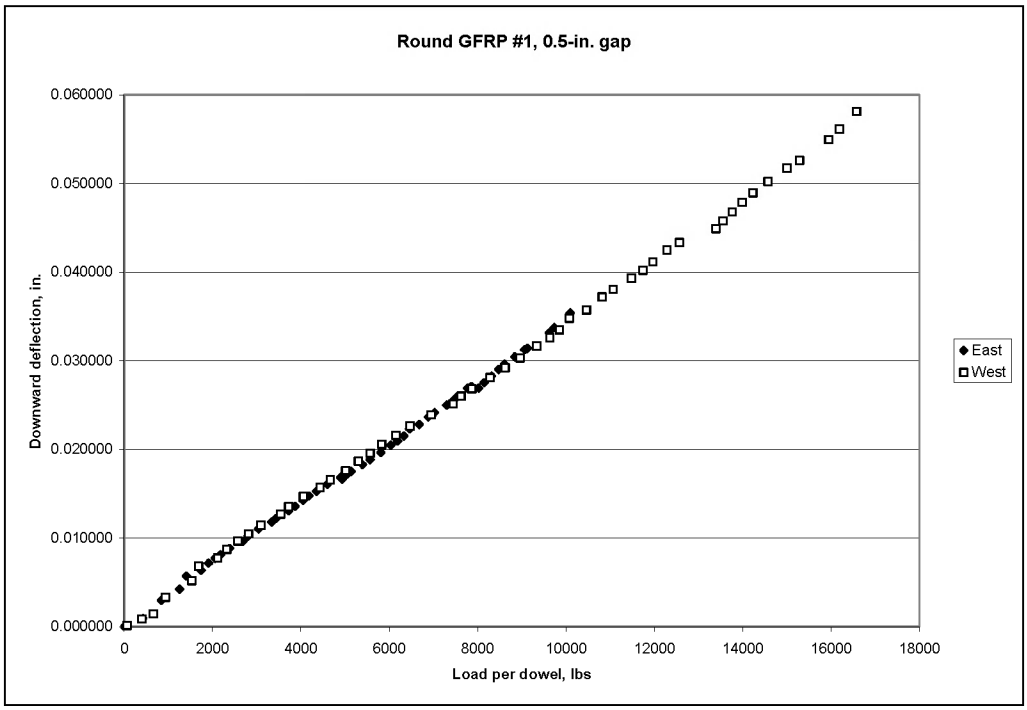

Figure A.18. Round GFRP #1, 0.5-in. gap load vs. deflection

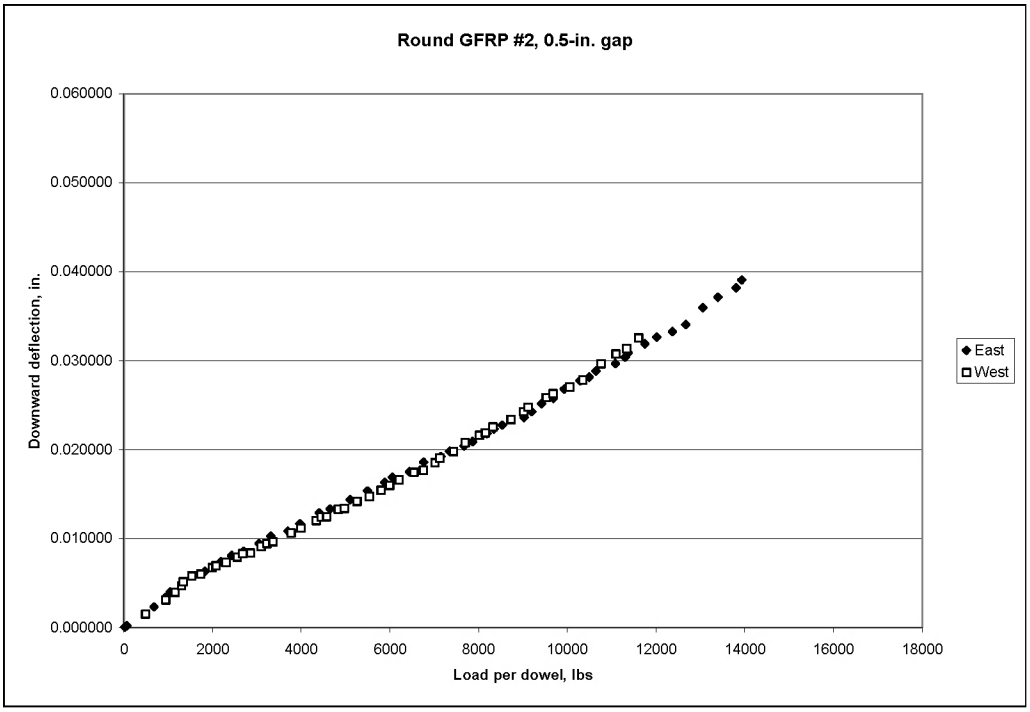

Figure A.19. Round GFRP #2, 0.5-in. gap load vs. deflection

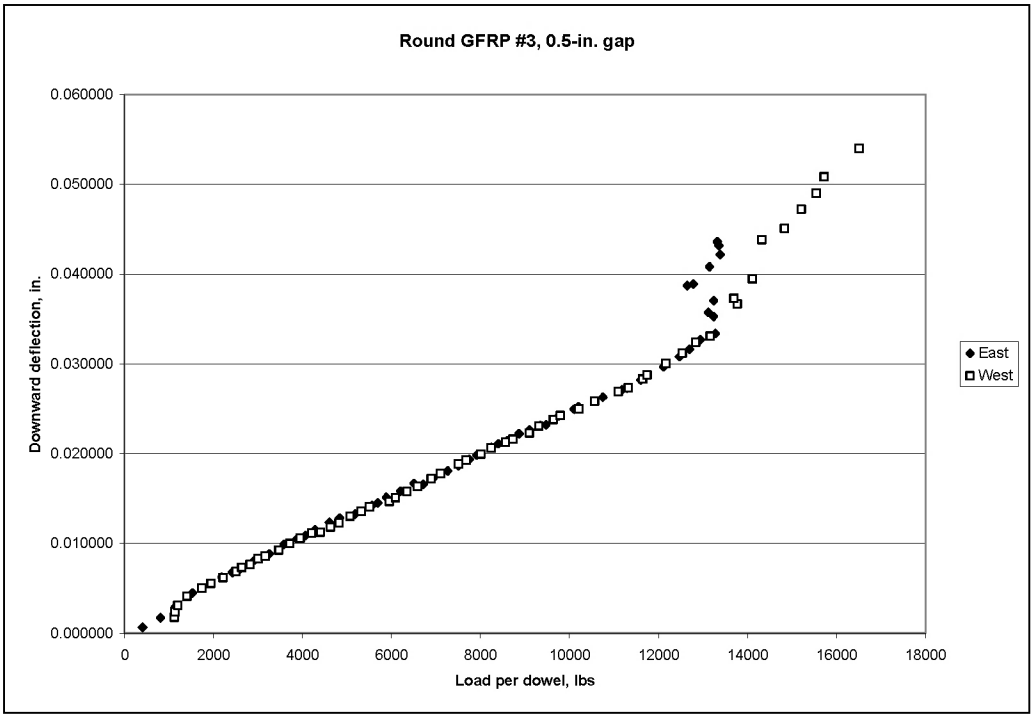

Figure A.20. Round GFRP #3, 0.5-in. gap load vs. deflection

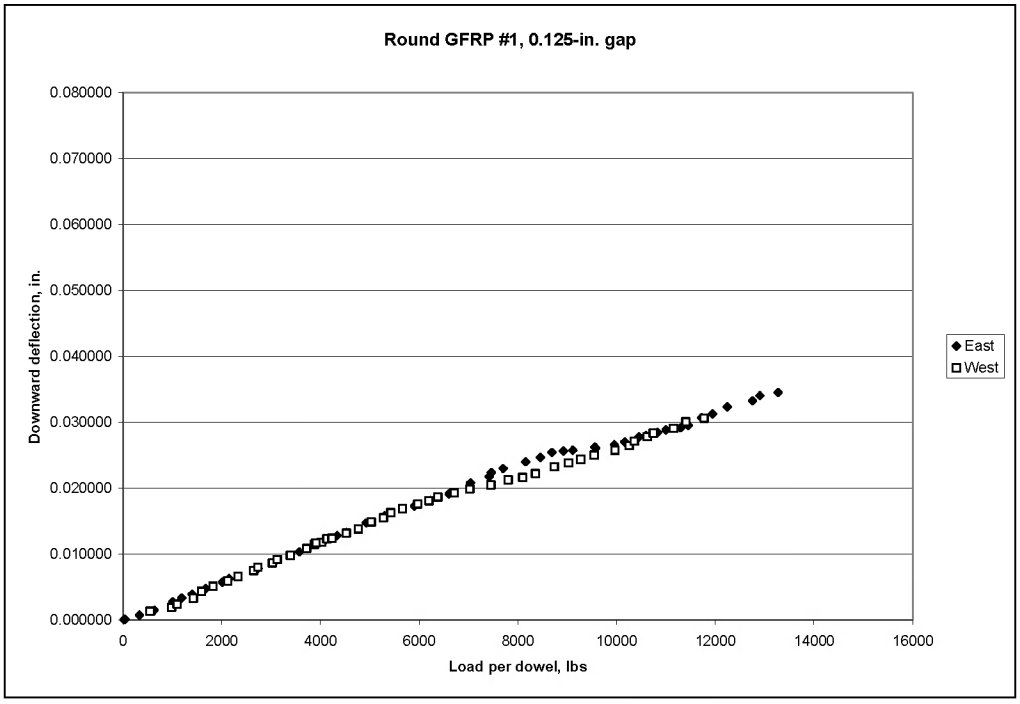

Figure A.21. Round GFRP #1, 0.125-in. gap load vs. deflection

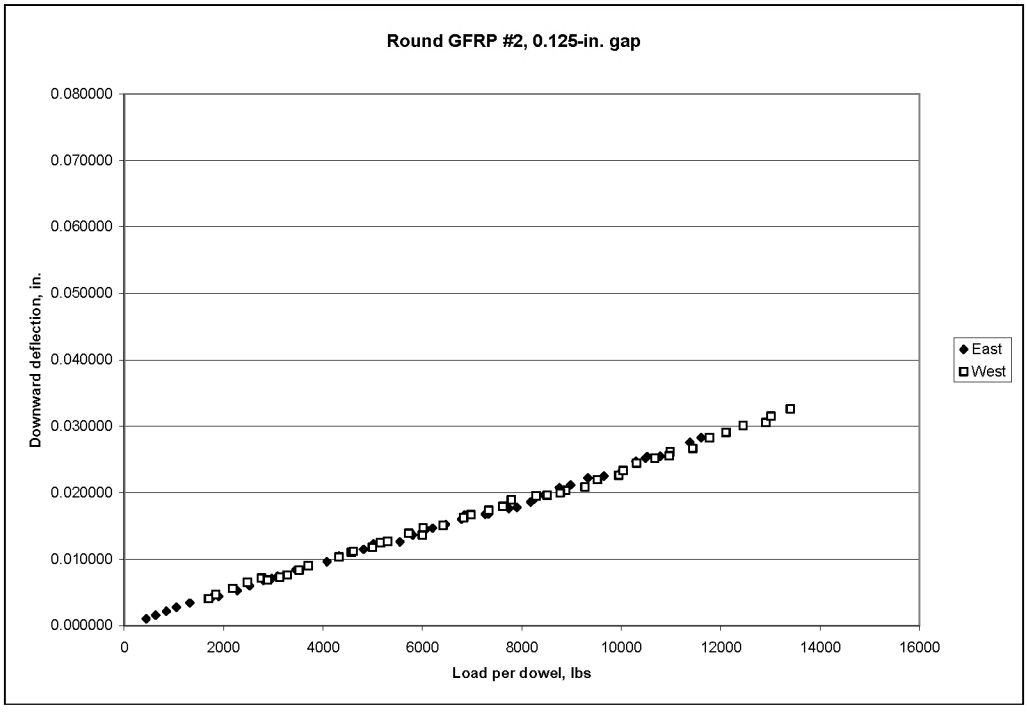

Figure A.22. Round GFRP #2, 0.125-in. gap load vs. deflection

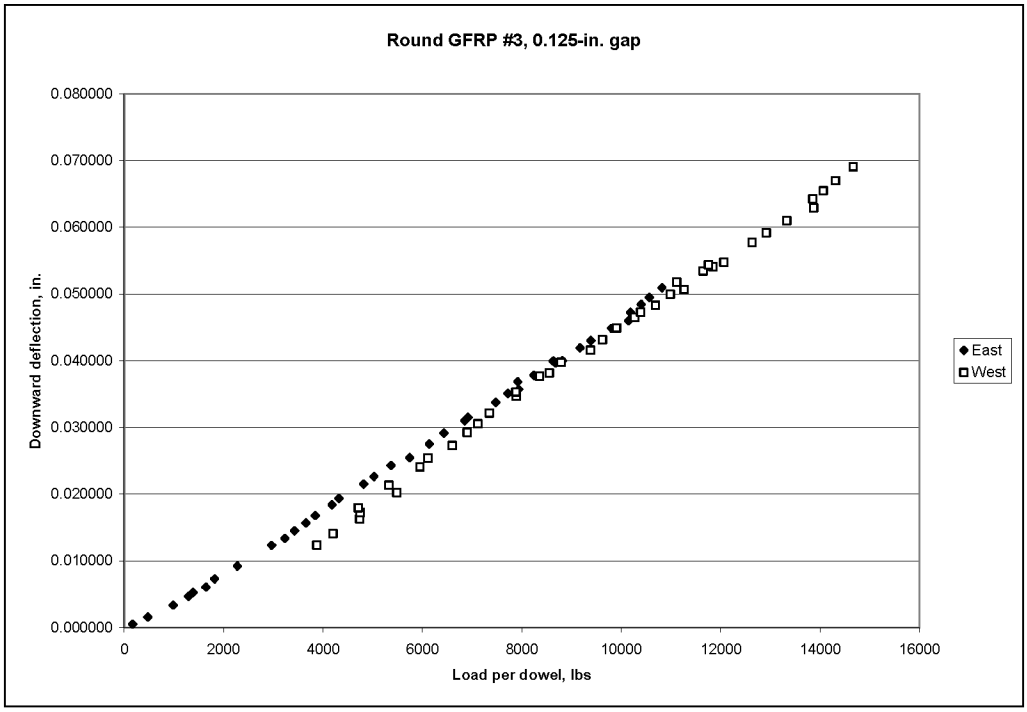

Figure A.23. Round GFRP #3, 0.125-in. gap load vs. deflection

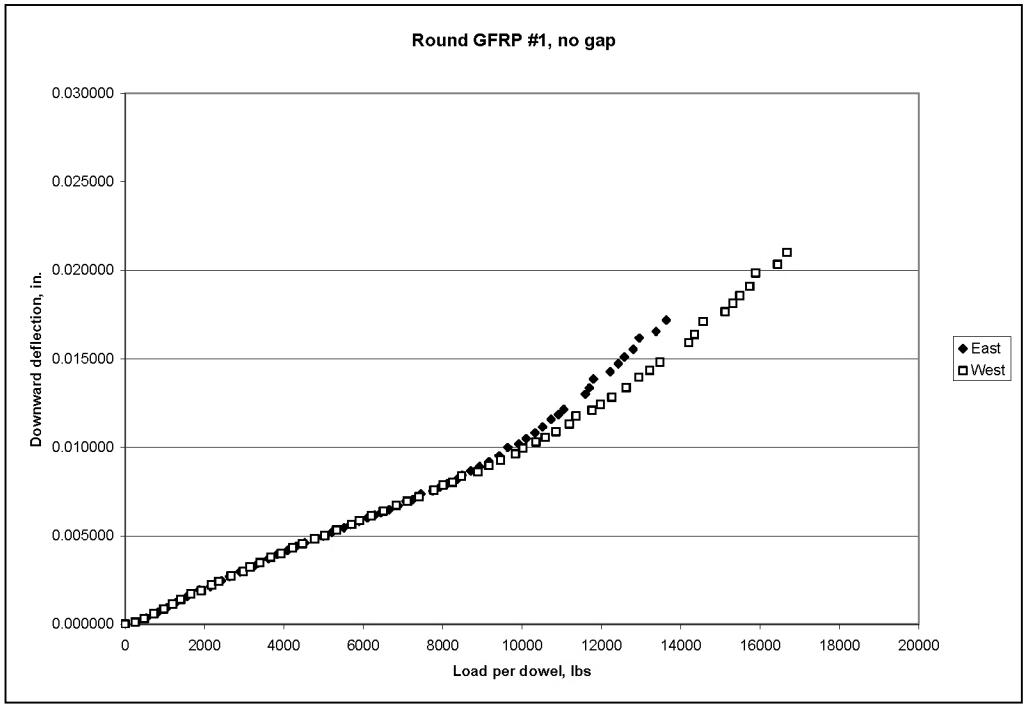

Figure A.24. Round GFRP #1, no gap load vs. deflection

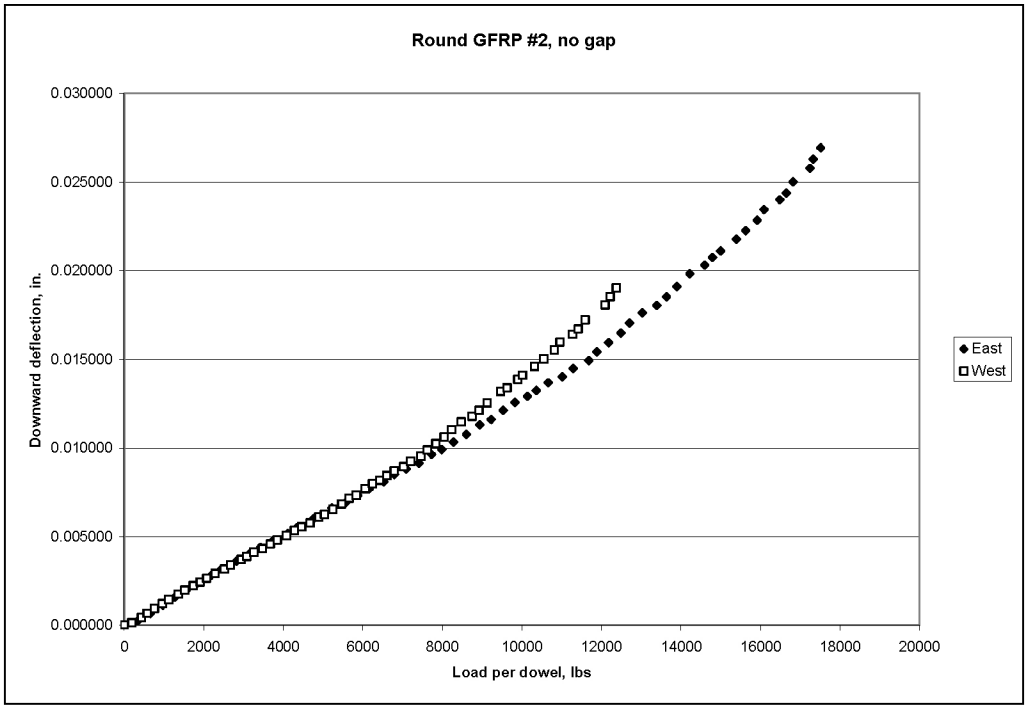

Figure A.25. Round GFRP #2, no gap load vs. deflection

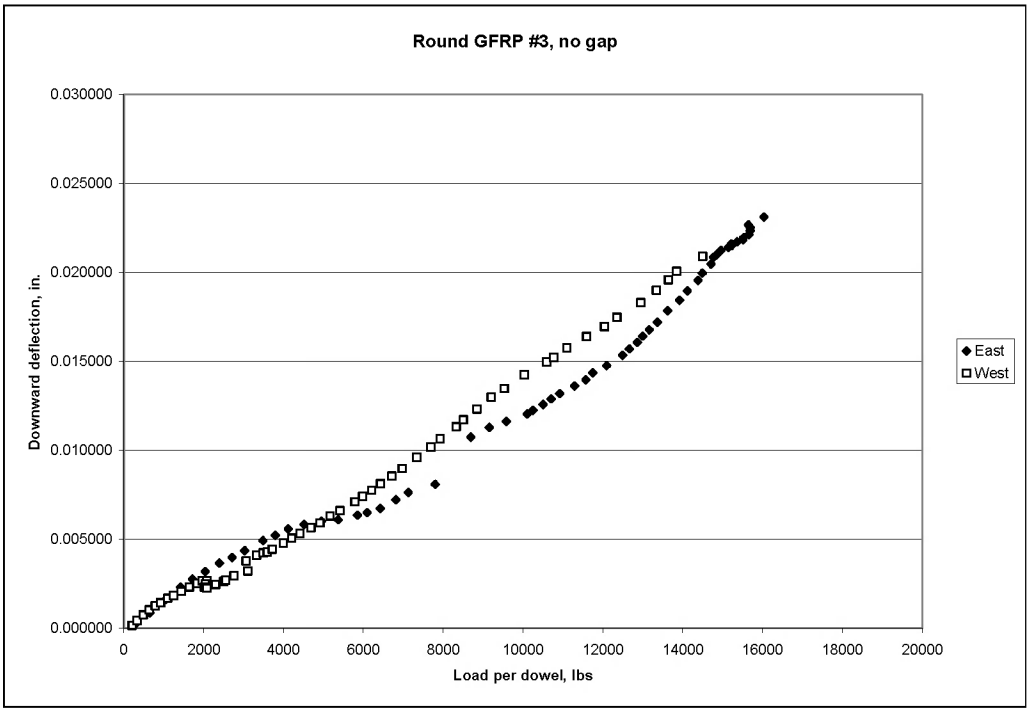

Figure A.26. Round GFRP #3, no gap load vs. deflection

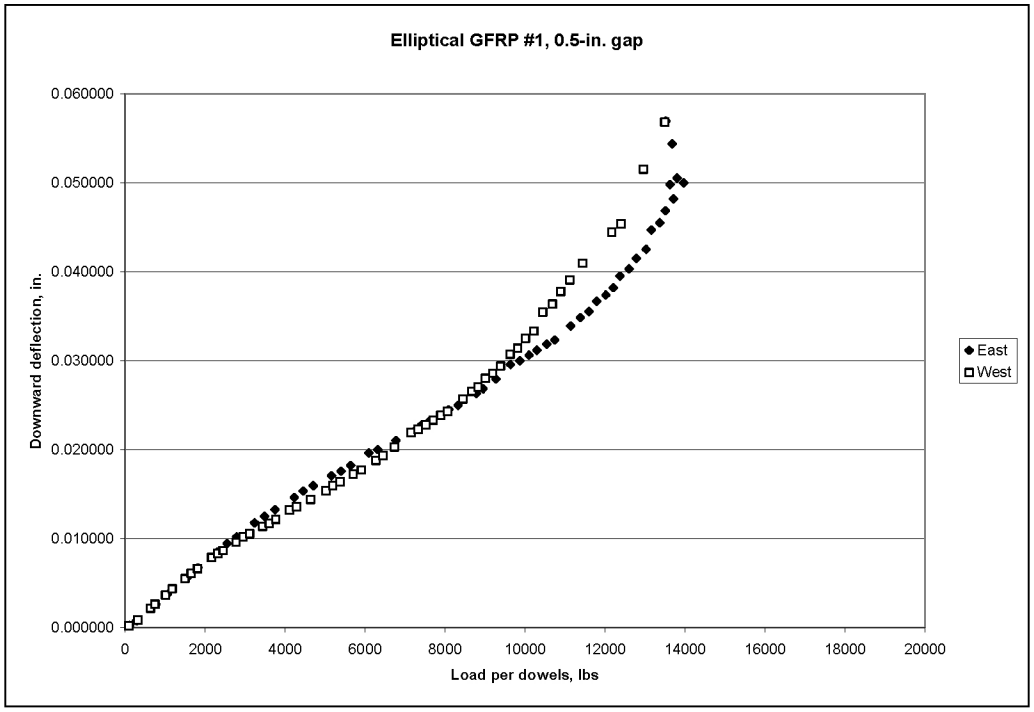

Figure A.27. Elliptical GFRP #1, 0.5-in. gap load vs. deflection

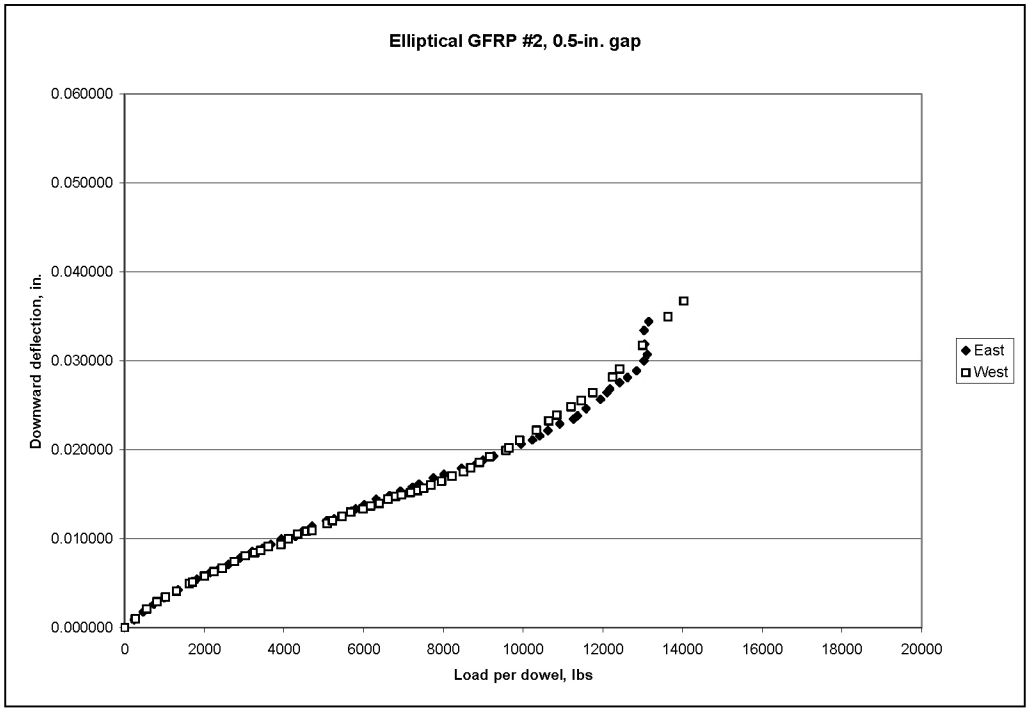

Figure A.28. Elliptical GFRP #2, 0.5-in. gap load vs. deflection

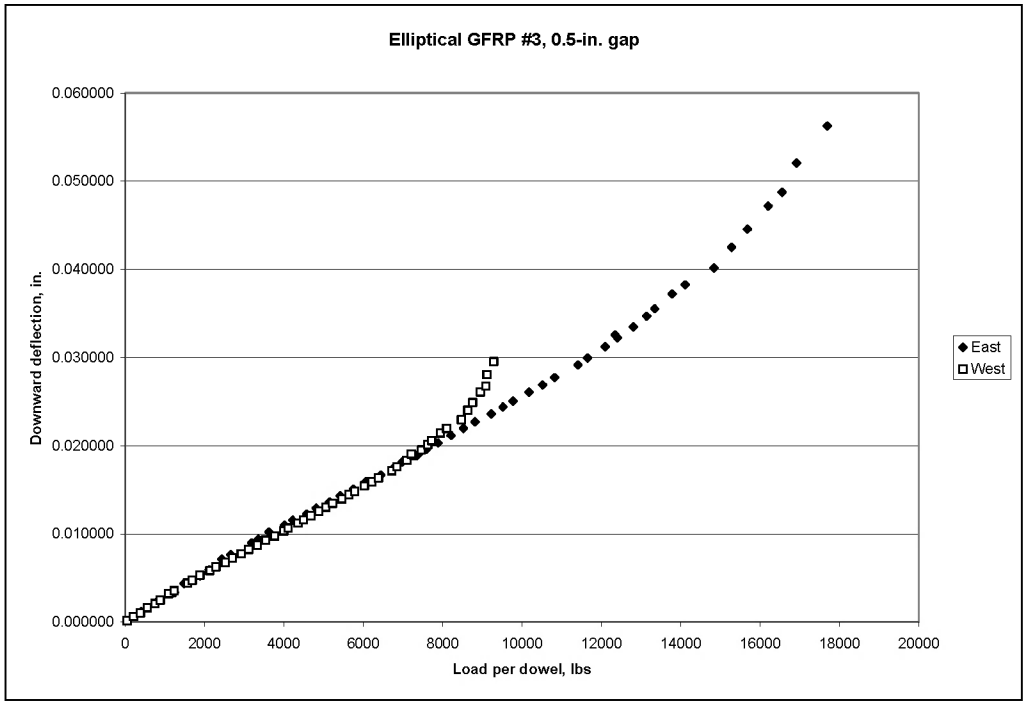

Figure A.29. Elliptical GFRP #3, 0.5-in. gap load vs. deflection

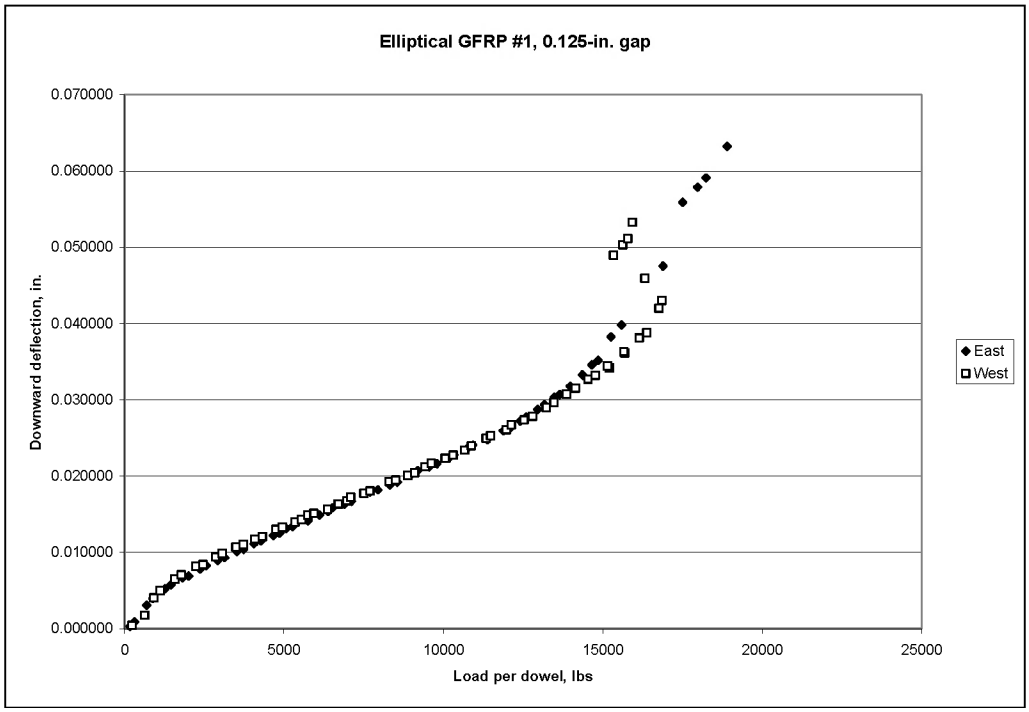

Figure A.30. Elliptical GFRP #1, 0.125-in. gap load vs. deflection

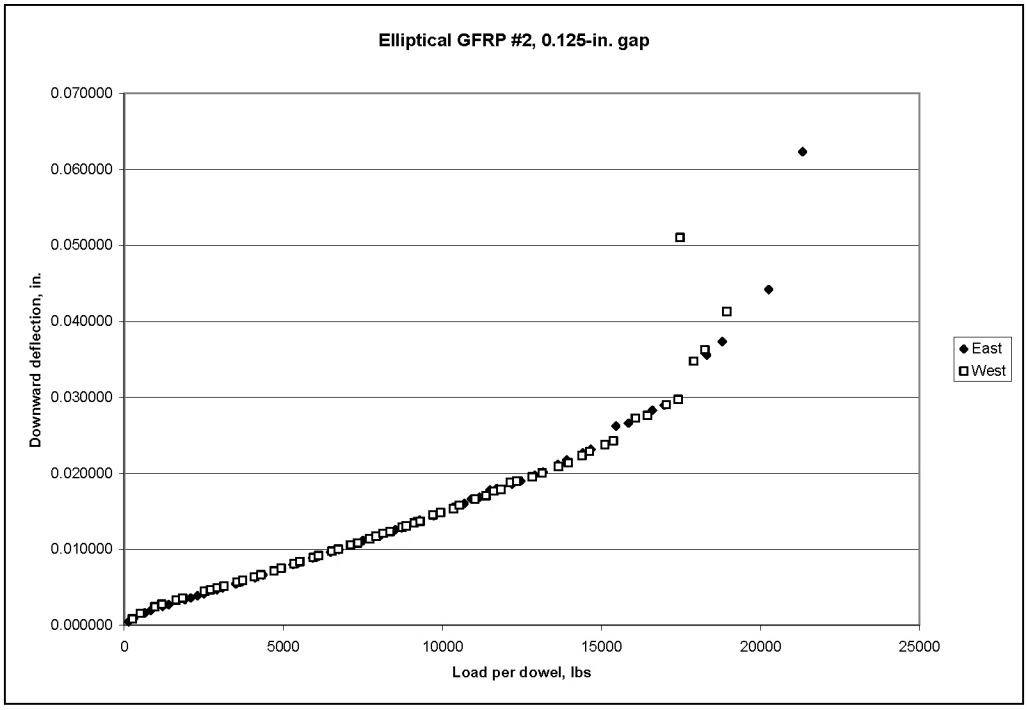

Figure A.31. Elliptical GFRP #2, 0.125-in. gap load vs. deflection

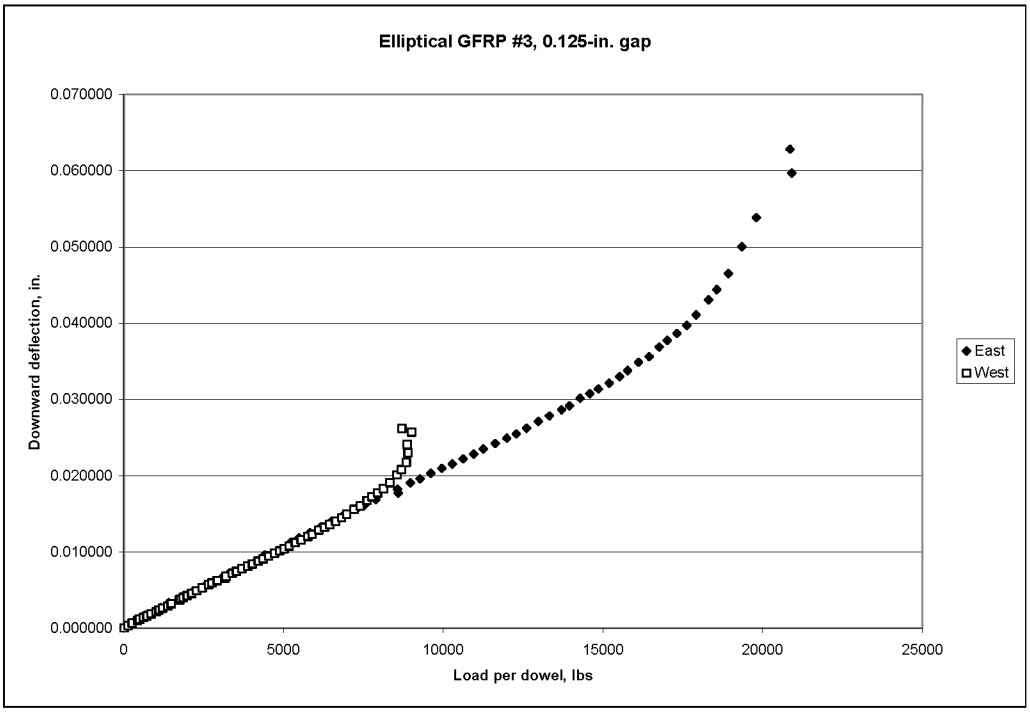

Figure A.32. Elliptical GFRP #3, 0.125-in. gap load vs. deflection

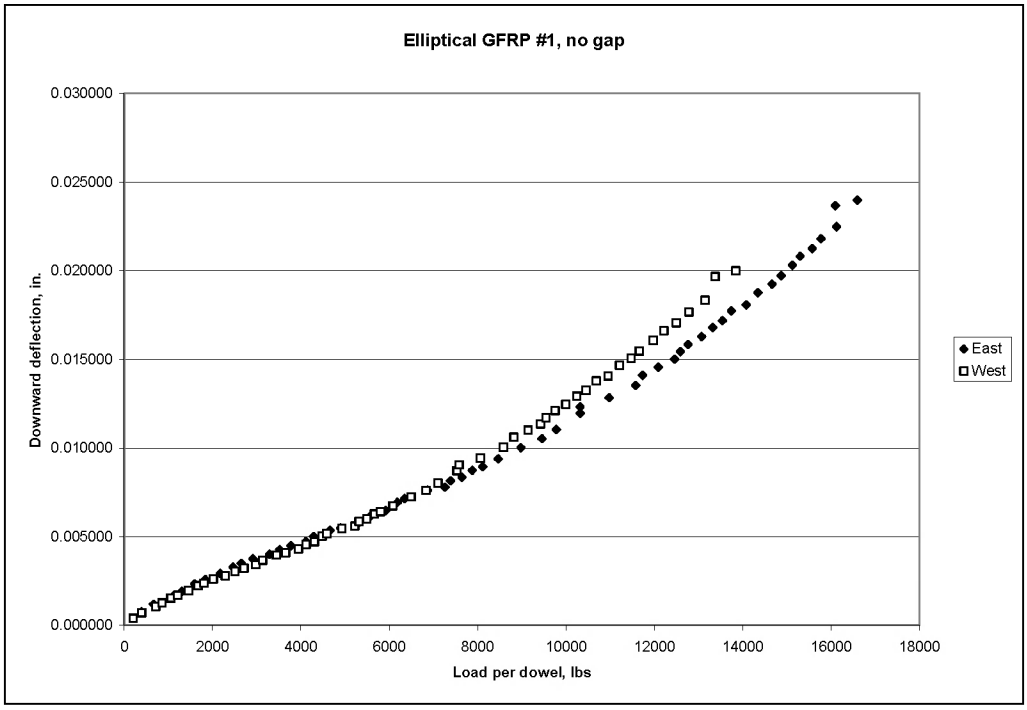

Figure A.33. Elliptical GFRP #1, no gap load vs. deflection

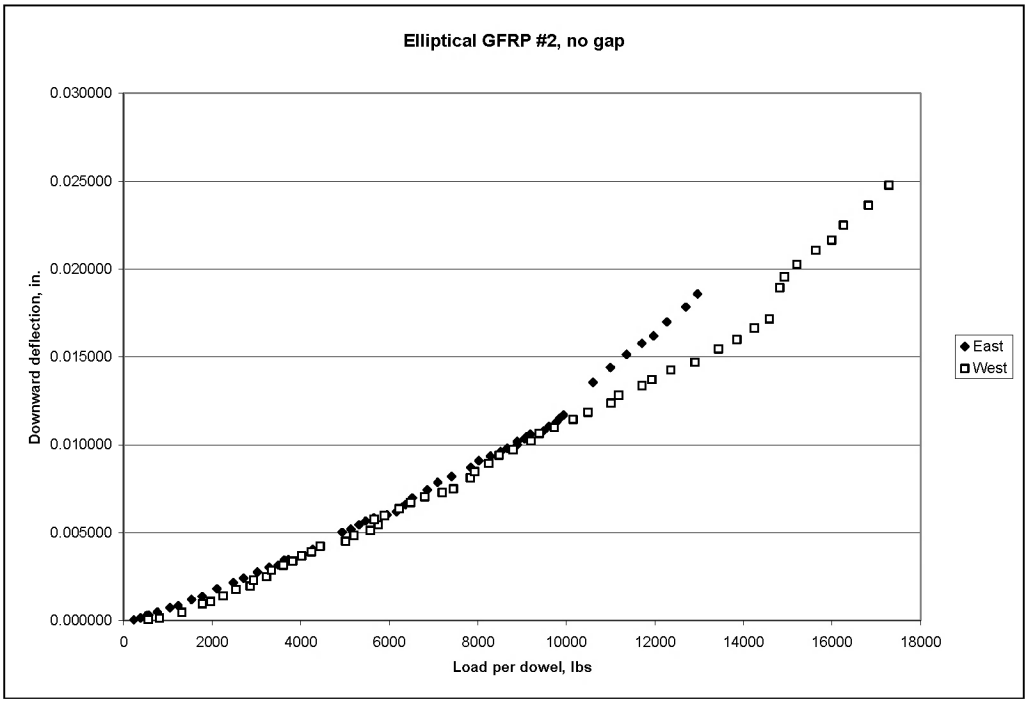

Figure A.34. Elliptical GFRP #2, no gap load vs. deflection

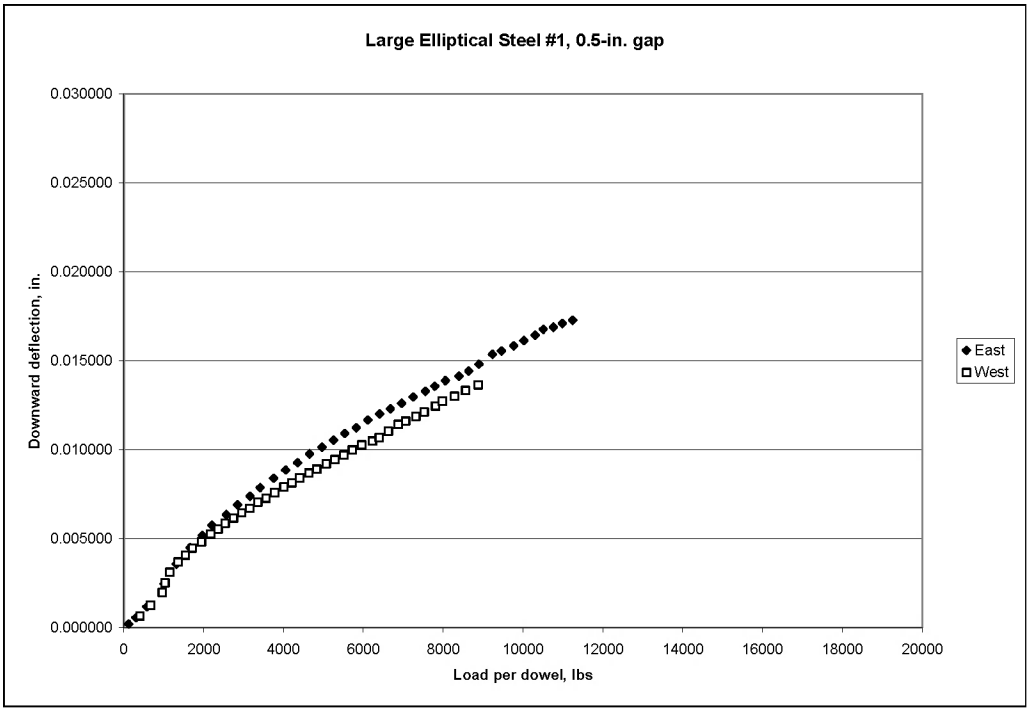

Figure A.35. Large elliptical steel #1, 0.5-in. gap load vs. deflection

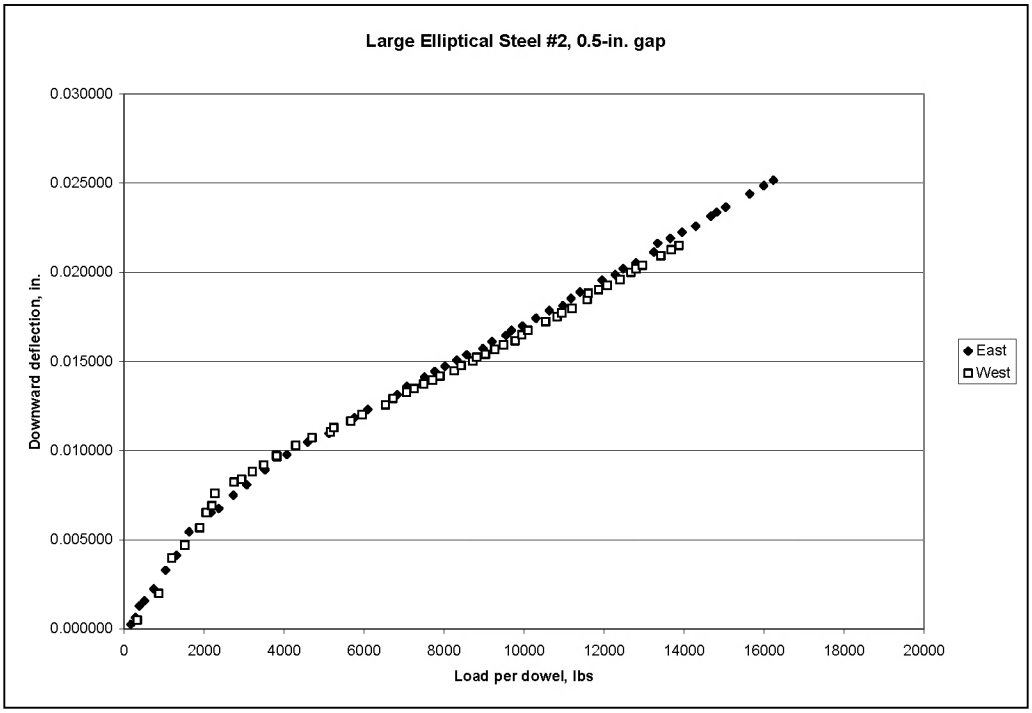

Figure A.36. Large elliptical steel #2, 0.5-in. gap load vs. deflection

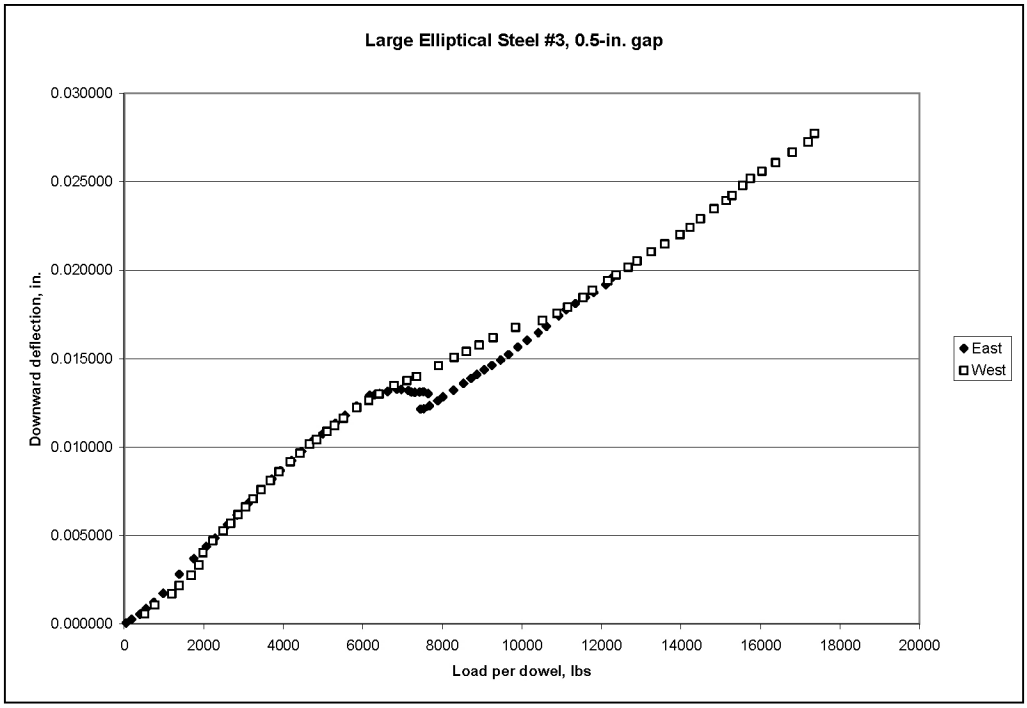

Figure A.37. Large elliptical steel #3, 0.5-in. gap load vs. deflection

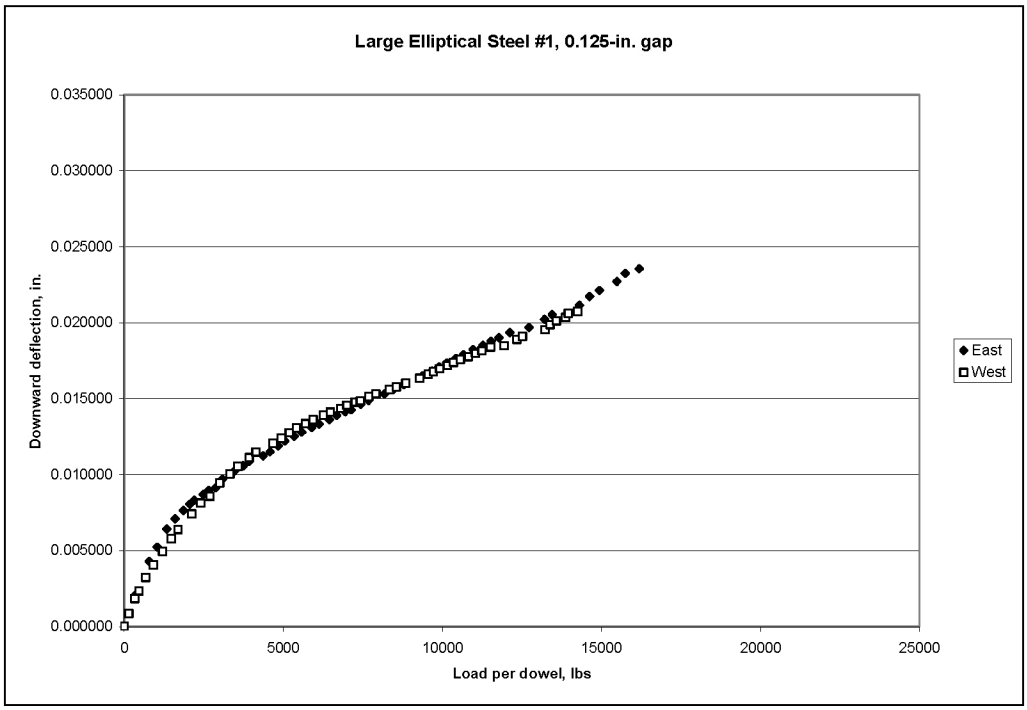

Figure A.38. Large elliptical steel #1, 0.125-in. gap load vs. deflection

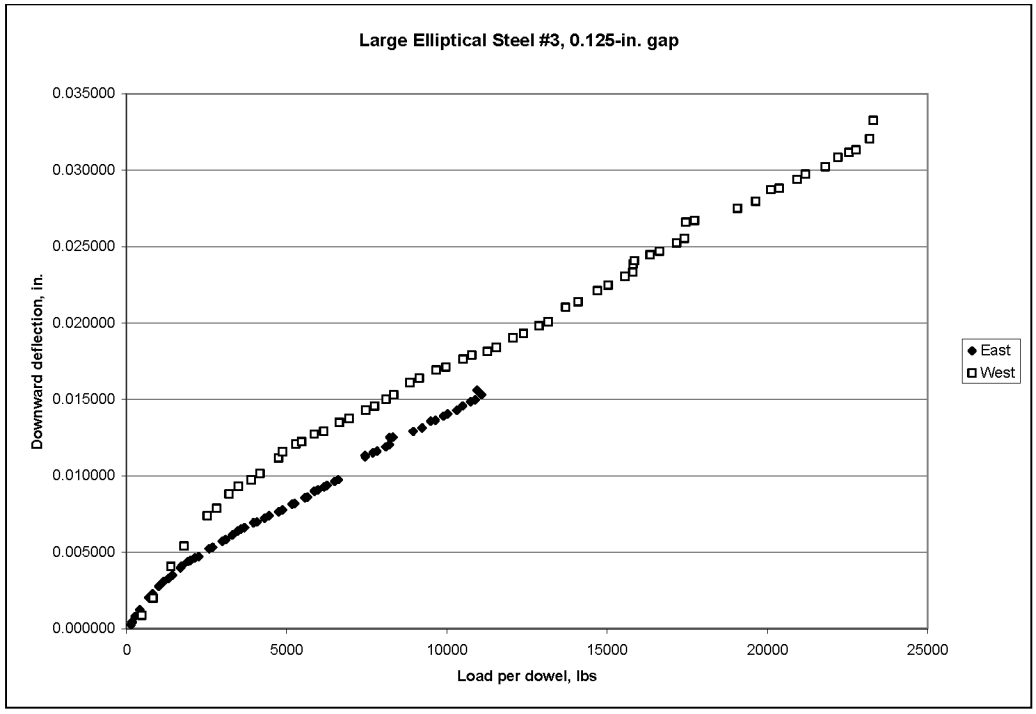

Figure A.39. Large elliptical steel #3, 0.125-in. gap load vs. deflection

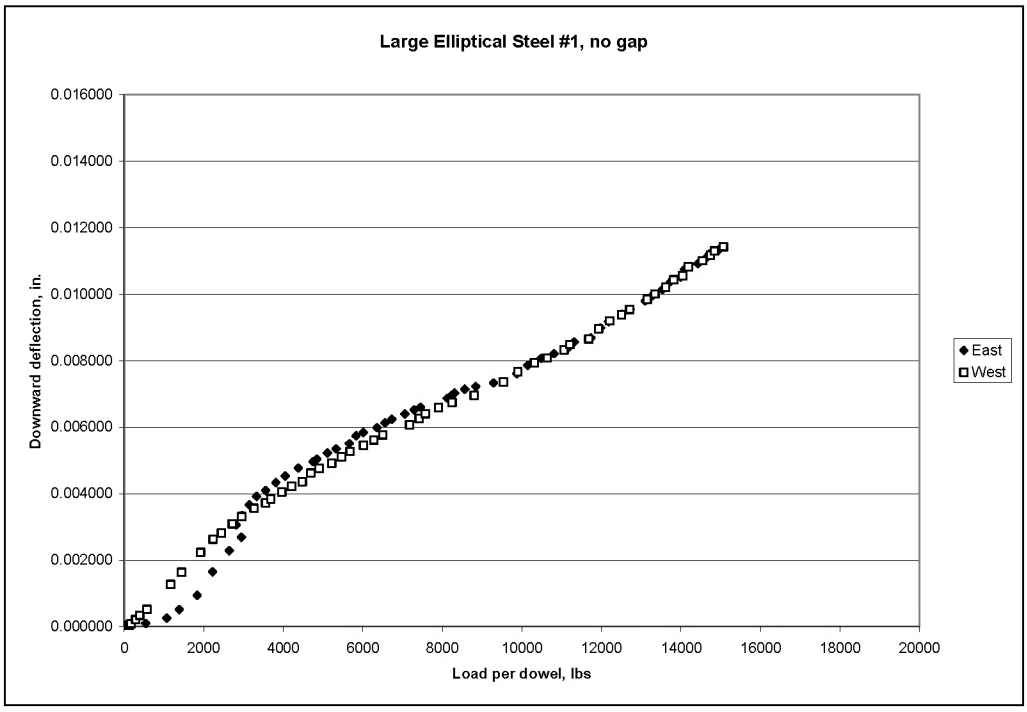

Figure A.40. Large elliptical steel #1, no gap load vs. deflection

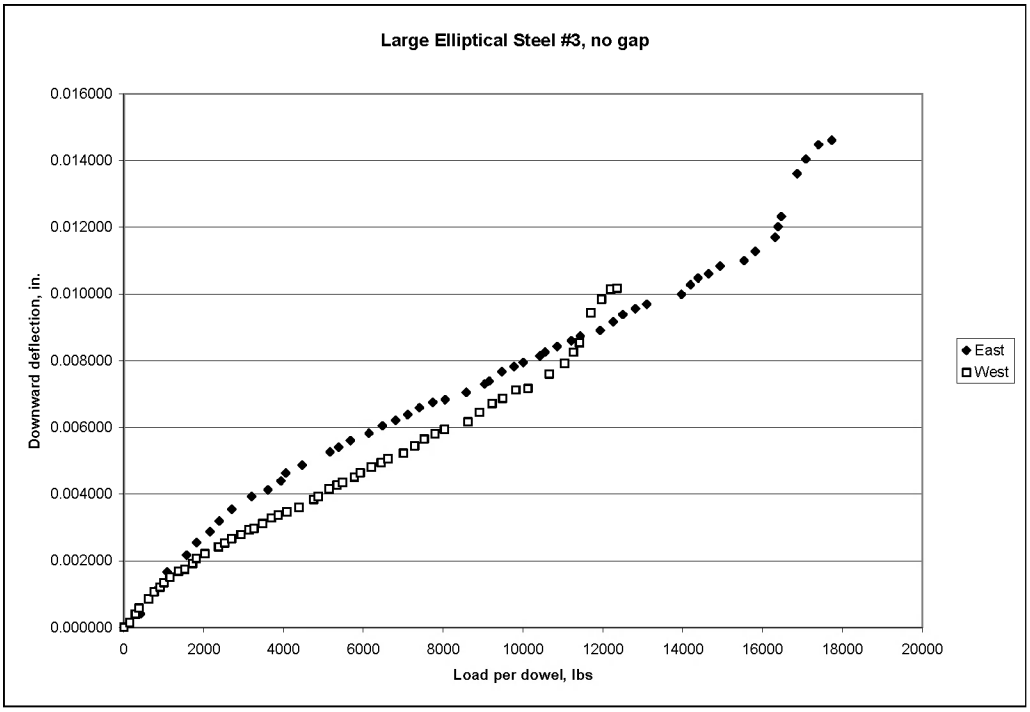

Figure A.41. Large elliptical steel #3, no gap load vs. deflection

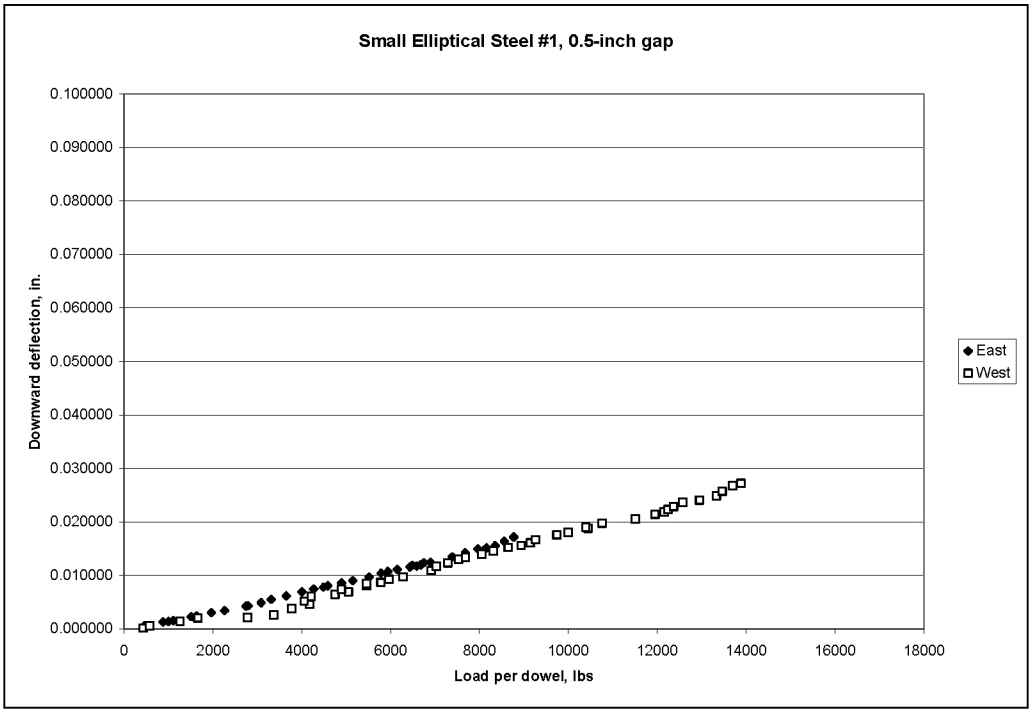

Figure A.42. Small elliptical steel #1, 0.5-in. gap load vs. deflection

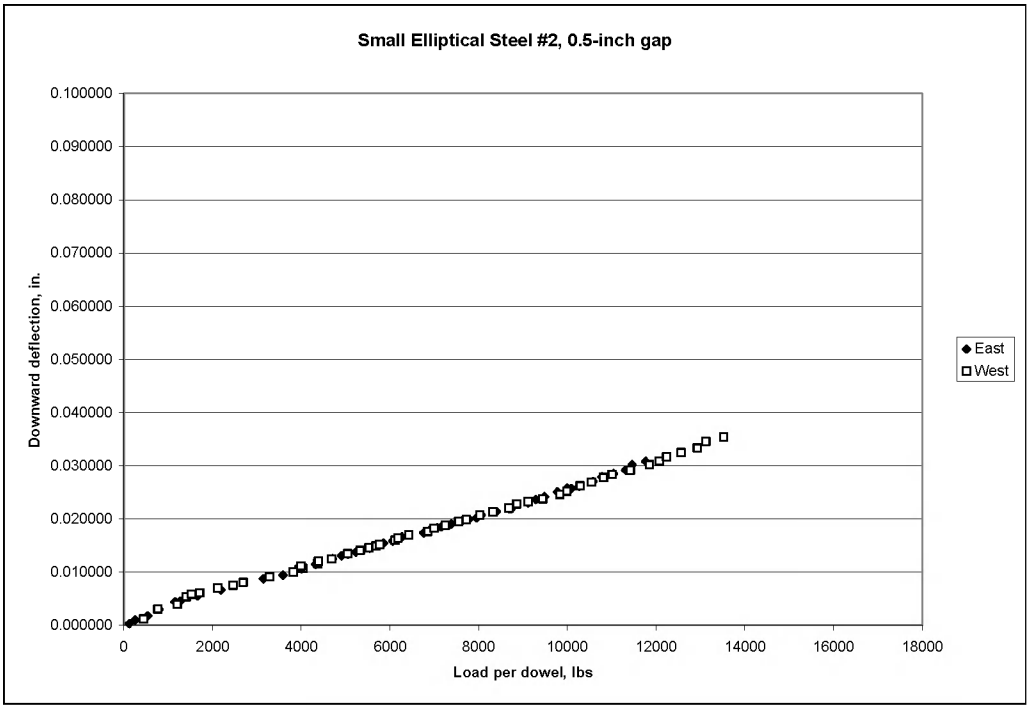

Figure A.43. Small elliptical steel #2, 0.5-in. gap load vs. deflection

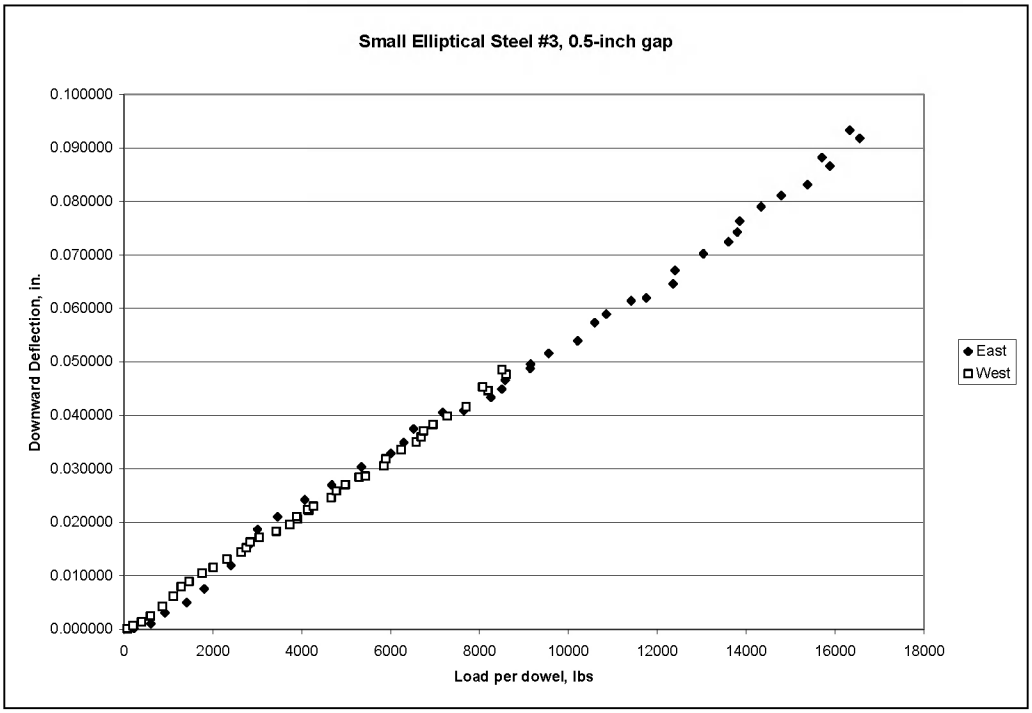

Figure A.44. Small elliptical steel #3, 0.5-in. gap load vs. deflection

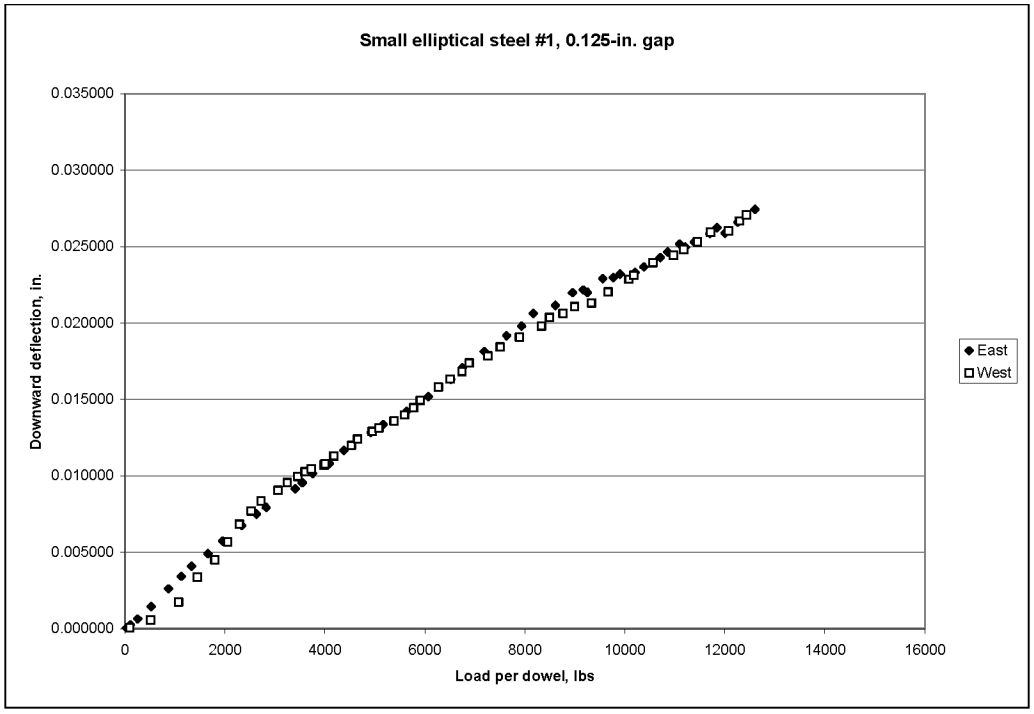

Figure A.45. Small elliptical steel #1, 0.125-in. gap load vs. deflection

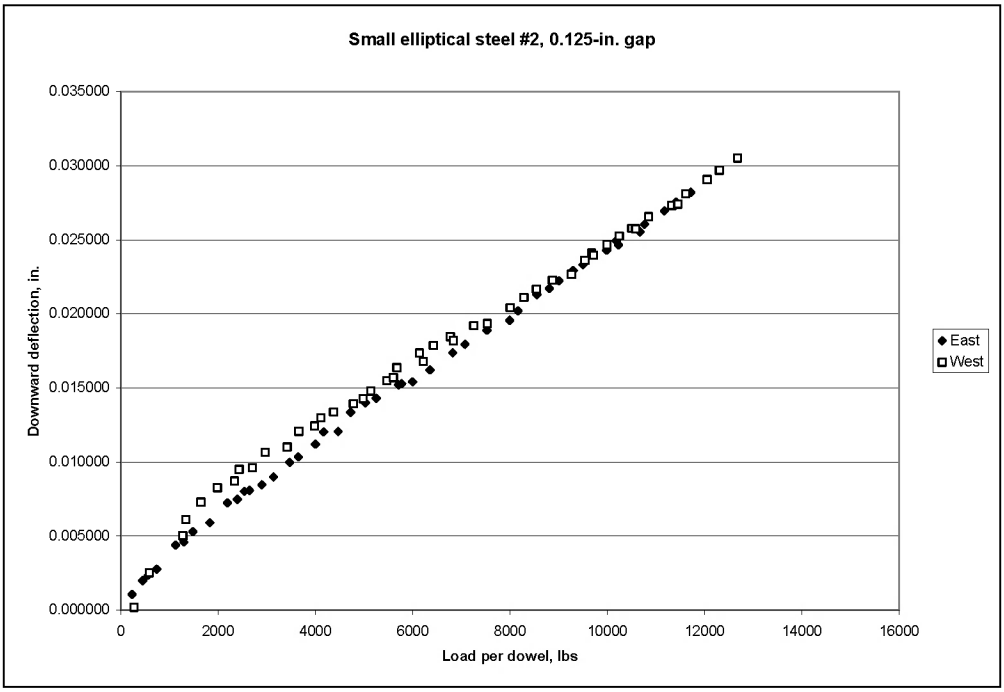

Figure A.46. Small elliptical steel #2, 0.125-in. gap load vs. deflection

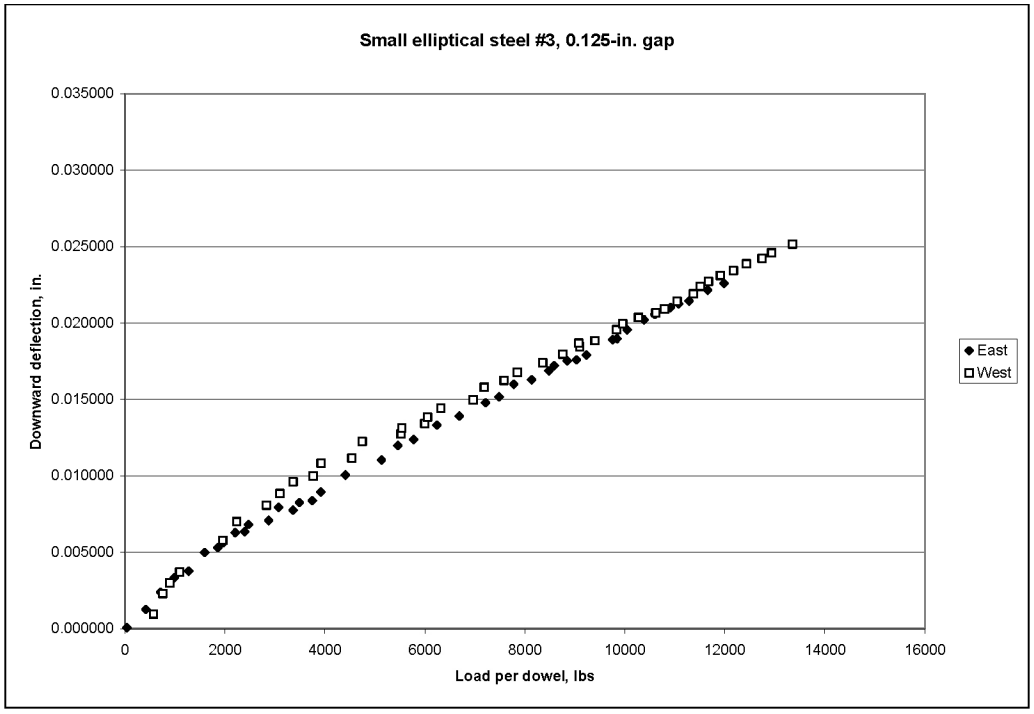

Figure A.47. Small elliptical steel #3, 0.125-in. gap load vs. deflection

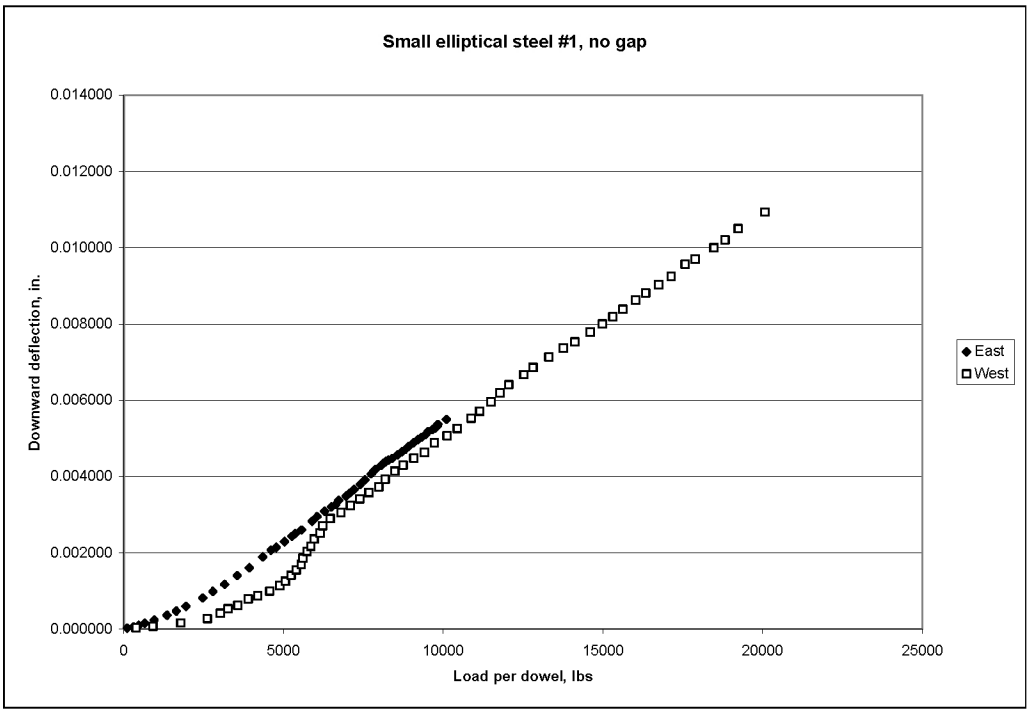

Figure A.48. Small elliptical steel #1, no gap load vs. deflection

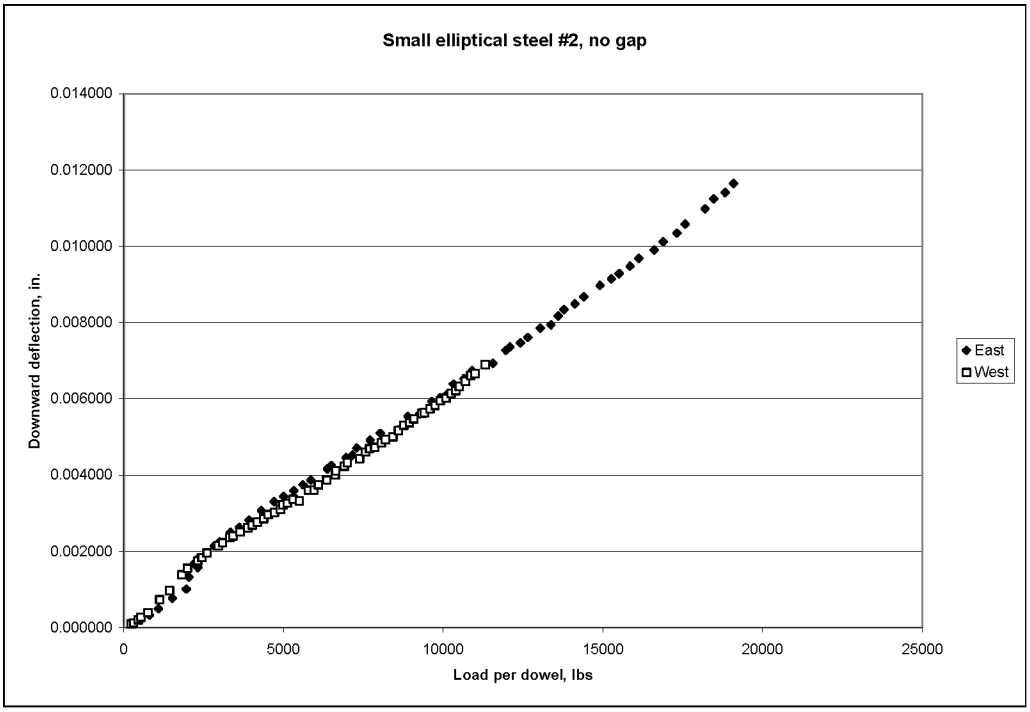

Figure A.49. Small elliptical steel #2, no gap load vs. deflection

APPENDIX B. CANTILEVER TEST LOAD VS. DEFLECTION PLOTS.

This section displays all deflections recorded by the string line transducer with respect to the recorded applied load corresponding to each deflection. The x-and y-axis scales are the same for plots of each specimen type to display the significant difference in deflection results obtained from the cantilever test.

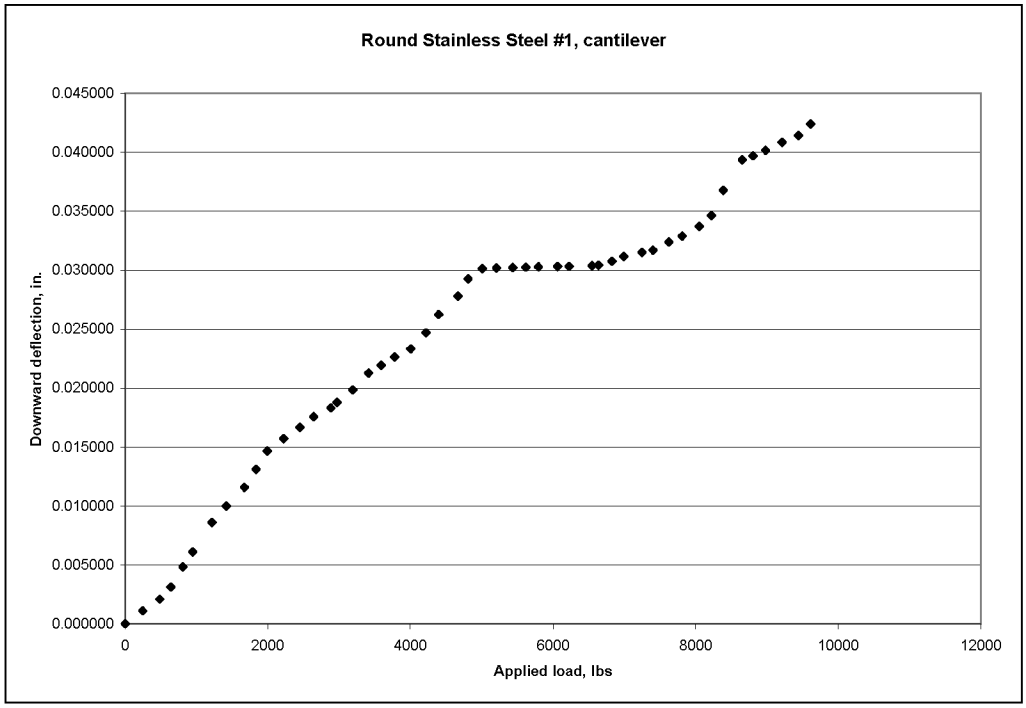

Figure B.1. Round stainless steel #1 cantilever load vs. deflection

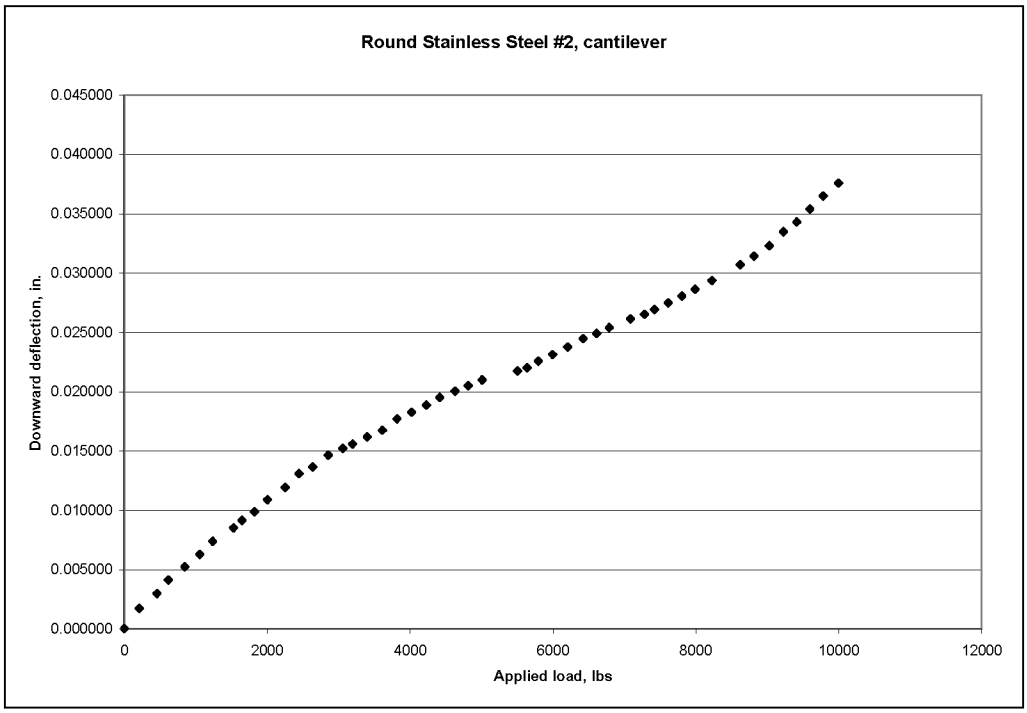

Figure B.2. Round stainless steel #2 cantilever load vs. deflection

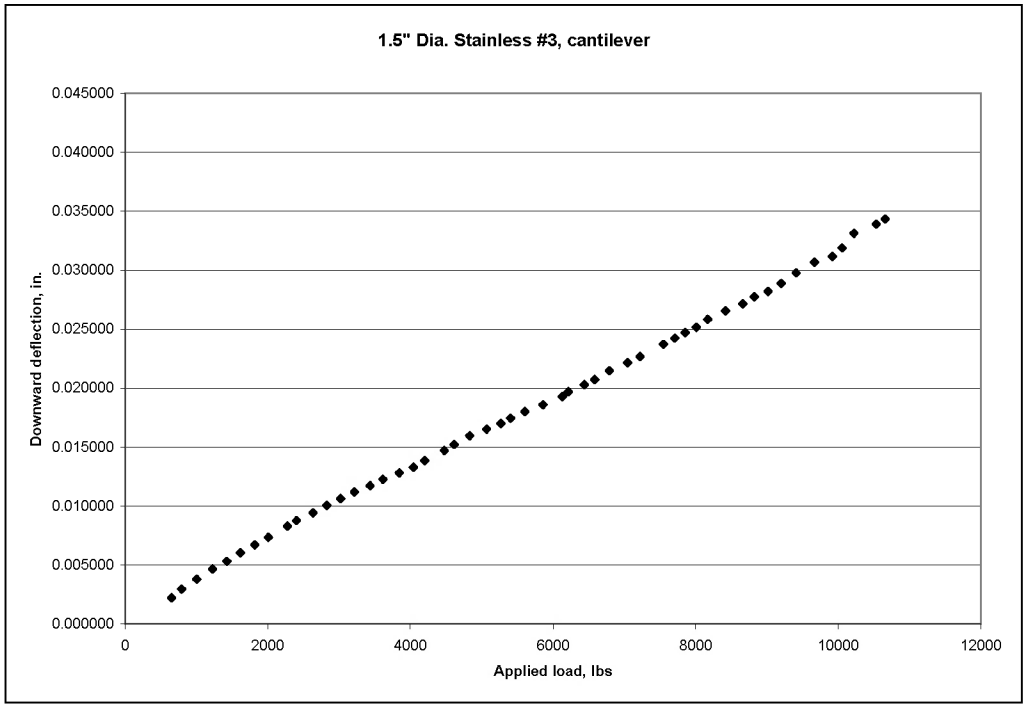

Figure B.3. Round stainless steel #3 cantilever load vs. deflection

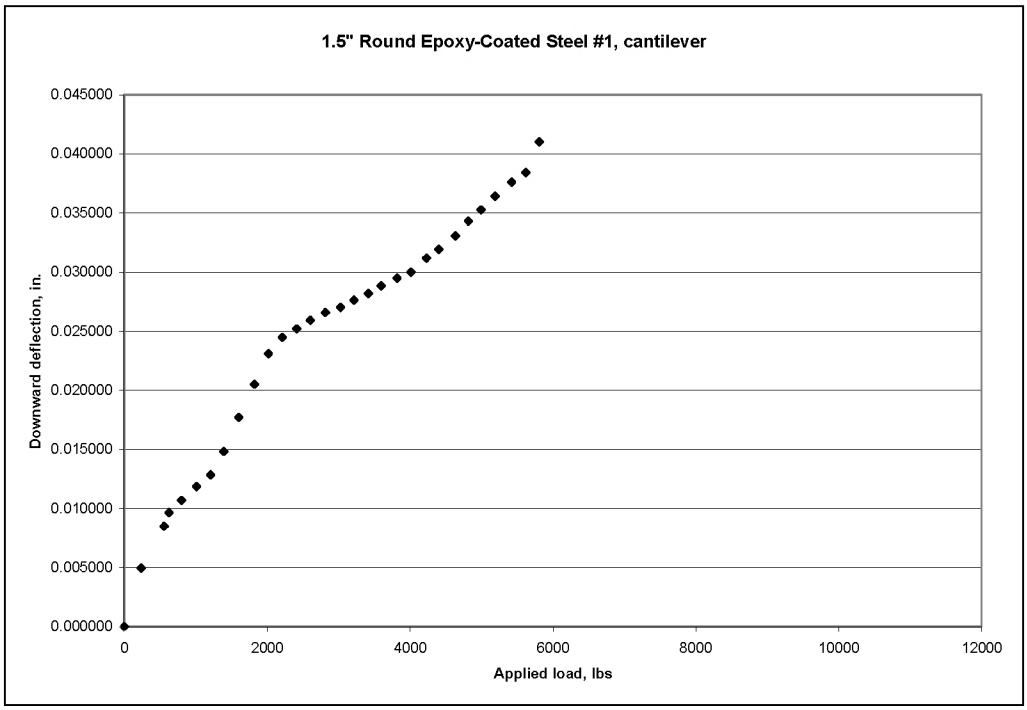

Figure B.4. Round epoxy-coated steel #1 cantilever load vs. deflection

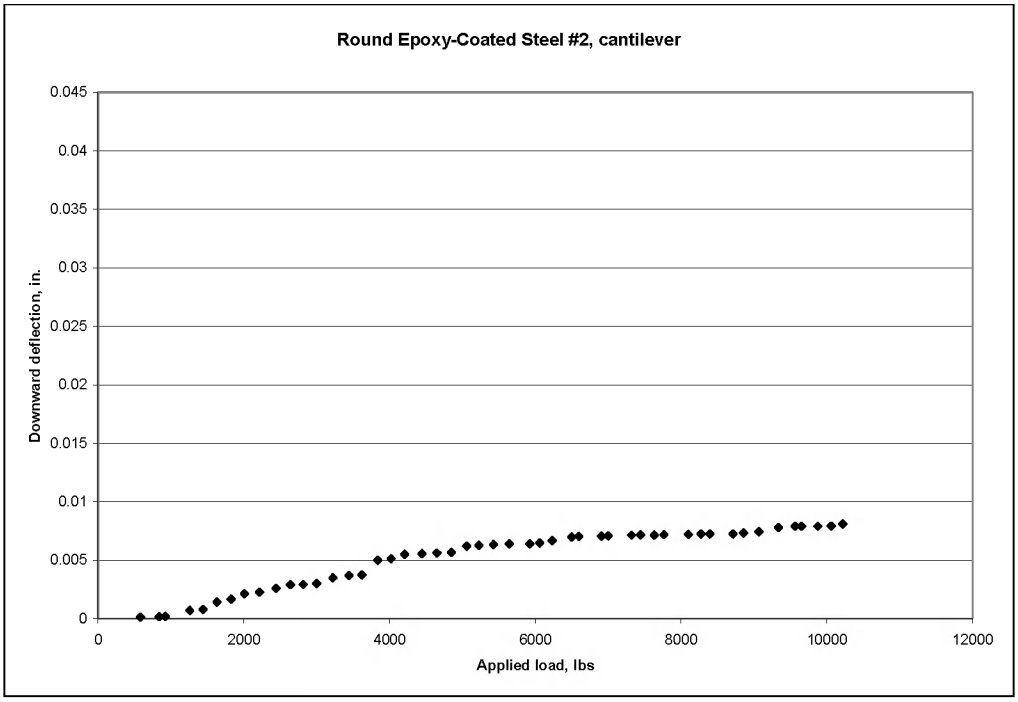

Figure B.5. Round epoxy-coated steel #2 cantilever load vs. deflection

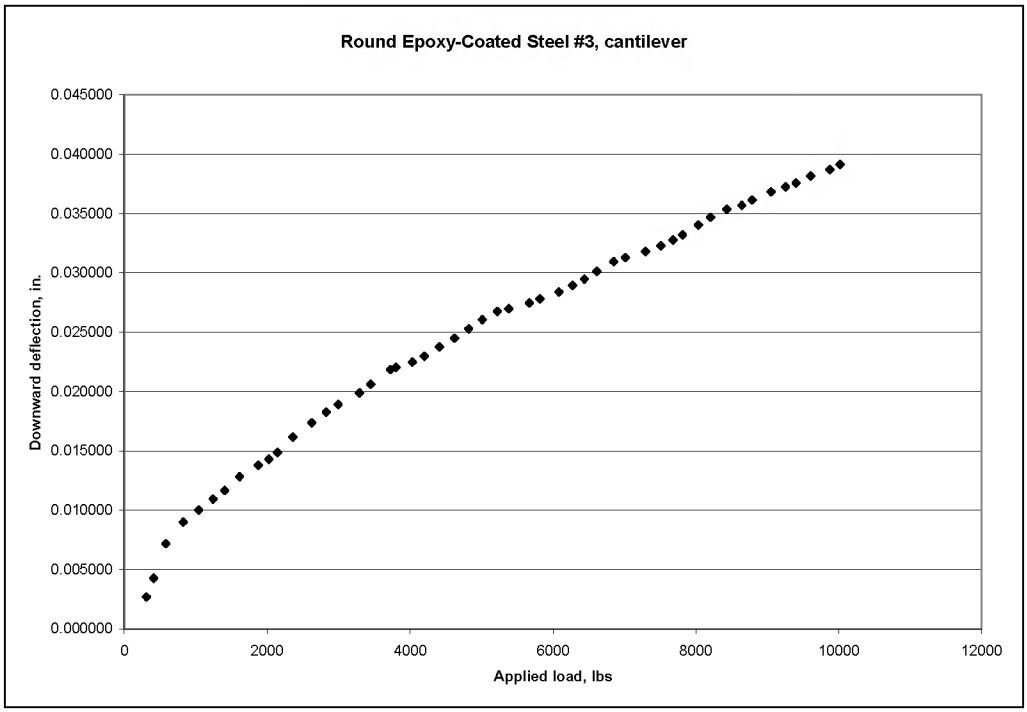

Figure B.6. Round epoxy-coated steel #3 cantilever load vs. deflection

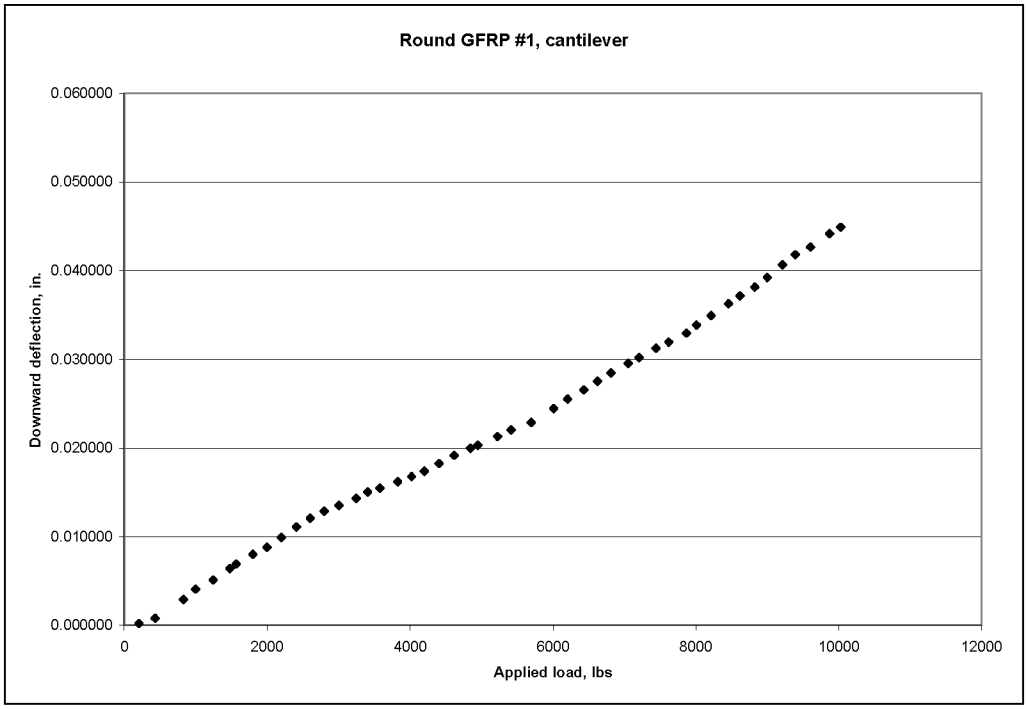

Figure B.7. Round GFRP #1 cantilever load vs. deflection

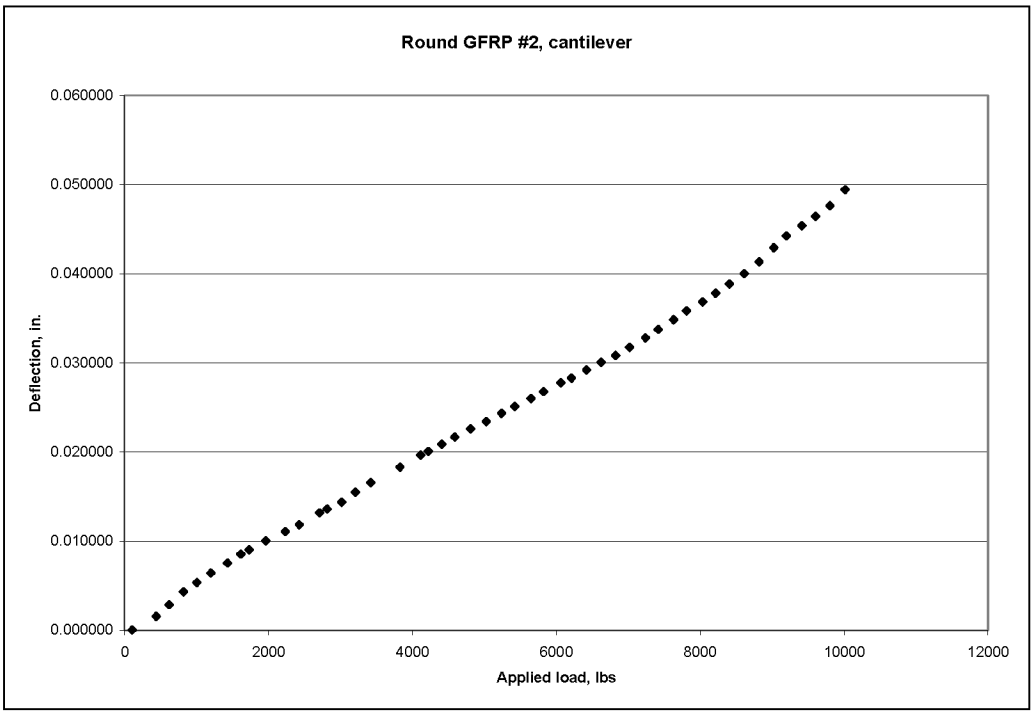

Figure B.8. Round GFRP #2 cantilever load vs. deflection

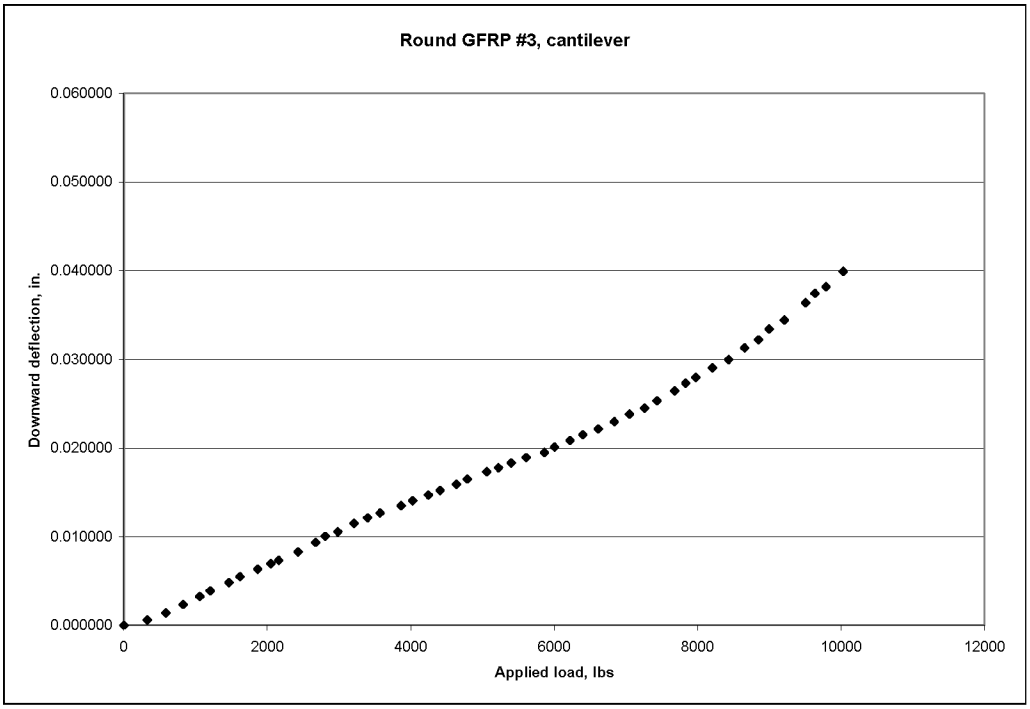

Figure B.9. Round GFRP #3 cantilever load vs. deflection

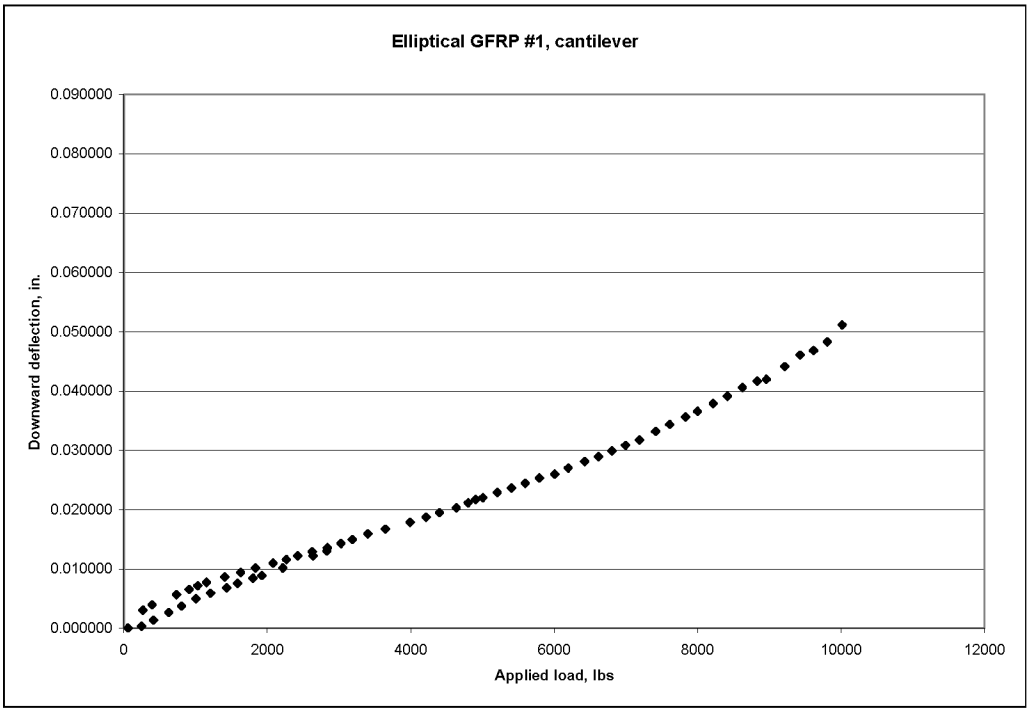

Figure B.10. Elliptical GFRP #1 cantilever load vs. deflection

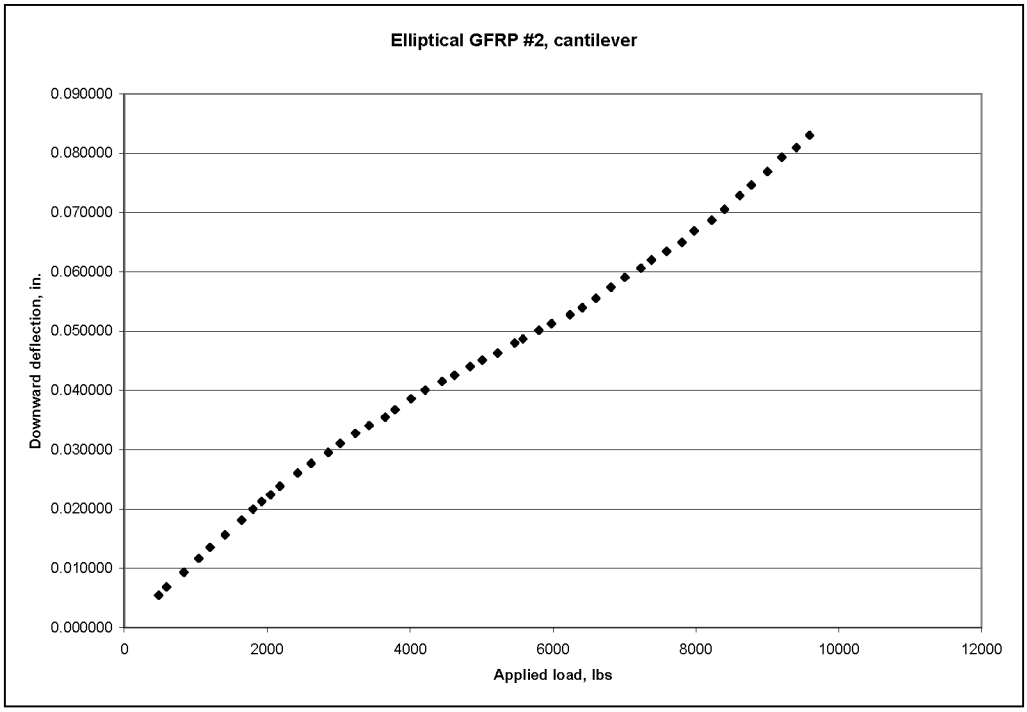

Figure B.11. Elliptical GFRP #2 cantilever load vs. deflection

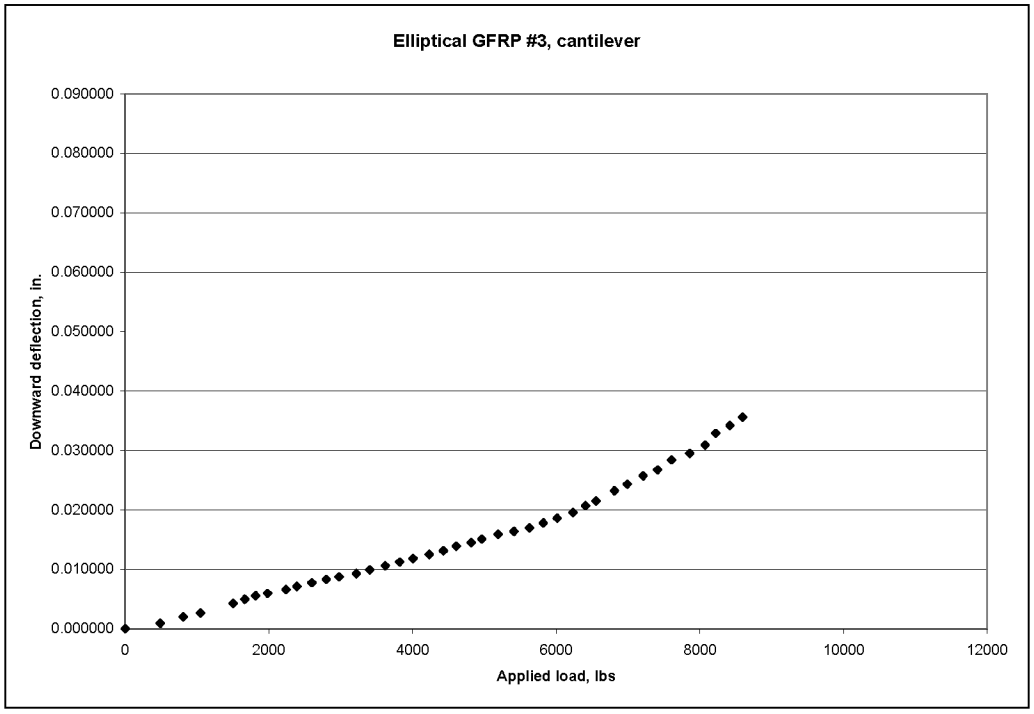

Figure B.12. Elliptical GFRP #3 cantilever load vs. deflection

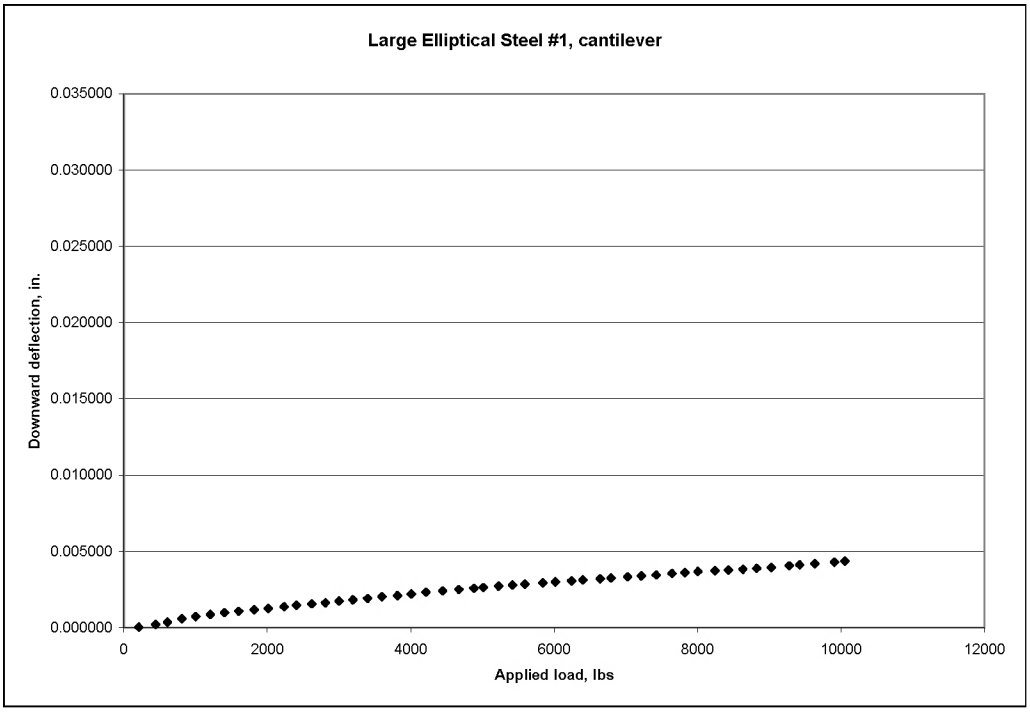

Figure B.13. Large elliptical steel #1 cantilever load vs. deflection

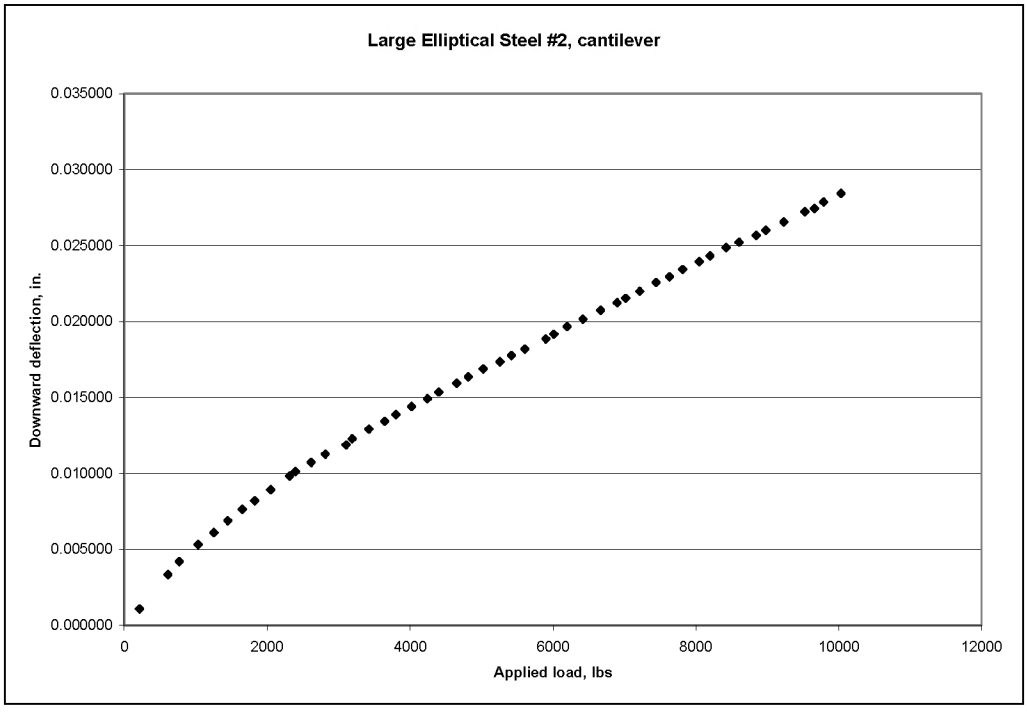

Figure B.14. Large elliptical steel #2 cantilever load vs. deflection

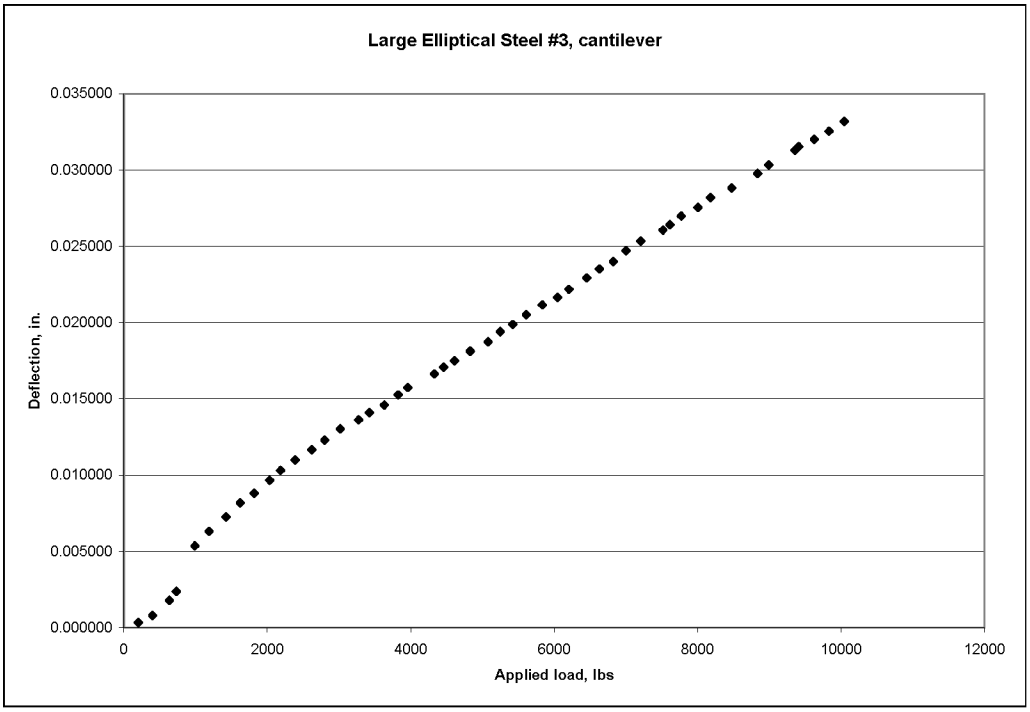

Figure B.15. Large elliptical steel #3 cantilever load vs. deflection

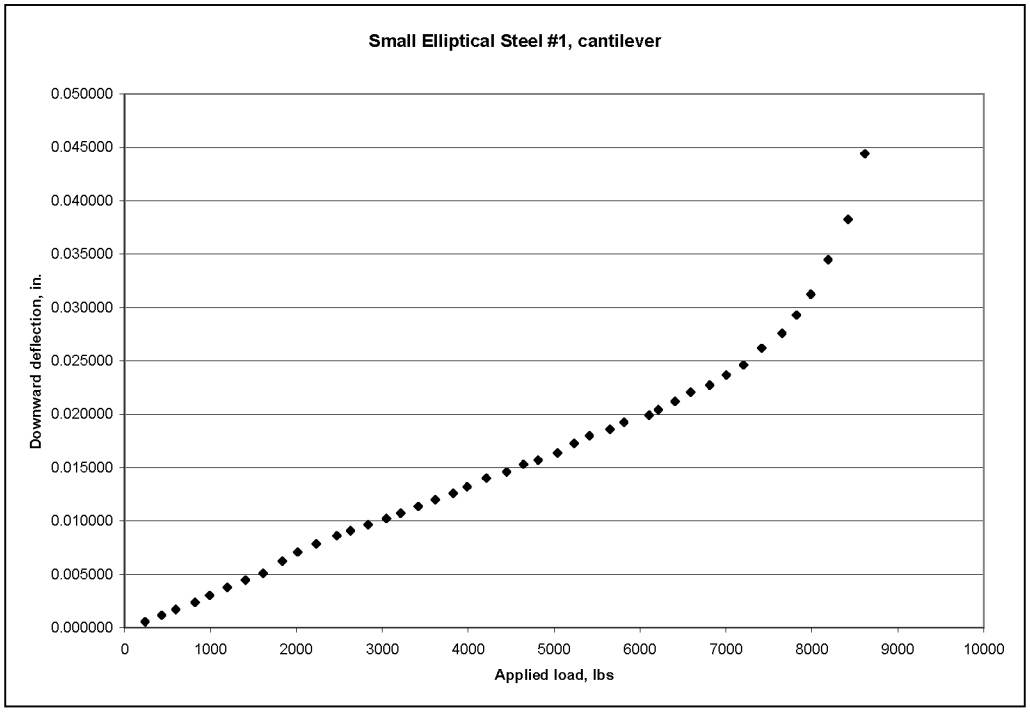

Figure B.16. Small elliptical steel #1 cantilever load vs. deflection

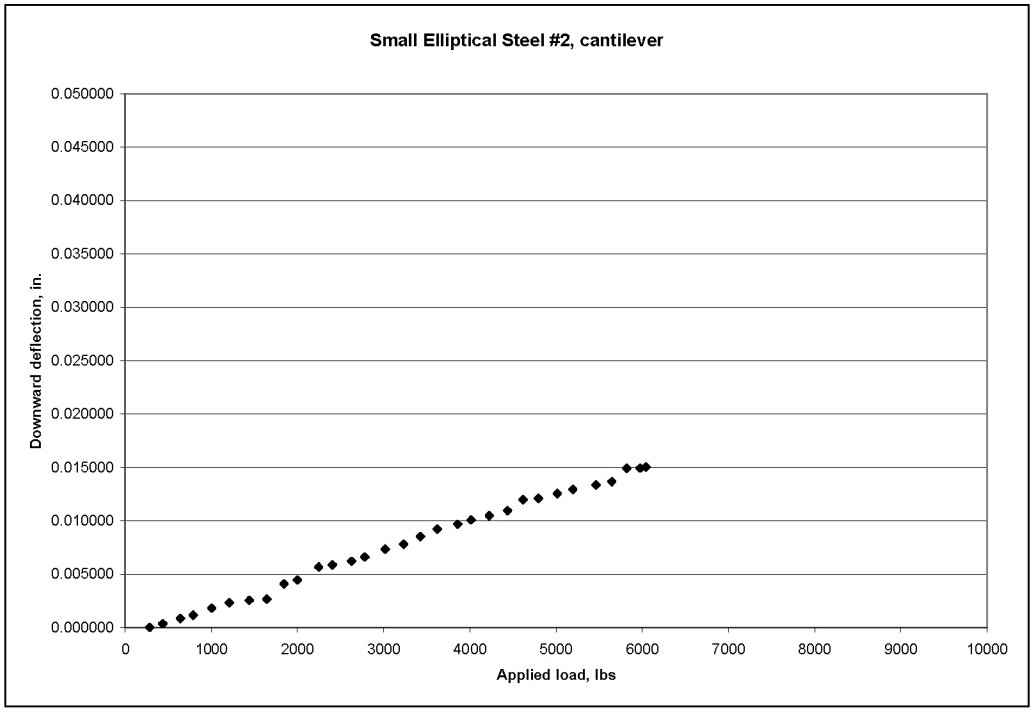

Figure B.17. Small elliptical steel #2 cantilever load vs. deflection

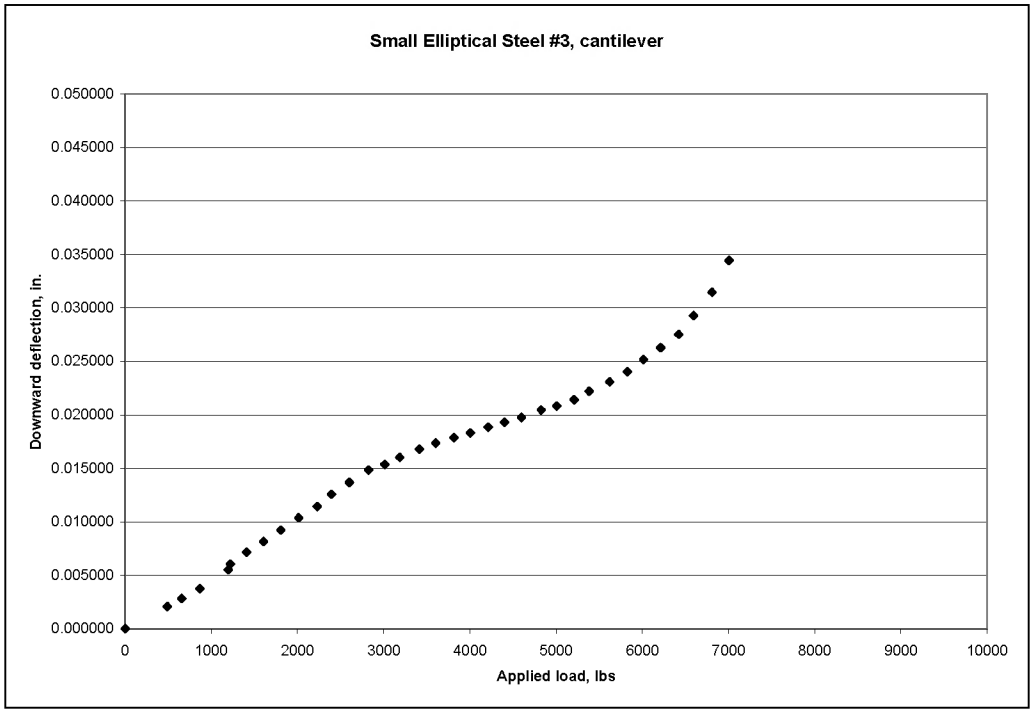

Figure B.18. Small elliptical steel #3 cantilever load vs. deflection

APPENDIX C. MODULUS OF DOWEL SUPPORT PLOTS.

This section displays the plots of k_0 for every modified AASHTO specimen and cantilever specimen. The k_0 values were plotted on the same graph to compare results of all tests with one another. The plots in Appendix C display the significant difference between the modified AASHTO procedure and the experimental cantilever test.

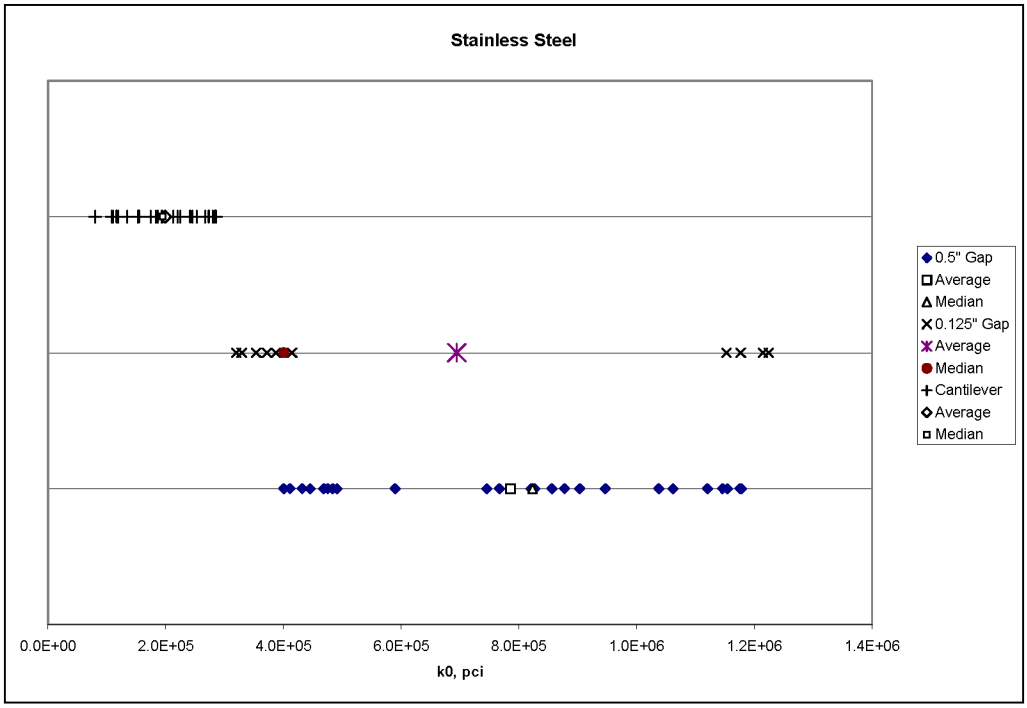

Figure C.1. Round stainless steel k_0 comparison

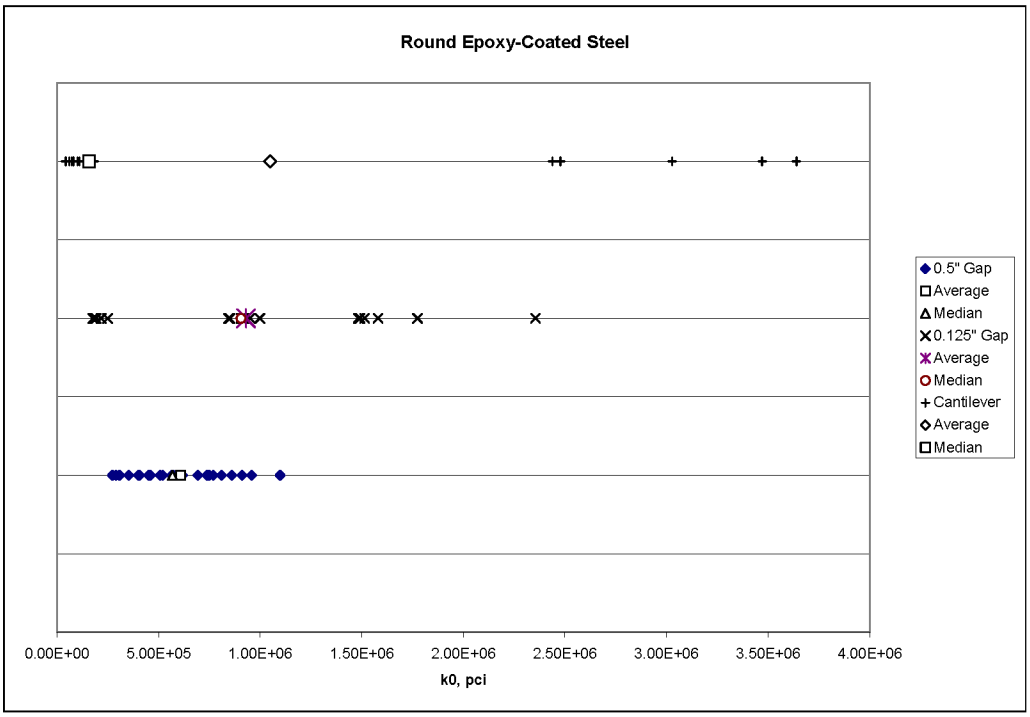

Figure C.2. Round epoxy-coated steel k_0 comparison

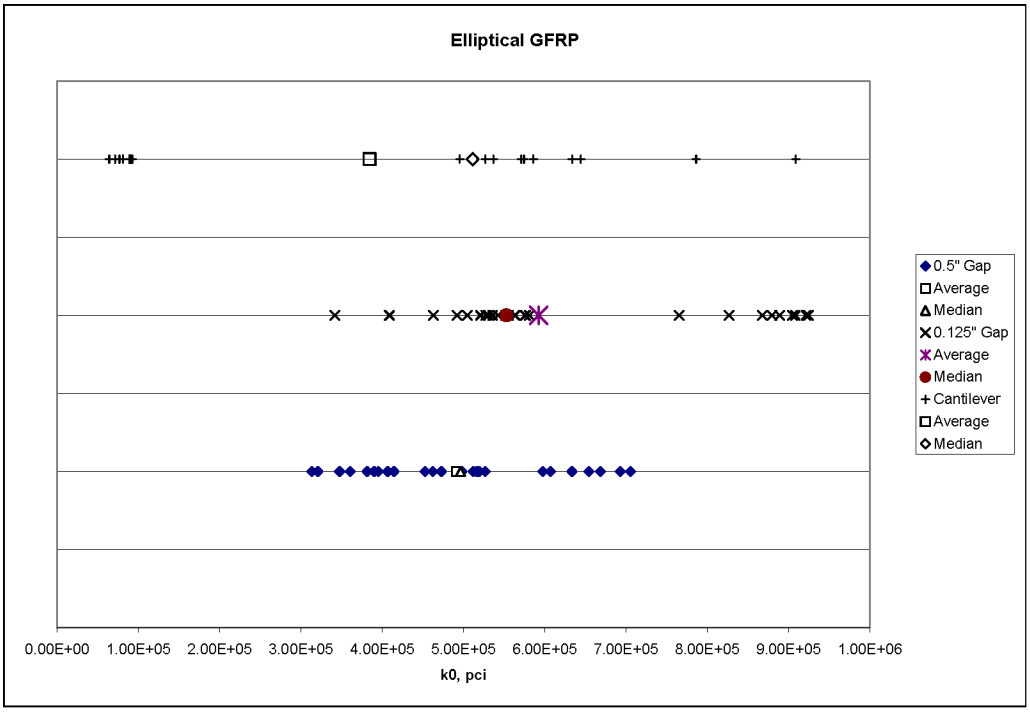

Figure C.3. Elliptical GFRP k_0 comparison

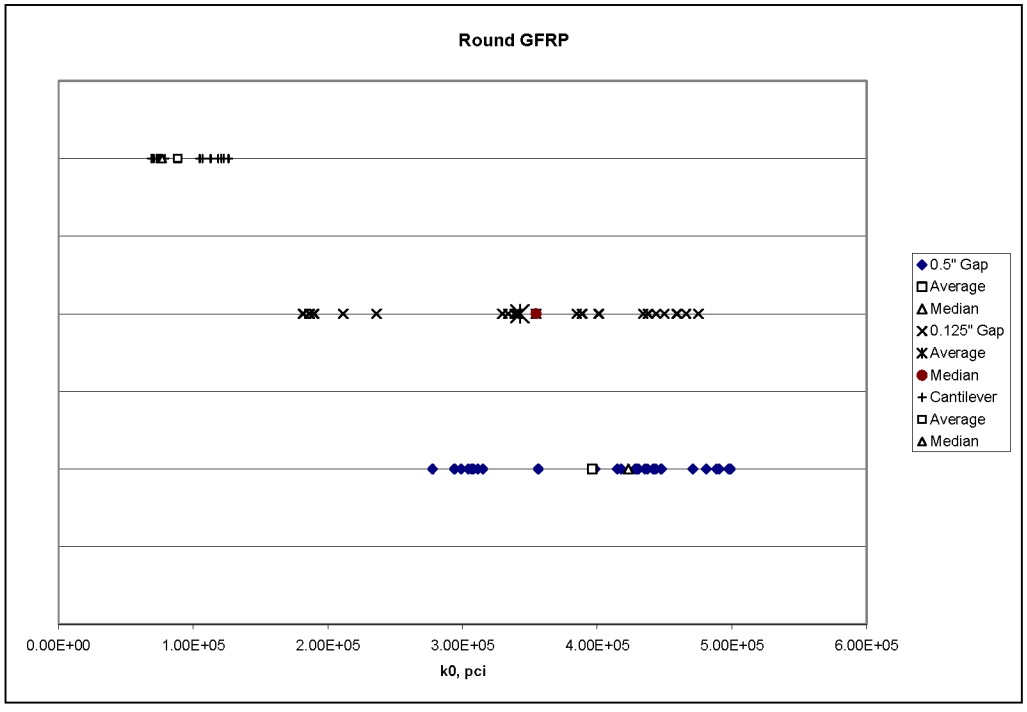

Figure C.4. Round GFRP k_0 comparison

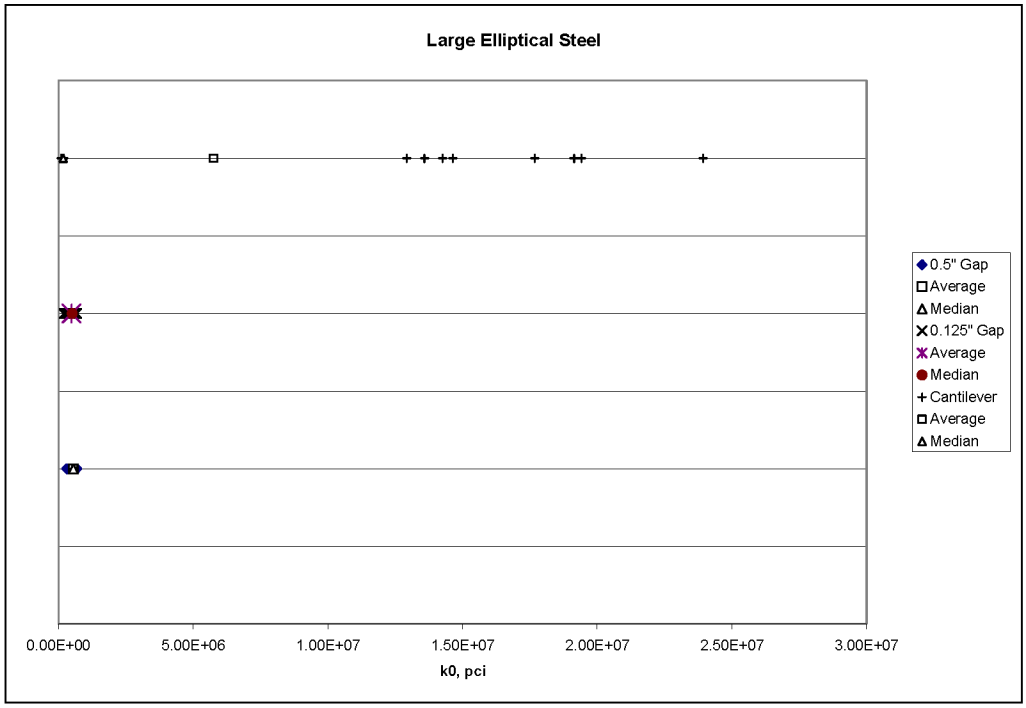

Figure C.5. Large elliptical steel k_0 comparison

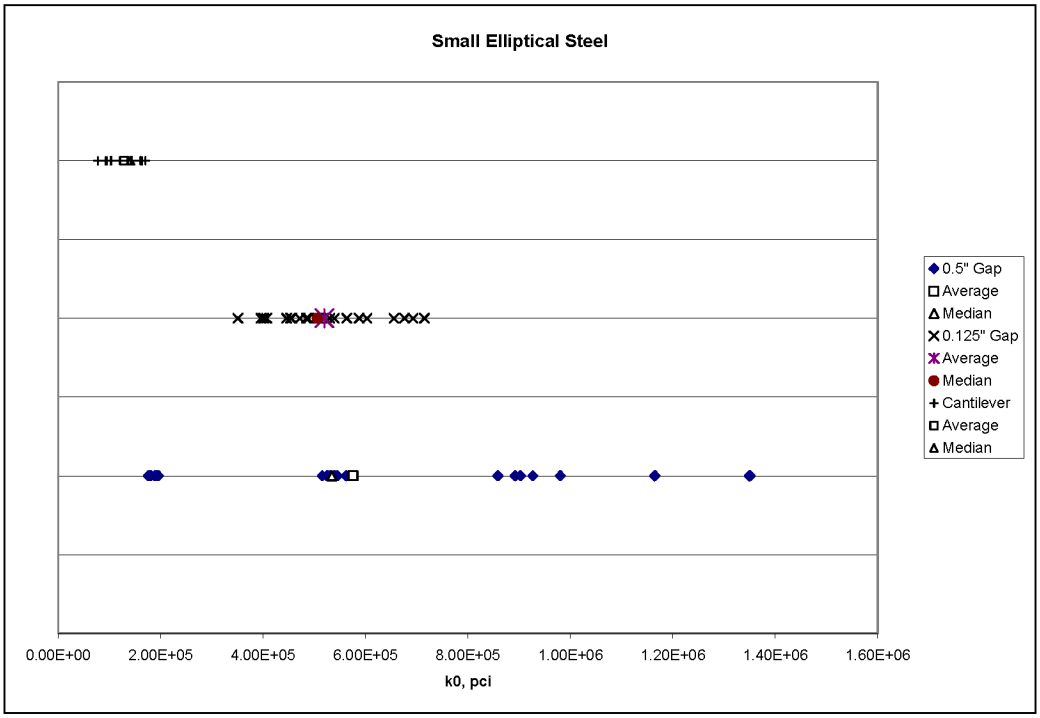

Figure C.6. Small elliptical steel k_0 comparison

APPENDIX D. SUGGESTED REVISION OF AASHTO T273 DOWEL TEST.

This section is a proposed procedural change to the current ***Standard Method for Testing Coated Dowel Bars, AASHTO DESIGNATION: T253***.

Revised ***Standard Method for Testing Coated Dowel Bars, AASHTO DESIGNATION: T-253***.

1 - Scope

1.1 This test method prescribes the test requirements for determining the Modulus of Dowel Support, k_o and the load-deflection behavior in concrete slab joint dowel bars.

1.2 This method is intended to improve the current dowel shear test portion of the AASHTO T253-76

2 - Referenced Documents

T253-76 - Standard Method for Testing Coated Dowel Bars

3 - Significance and Use

3.1 This test method is used to determine the Modulus of Dowel support of dowel bars to be used as shear load transfer mechanisms in paved concrete slabs.

3.2 This test method is designed to improve the consistency of test results by limiting end block rotation and specifying placement of applied loads and instrumentation.

3.3 End block rotation shall be mitigated through the placement of dual clamp mechanisms per end block.

3.4 This test method may also be used to study the load vs. deflection behavior of dowel bar specimens.

4 - Terminology

4.1 Modulus of Dowel Support (k_o): Stress between the dowel bar and surrounding concrete produced by a unit deflection of the dowel bar.

4.2 Relative Deflection: The vertical distance between two concrete surfaces separated by a joint under applied loading.

4.3 Embedment Length: The length of a dowel bar surrounded by concrete.

5 - Test Equipment and Requirements

5.1: A reaction frame capable of resisting a minimum of 30000 pounds of force and 54000 inch-pounds of moment with negligible deflection is required.

5.2: Load shall be applied to the concrete block through the use of a 50000-pound minimum capacity hydraulic actuator.

5.3: Deflection measurement shall be achieved through the use of 0.25-inch stroke direct current deflection transducers (DCDTs).

5.4: End block clamping mechanisms shall be constructed using high-strength steel connection members.

6 - Specimen Preparation

6.1: All concrete formwork shall be prefabricated steel formwork.

6.2: Sheets of polyvinyl chloride (PVC) shall be utilized for concrete joint construction.

6.3: Concrete joints shall be free of debris, especially at the dowel bar location.

6.4: Dowel bars must be level and centered within the transverse direction of the

specimen formwork.

7 - Test Atmosphere

7.1: Tests shall be conducted within standard laboratory conditions (23 ± 3 °C and 50 ± 10 % relative humidity) unless specified otherwise.

8 - Test Method

8.1: The end blocks shall be restrained from rotation and translation in all directions. Clamping forces shall be applied at the outside edges of the end blocks with enough space to allow for instrumentation. A minimum 1-in. clearance is recommended.

8.2: Loading shall be applied as shown below in Figure A-1.

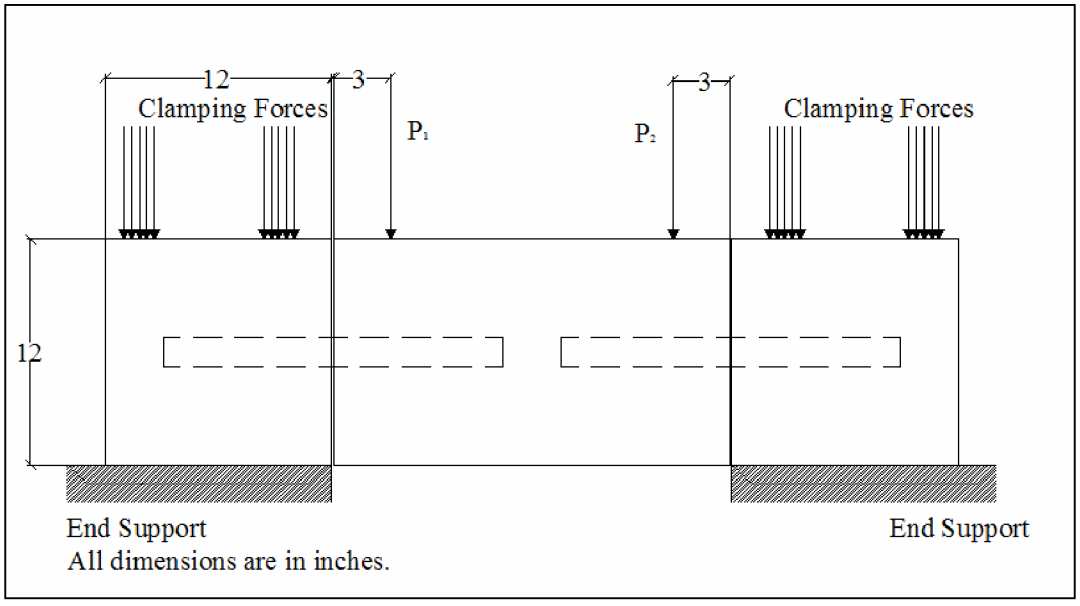

Figure D-1. Modified dowel test procedure.

8.3: Loading shall be applied at a maximum rate of 2,000 lbs per minute.

8.4: Deflection readings shall be recorded in 500-lb increments.

8.5: End load application at 20,000 lbs (10,000 lbs per dowel) or block shear failure.

9 - Calculations

9.1: Relative deflection, Δ, shall be calculated by subtracting the end block deflection reading from the middle block deflection reading at each joint location.

9.2: The load, P, transferred by each dowel bar shall be calculated as one-half of the applied actuator force.

9.3: The shear deflection, δ, per dowel bar shall be calculated using Equation 9.1.

$$\delta = \frac{\lambda P z}{AG}, \text{ in.} \tag{9.1}$$

Where,

λ = shear shape factor=10/9 for round and elliptical bars

P = shear force transferred by dowel, lbs

A = cross-sectional area of dowel bar, in.^{2}

G = dowel bar shear modulus, psi

9.4: Dowel bar deflection, y_0 shall be calculated using Equation 9.2.

$$y_0 = \frac{\Delta - \delta}{2} \tag{9.2}$$

9.5: The Modulus of Dowel Support, k_0, is determined through simultaneous solving of Equations 9.3 and 9.4.

$$y_0 = \frac{P}{4\beta_0^3 EI}(2 - \beta_0 z) \tag{9.3}$$

$$\beta_0 = \sqrt[4]{\frac{k_0}{4EI}} \tag{9.4}$$

Where,

β_0 = Relative stiffness of a beam on an elastic foundation, in.$^{-1}$

k_0 = Modulus of Dowel Support, pci

y_0 = Dowel bar deflection within concrete, in.

P = Shear load transferred by dowel bar, lbs

E = Dowel bar Modulus of Elasticity, psi

I = Dowel bar moment of inertia of, in.^{4}

Equations 9.3 and 9.4 are solved simultaneously using a spreadsheet computer program. A trial column of k_0 values are established to initially calculate k_0. The trial values of k_0 are used to calculate an initial value of β. Once the initial value of β is calculated, an initial theoretical value of y_0 can be calculated using Equation 9.3. The Solve function is then used to set Equation 9.3 equal to the measured value of y_0 (Equation 9.2) by changing the value of k_0. A sample spreadsheet is displayed below.

d=	1.50 (in)	Rows with highlighting and bold text contain correct k0 values.
h=	1.50 (in)	All other rows display initial conditions before calculations are executed.
I=	0.2485 (in^4)	
E=	28000000 (psi)	
z=	0.125 (in)	
A=	1.77 (in^2)	
υ=	0.31	
G=	10687023 (psi)	
λ=	1.11	

Load	Δ East	Δ West	δ East	δ West	y_0 East (Δ−δ)/2	y_0 West (Δ−δ)/2	y_0 East calc	y_0 West calc	β East	β West	k_0 East	k_0 West
0	0.000028	-0.000034	0.000000	0.000000	0.000014	-0.000017	0.000001	0.000001	0.322	0.322	200000	200000
232	-0.000040	-0.000015	0.000002	0.000002	-0.000021	-0.000008	0.000509	0.000509	0.322	0.322	200000	200000
645	-0.000067	0.000604	0.000005	0.000005	-0.000036	0.000300	0.001414	0.001414	0.322	0.322	200000	200000
1211	-0.000204	0.001637	0.000009	0.000009	-0.000106	0.000814	0.002654	0.002654	0.322	0.322	200000	200000
1450	0.000600	0.002219	0.000011	0.000011	0.000295	0.001104	0.003176	0.003176	0.322	0.322	200000	200000
1770	0.000824	0.002691	0.000013	0.000013	0.000405	0.001339	0.003880	0.003880	0.322	0.322	200000	200000
2097	0.001277	0.003307	0.000015	0.000015	0.000631	0.001646	0.004596	0.004596	0.322	0.322	200000	200000
2488	0.001583	0.003941	0.000018	0.000018	0.000782	0.001962	0.005451	0.005451	0.322	0.322	200000	200000
2571	0.001721	0.004194	0.000019	0.000019	0.000851	0.002088	0.005633	0.005633	0.322	0.322	200000	200000
3107	0.002092	0.004869	0.000023	0.000023	0.001034	0.002423	0.006808	0.006808	0.322	0.322	200000	200000
3665	**0.003134**	**0.005652**	**0.000027**	**0.000027**	**0.001553**	**0.002812**	**0.001552**	**0.002812**	**0.560**	**0.458**	**1824269**	**819335**
4116	0.003902	0.006470	0.000030	0.000030	0.001936	0.003220	0.009019	0.009019	0.322	0.322	200000	200000
5022	0.004476	0.007431	0.000037	0.000037	0.002219	0.003697	0.011005	0.011005	0.322	0.322	200000	200000
5872	0.005577	0.008453	0.000043	0.000043	0.002767	0.004205	0.012868	0.012868	0.322	0.322	200000	200000
6535	0.006133	0.009192	0.000048	0.000048	0.003042	0.004572	0.014321	0.014321	0.322	0.322	200000	200000
7040	**0.006730**	**0.009889**	**0.000052**	**0.000052**	**0.003339**	**0.004918**	**0.003339**	**0.004918**	**0.539**	**0.473**	**1566191**	**929693**
7834	0.006929	0.010723	0.000058	0.000058	0.003436	0.005333	0.017167	0.017167	0.322	0.322	200000	200000
8354	0.007668	0.011229	0.000061	0.000061	0.003803	0.005584	0.018306	0.018306	0.322	0.322	200000	200000
8850	0.008139	0.011741	0.000065	0.000065	0.004037	0.005838	0.019394	0.019394	0.322	0.322	200000	200000
9113	0.008880	0.012091	0.000067	0.000067	0.004407	0.006012	0.019971	0.019971	0.322	0.322	200000	200000
9853	**0.009857**	**0.012864**	**0.000072**	**0.000072**	**0.004893**	**0.006396**	**0.004892**	**0.006396**	**0.531**	**0.485**	**1472647**	**1026321**
10601	0.011112	0.013618	0.000078	0.000078	0.005517	0.006770	0.023231	0.023231	0.322	0.322	200000	200000
10917	0.011273	0.013792	0.000080	0.000080	0.005596	0.006856	0.023922	0.023922	0.322	0.322	200000	200000
11416	0.011435	0.014347	0.000084	0.000084	0.005676	0.007132	0.025017	0.025017	0.322	0.322	200000	200000
12112	0.011142	0.015021	0.000089	0.000089	0.005526	0.007466	0.026543	0.026543	0.322	0.322	200000	200000
12546	**0.012841**	**0.015921**	**0.000092**	**0.000092**	**0.006374**	**0.007914**	**0.006374**	**0.007914**	**0.527**	**0.490**	**1427799**	**1066676**

The dowel load and deflection readings for the calculation of k_0 shall be taken from the 2,000 lb/dowel – 10,000 lb/dowel range.